DISSERTATION

COMPUTED TOMOGRAPHIC CHARACTERIZATION OF THE EQUINE THIRD METACARPAL BONE

Submitted by

Martha G. Drum

Department of Clinical Sciences

In partial fulfillment of the requirements

for the Degree of Doctor of Philosophy

Colorado State University

Fort Collins, Colorado

Fall 2006

COLORADO STATE UNIVERSITY

July 12, 2006

WE HEREBY RECOMMEND THAT THE DISSERTATION PREPARED UNDER OUR
SUPERVISION BY MARTHA G DRUM ENTITLED COMPUTED TOMOGRAPHIC CHARACTERIZATION OF THE EQUINE THIRD METACARPAL BONE BE ACCEPTED AS FULFILLING IN PART REQUIREMENTS FOR THE DEGREE OF DOCTOR OF PHILOSOPHY.

Committee on Graduate Work

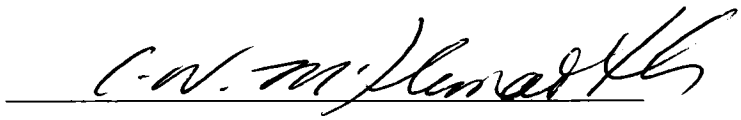

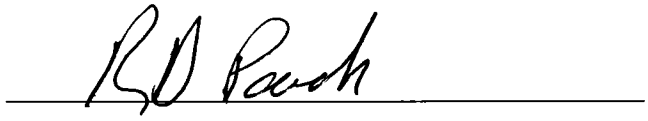

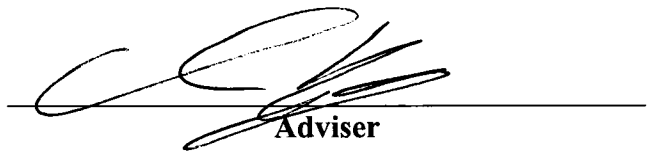

Adviser

Co-Adviser (if applicable)

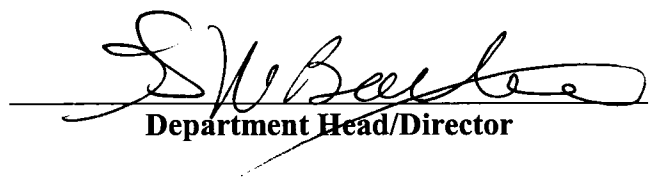

Department Head/Director

ABSTRACT OF DISSERTATION

COMPUTED TOMOGRAPHIC CHARACTERIZATION OF THE EQUINE THIRD METACARPAL BONE

Changes in subchondral bone (SCB) density attributable to disease pathogenesis or to normal aging and exercise related changes in horses are unclear. This project investigated equine (SCB) density characteristics using computed tomographic osteoabsorptiometry (CTO) and quantitative computed tomography (QCT). Results will provide objective measures of SCB density in horses.

Five metacarpophalangeal joints were CT scanned and four 1-cm^3 regions of interest were obtained for ash analysis to determine apparent bone density. A good correlation exists between 3D-QCT SCB densities and ash density in the distal third metacarpal bone of horses.

Metacarpophalangeal joints from non-racing, exercised, and racing horses were CT scanned, disarticulated, and subjectively evaluated for gross pathologic damage. A 3D surface model and a model with eight surface ROIs of the distal third metacarpal condyle were created from the CT scans, with mean density and mean voxel standard deviation(MVSD) measured. CTO patterns of SCB density were assessed subjectively for distribution trends by applying colors to specific SCB density ranges.

Racehorses had significantly lower mean density values than exercised and non-racing horses, and exercised horses had significantly lower mean density values than non-racing horses. Gross pathologic lesions were not associated with SCB density. Palmar abaxial sites were the only ROI with consistent significant differences between groups, and was supported by CTO maps.

Finally, histologic lesions, gross pathologic lesions, and QCT bone density measurements in nine racehorses were compared. Histologic specimens were evaluated for presence of osteochondral lesions. Mean CT density proved to be of little value in predicting osteochondral lesions typical of racing horses. However, mean voxel standard deviation was mildly associated with osteochondral lesions in racing horses, and should be investigated in future studies with a larger sample size.

QCT was a useful tool for characterizing SCB density in horses, but a poor predictor of gross pathologic change. CTO mapping contributed valuable SCB density characteristics in horses. While the predictive value of QCT and CTO was limited in this study, few pathologic lesions occurred in the sample. Even so, this study provides a foundation for using QCT and CTO prediction for larger studies on subtle joint disease in horses.

Martha G. Drum
Department of Clinical Sciences
Colorado State University
Fort Collins, Colorado 80523
Fall 2006

ACKNOWLEDGEMENTS

Multiple agencies, organizations and fantastic individuals were essential in the development and implementation of this study.

I would like to acknowledge my committee members for all their help and guidance. Dr. Kawcak was instrumental in fostering my education through my doctoral program while mediating the many technical difficulties encountered during this research. Dr. McIlwraith was also essential in my professional development as he is a brilliant teacher and compassionate motivator. His encouragement, support, and clinical expertise were crucial to the completion of this dissertation. I would also like to thank Dr. Norrdin for his help and eagerness in developing the gross pathologic and histologic grading schemes developed in this dissertation, Dr. Park for his input on the imaging portion, especially the osteoabsorptiometry maps, and Dr. Les for his attention to detail and overall expertise.

This study was funded by several organizations including the College Research Council at Colorado State University, the Southern California Equine Foundation, the Global Equine Research Alliance, the Marilyn Simpson Trust, High Medical Technologies, and the Grayson Jockey Club.

Several people generously gave their time to help me with this study. Billie Arceneaux spent numerous hours CT scanning, troubleshooting, and maintaining

data for the nearly 200 CT scans used in this study. Dan Carr was vital to the study, as he not only wrote the program used to create the three-dimensional models, but provided countless hours of instruction as to the premise of the computer software. I would also like to thank Bob Zink for his input on decalcification techniques and troubleshooting in the histologic analyses, Carola Pechey for donating her time to perform ash analysis, and Dr. Phillip Chapman for his countless hours of statistical guidance and advice.

I cannot forget my fellow graduate students, colleagues and laboratory staff: Dr. Katja Duesterdieck, Katrina Easton, Kindra Orr, Dr. Natasha Werpy, Erin Duffy, and everyone at the EORC.

Most of all I'd like to thank my friends and family for their support during my seven years in the combined DVM/PhD program, namely my husband Jeff for letting me follow my dreams and enabling me to accomplish them.

TABLE OF CONTENTS

Chapter 1

Introduction

Background and Rationale

Joint Disease in Animals and Humans

Musculoskeletal disease causing pain and disability is tremendously common in humans and horses. In the general U.S. horse population, the United States Department of Agriculture (USDA) found 50% of horse operations surveyed had at least one horse with a lameness that prevented the horse from performing its intended duties during the previous year[1]. This estimate may be low because racetracks were excluded from the sample population and musculoskeletal injuries are the most common cause of injury and death in racehorses[2]. Also, the USDA found that the majority of lamenesses reported during the survey year were chronic, lasting four months or more, and joint or leg problems the most common cause of lameness. Thus, joint disease is of great importance in the horse industry and attempts to improve detection and treatment will benefit the general horse population.

In 2001, 33% or 69.9 million adults in the United States self-reported having pain, aching, stiffness, or swelling in or around a joint on most days for at least a month[3], and approximately 21 million of the respondents actually had arthritis diagnosed by a physician. Arthritis and other rheumatic conditions

(AORC) were found to be the leading cause of disability in CDC survey respondents[4], and annual medical costs for AORC disability claims are reported to be $86 billion[5]. Unfortunately this scenario is likely to worsen as the CDC estimates 20 million new arthritis cases total by 2020.

Clearly the impact of joint disease is far reaching in both humans and horses. Treatment of osteoarthritis is difficult because it is often not diagnosed until joints are already symptomatic, and symptoms frequently result because of irreversible joint damage. Hence, a huge effort, ranging from advanced diagnostic imaging to biomarker research, has been initiated towards the early diagnosis of subtle joint damage in humans and animals aiming to slow the progression of degenerative joint disease and maximize therapeutic potential.

Subchondral Bone Structure

Subchondral bone can loosely be defined as the bone just beneath the articular cartilage. Structurally, osteochondral tissues are composed of the subchondral mineralized tissues, which include the calcified cartilage layer and subchondral bone plate, and the overlying articular cartilage. Calcified cartilage is highly mineralized cartilage that mechanically links the stiff subchondral bone to the pliable articular cartilage, which may do so by a gradual transition in stiffness afforded by the calcified cartilage[6]. The subchondral bone plate generally refers to the bony layer separating the calcified cartilage layer from

marrow spaces[6]. Composition of the subchondral bone plate varies from osteonal bone, as in the cortex, to appositional new bone laid down in a lamellar pattern which can obscure the junction between the subchondral plate and trabecular bone[7].

The function of osteochondral tissues is to form the shape of the joint surface, and to provide a means to transfer load between bones and maintain homeostasis in the joint[8]. Subchondral bone absorbs the majority of impact loading while articular cartilage functions to lubricate and distribute load evenly across the joint surface[9]. The calcified cartilage layer plays a role in maintaining the stiffness gradient between subchondral bone and articular cartilage[10]. The even transfer of forces across the joint is imperative for efficient utilization of the shock-absorbing properties of bone. The importance of this relationship is demonstrated during intense exercise[11] and osteoarthritic[12] induced changes in the calcified cartilage layer resulting in increases in subchondral bone density. The increased subchondral bone density causes stiffening and a decreased ability to efficiently absorb loading forces[9].

Mechanisms of Increasing Bone Density

Rheumatic disease, including arthritis, is a general label for a disease process that involves inflammation and loss of function of one or more connective tissue structures of the body[13]. Typically, arthritis can be divided

into rheumatoid arthritis and the more common osteoarthritis. Rheumatoid arthritis is an inflammatory disease of the synovium usually occurring in multiple bilateral sites [14], in contrast to osteoarthritis which frequently involves a single joint. In rheumatoid arthritis, the immune system is stimulated, and local inflammatory mediators in the joint increase articular cartilage catabolism. Focal subchondral and periarticular erosions, periarticular osteopenia and generalized osteopenia are bony changes common with rheumatoid arthritis[14]. Conversely, osteoarthritis occurs when there is an intrinsic failure of the osteochondral tissues. Historically thought to be a disease of articular cartilage, there is increasing evidence for the role of subchondral bone in the initiation and progression of osteoarthritis in humans and animals [15-21].

Pathophysiologically, osteoarthritis is characterized by cartilage degradation and changes in proteoglycan and collagen structure resulting from a disturbance in homeostasis[22]. Loss of proteoglycans and collagen alter the mechanical properties of articular cartilage[22]. However, subchondral bone sclerosis is also considered a cardinal feature of osteoarthritis.

Accumulation of microfractures is a step in triggering subchondral sclerosis via bone remodeling [23], but not all microfractures are repaired immediately, if at all[24]. Radin et al, [25] found no difference in number of microfractures in end stage osteoarthritic femoral heads as compared with age matched controls. In a study of human OA patients, femoral head

histomorphometry revealed that subchondral bone OA changes were associated with a lower degree of mineralization and an increase in unmineralized osteoid parameters in all OA specimens[20]. Another study examining biomechanical properties and density parameters of cancellous cores of human femoral heads found an increase in stiffness and bone volume, but a decrease in mineralized density in OA femoral heads compared to osteoporotic and normal age-matched controls[26]. Increasing osteoid may account for microfractures seen in osteoarthritis as increases in osteoid volume increase trabecular stiffness which in turn reduces the elastic modulus causing accumulation of microdamage in mineralized bone[27, 28]. Although this is one possible explanation of how microdamage and subsequent microfractures may occur, the precise role of microfractures in subchondral sclerosis and OA remains unclear.

A more recent explanation for the subchondral bone sclerosis seen in OA patients has recently been proposed by Hilal et al., to be a result of abnormal osteoblastic behavior[29]. Insulin growth factor (IGF) production may influence osteoblastic homeostasis pathways causing upregulation of osteoblastic activity. Further, subchondral thickening, via mechanical or cytokine stimulation of osteoblasts (or both), may increase microfractures in calcified cartilage causing bone matrix damage and activation of IGF regulated articular cartilage matrix repair. Thus, Hilal et al., felt that the enhancement of these systems by abnormal osteoblasts may be the cause of subchondral sclerosis and subsequent articular

cartilage degradation in early OA, which supports the role of subchondral bone in early joint disease.

Subchondral bone not only thickens in response to disease processes, but also as a normal adaptation to exercise and applied loads[30]. Bone is a dynamic tissue that is continuously responding to external forces by creating new, incompletely mineralized bone and resorbing mature lamellar bone to maximize stability and elasticity. Relative to other tissues, such as articular cartilage, bone has the potential for successful repair following damage.

Subchondral sclerosis is a physiologic response geared to strengthen bone architecture with the least amount of material in order to avoid ultimate failure[31]. This can occur by increased horizontal connections within the vertically oriented trabecular bone framework[32, 33] or by increasing the thickness of the trabeculae and subchondral plate[9]. Bone remodeling is the coupled process of bone resorption followed by bone formation, and is thought to be the dominant mechanism by which bone thickens in adults. Signaling of bone remodeling occurs at a certain strain threshold[34]. Below this threshold, resorption occurs; above it, remodeling is turned on to create biomechanically stable bone. It is thought[35] that when the signals for remodeling are sustained for long periods, as in repetitive cyclic loading, remodeling continues and bone becomes sclerotic and stiffens. Increased bone remodeling in exercised horses

has been demonstrated by several investigators[Kawcak, 2000 #27[36-39], and is useful as an experimental model of bony remodeling in racing horses[39].

Microdamage of bone is thought to be another protective mechanism to help bone withstand variations in applied loads[40]. Coalescence of microdamage creates grossly visible microcracks or microfractures and stimulates bony remodeling to remove old or damaged bone and replace it with new stronger bone. A correlation has been found between microdamage incurred from normal physiologic loads and initiation of intracortical bone remodeling[30, 40], and diffuse microdamage has been observed in exercised horses[39].

Another way that bone may increase in volume is by the process of bone modeling which predominates during periods of skeletal development. Bone modeling is the process by which bone is actively changed to respond appropriately to mechanical force. The overall gross shape of the bone is changed as seen in young and growing animals. Bone modeling can account for trabecular drift where there is formation of new bone on one side and opposing resorption, but is largely ineffective in adult bone. Modeling by forming bone on either side of a trabecular strut was found to continue well into adulthood in humans. In horses, Boyde[24] found an increased amount of bone in cancellous marrow tissues in immature exercised horses as compared to controls and in racing horses. However, he found no evidence to suggest that increased bone

density in racing horses was the result of the coupled remodeling sequence suggesting modeling is occurring concurrently with remodeling in racing horses.

Ultimately bone density is increased by several different pathways. If certain repeatable, predictable relationships between pathologic joint changes, adaptive bone formation, and subchondral density changes can be determined in a joint on the whole, then it may be possible to diagnose pathologic joint damage earlier in the course of disease.

The Connection between Subchondral Bone and Articular Cartilage

The events controlling the progression of mild cartilage damage to osteoarthritic lesions of cartilage fibrillation, osteophyte formation and full thickness cartilage loss with eburnation of subchondral bone are unclear. Although early cartilage changes can be induced both mechanically and biochemically in many models[41, 42], it seems that joint instability or impulsive loading are key in the progression of cartilage damage to osteoarthritis[21, 43, 44].

Increases in cartilage water content are an early degenerative change, and may result from a loss of collagen fibrils or collagen damage. This creates a cartilage matrix that is softer in compression and weaker in tension, which may cause an increased susceptibility to fibrillation and cleft formation. Instantaneous

deformation, a test of tensile stiffness in collagen, was found to correlate strongly to cartilage swelling, and both were associated with increases in degraded collagen molecules[45].

Both subchondral bone and calcified cartilage are implicated in the pathogenesis of osteoarthritis, but there is still disagreement as to the primary initiating factor, articular cartilage damage or subchondral remodeling. E.L. Radin proposed changes in subchondral bone precede cartilage changes and a high stiffness gradient in the calcified cartilage layer leads to increased stress in the overlying cartilage[46]. Experimental osteoarthritis models have led to the theory that the slow progression of cartilage erosion in the course of osteoarthritis increases sclerosis in subchondral bone which increases stiffness and contributes to further mechanical cartilage damage[47].

Although the exact role of subchondral bone in the initiation of OA is still unclear, subchondral density changes affect the progression of osteoarthritis [21, 22, 43, 48, 49]. In studies of human patients, treatment of subchondral lesions significantly improved pain levels and slowed progression of disease. Also, experimental models of osteoarthritis have shown that cartilage lesions may not progress without impact loading and subchondral change[21]. Therefore, the ability to monitor subchondral bone changes, and more specifically detect subchondral sclerosis in early stages of joint disease, has the potential to greatly affect the outcome and prognosis of joint disease.

Qualitative Subchondral Bone Imaging

Lameness is a leading cause of lost days in race training[50, 51], but current diagnostics struggle with sensitivity in detecting and prevention of subtle joint disease[52]. Radiographs, subjective lameness evaluations, nuclear scintigraphy, magnetic resonance imaging (MRI), and computed tomography (CT) are widely used diagnostic techniques in humans and animals, but each has their own specific limitations.

Radiography has been a first line diagnostic tool since the discovery of x-rays in 1895. It is relatively inexpensive, safe and easy to use. The majority of physicians and veterinarians around the world receive formal training in acquiring and interpreting radiographs, thus making it a very familiar diagnostic modality. Unfortunately, subchondral density assessment via radiography has several limitations. A radiographic latent period exists where simple radiographs are insensitive until approximately a 30-50% change in bone mineral density occurs[53]. As an example, 40% of equine femoropatellar joints appeared radiographically normal, but had cartilage changes present when arthroscopically examined[54]. However, it cannot be said for certain that those joints with cartilage changes would have progressed to exhibit radiographic evidence of bony change.

Radiologic imaging of bony structures provides excellent spatial resolution, which is simply the smallest discernable distance between two structures. Spatial resolution can be measured in millimeters or line pairs per centimeter[55]. Typical spatial resolution for CT scanners is 10 line pairs per centimeter or 0.5 mm resolution, but some newer scanners have resolutions as low as 0.3 mm[55]. However, the contrast resolution, or ability to assess the amount of radiodensity differences, is poor with radiographs; thus, the inability to discretely discern soft tissue structures with x-rays. Radiographs are a two-dimensional representation of a three-dimensional object, but orthogonal (perpendicular) and oblique views improve defining or detecting lesions. The effect of summation or superimposition of structures is a weakness of radiography particularly in complex joints such as the carpus or tarsus. However, high detail radiographs have been found to image trabecular structure of a single bone that directly correlates to the three-dimensional architecture[56].

With regards to osteoarthritis, it is well documented that radiographic severity correlates to clinical symptoms in humans, but the converse has not been proven reliably[57]. No consistent correlation between severity of radiographic OA lesions and clinical signs in horses has been found[53]. Osteophyte score, joint space narrowing and bony contour changes are considered reliable indices of degenerative joint disease on radiographs in humans[58, 59] and dogs, while subchondral sclerosis and cysts were not reliable indices[60]. Radiographic joint space narrowing is considered the most

sensitive but least specific indicator of human hip osteoarthritis, while also being neither sensitive nor specific for human knee osteoarthritis[61]. Also, radiographic scoring systems imply that disease progression is temporally linear[60], but this has not been proven in animals. Furthermore, osteophyte score, joint space narrowing and bony contour changes are representative of more advanced degenerative joint disease whereas subchondral bone sclerosis can be an early change as well as a feature of end-stage osteoarthritis[61]. The inconsistency of subjective radiographic evaluations and structural limitations of radiographs make it obvious that more reliable methods of diagnosing early or subtle joint disease are needed.

Nuclear scintigraphy is a highly sensitive means to determine early joint disease[62], and the ability to image entire limbs or skeletal regions makes it ideal for screening tests. Scintigraphy employs injecting a radioactive compound, such as Technecium-99, into the patient, then a specialized gamma camera is used to detect the amount of radiation emitted by the patient. The radioactive compound is taken up by metabolically active cells, thus sites of mild bone remodeling can be detected using nuclear scintigraphy. Although this is a major advantage in localizing lameness, it is also directly related to the limited specificity of scintigraphy as changes in bone metabolism can occur in multiple disease processes such as exercise induced bone remodeling and osteochondral damage[63, 64].

Magnetic resonance imaging (MRI) has superior soft tissue resolution due to its hydrogen-based imaging principles compared to computed tomography and radiography. Greater evidence is arising for using MRI to identify bone density changes such as third carpal bone sclerosis in horses[65]. However, the relatively homogenous MRI signal produced by subchondral bone makes it difficult to identify small changes in bone density.

Computed tomography (CT) allows one to clearly visualize individual anatomical structures without superimposition, particularly in joint spaces or joint surfaces. A few studies have demonstrated that CT was able to detect and define radiographically silent but clinically apparent fractures in horses[52, 66]. CT may be used to identify changes in cortical and subchondral bone in order to prevent or at least enhance treatment of bone injury. Computed Tomographic Osteoabsorptiometry (CTO) is the mapping of subchondral bone density distributions with specific density ranges assigned to specific colors or shades of gray and comparing differences in density distributions between subjects. This is in contrast to quantitative computed tomography (QCT), which measures the specific density of bone or other tissue over a certain area. Eckstein et al., [67] found CTO as a useful tool for determining loading history of subchondral bone in human elbows. The value of CT in horses has been limited due to cost and the need for general anesthesia. However, as demand for definitive lameness diagnosis increases, so does the popularity of CT since CT still remains one of the best clinical tools to identify early subchondral bone lesions in horses[68].

Quantitative Subchondral Bone Analysis

The most commonly used modalities to quantitate bone density are Dual-energy x-ray absorptiometry (DXA), QCT (including pQCT and vQCT), radiodensitometry, and quantitative ultrasound. By far, QCT and DXA have been used the most both clinically and experimentally. Although they both utilize ionizing radiation, the end result is quite different.

DXA measures the transmission of X-rays with high and low photon energies in order to separate bone from soft tissue. The two distinct energy peaks are created for bone and soft tissues using either the energy switching or rare earth filter methods. Soft-tissue and bone fractions are estimated using complex algorithms[69], such that total bone mineral density (BMD) and bone mineral content (BMC=BMD x area) are calculated and reported in g/cm^2. DXA is used extensively to measure bone mineral content, but is not able to image bone volumes. This is important as bone mass alone is not an indicator of bone strength[70]. DXA analysis of subchondral bone is relatively limited, particularly since the major market for DXA is monitoring osteoporosis which focuses on measuring trabecular bone turnover. This results in difficulty precisely measuring density of the entire subchondral bone area due to joint curvature and limitations in proprietary software package measurement tools.

However, subchondral bone mineral density from DXA studies has been found to increase in meniscectomized guinea pigs[71] and has correlated with radiographic subchondral sclerosis[72] and joint space narrowing[73] in humans. In horses, regional areas of subchondral density assessed using DXA were significantly different within the third metacarpal bone[74, 75]. DXA has been indispensable for determining bone mineral content in humans. It is traditionally used to assess vertebral bone mineral content to monitor osteporotic change. However, some studies show that QCT is actually more sensitive to changes in bone mineral density[76], but DXA is less expensive and more readily available to monitor longitudinal bone density in humans.

Since detection of early joint changes, such as subchondral sclerosis, is difficult to assess subjectively[60], one method of quantitatively evaluating radiographs is photodensitometry. This is done by placing an aluminum step-wedge in the radiographic field as a reference standard of bone mineral content. Using this method Nielsen et al, [77] documented a period of demineralization followed by remineralization in the lateral, medial, and dorsal third metacarpal cortices of two-year old quarter horses during their first racing season. Porr et al[78] found a decrease in bone mineral content of Arabian horses following a period of athletic deconditioning using photodensitometry. Although the step-wedge method is easy and repeatable, it cannot adequately measure subchondral bone density due to superimposition artifacts of joint surface contours.

Computed Tomography (CT) Principles

Computed Tomography (CT) was developed to in the early 1970's to address limitations of conventional two-dimensional radiography. The fundamental concept of CT is that internal structures can be reconstructed from multiple projections of the structure. This occurs by using multiple converging x-ray beams paired with multi-element detectors to create a cross-sectional tomogram or "slice" via complex algorithms processed by a peripheral computer, hence the name computed tomography.

Modern day CT scanners are very different from the first generation translate-rotate scanners of the 1970s. First generation scanners had a tube and detector that moved continuously across the patient to translate the degree of tissue attenuation, then rotated 1 degree and repeated another translation for 180 degrees, with second generation scanners being a step up by increasing the number of detectors. Third generation scanners utilize a fan beam that exposes the patient to the source x-rays, and a detector arc that collects between 600-1200 data points at once[55]. The detectors and tube rotate around the patient for 360 degrees. However only voxels in line of the center detectors are measured thus reducing scatter and image noise. Fourth generation scanners operate using the same fan beam width, but are in a stationary 360 arc. Developments with each generation of CT scanner have increased image spatial resolution, decreased scanning times, and reduced patient radiation dose.

Spatial resolution is the smallest size of an object that can be imaged with CT, and is influenced by many factors including the linear attenuation coefficient of a tissue and background noise. Typical spatial resolution for CT scanners is 10 line pairs per centimeter or 0.5 mm[55]. Linear attenuation coefficients tell how much attenuation can be expected from a certain thickness of tissue, and are specific for both the energy of the x-ray beam and the tissue type. It is classically represented by the equation:

$$N = N_o e^{-\mu X}$$

Where N = number of transmitted photons

N_O = number of incident photons

μ = linear attenuation coefficient

X = part thickness (in centimeters)

Obviously the better the spatial resolution, the more accurate the quantitative measurements, but this may come at the expense of increasing ionizing radiation dose to the patient.

CT images are made by a reconstruction algorithm that interprets the initial x-ray intensity and the exiting x-ray intensity summed over numerous segments within a slice to determine tissue attenuation for each picture element (pixel). Each voxel represents a volume element (voxel) whose length is determined by the slice thickness. To image the complicated matrix assembled during reconstruction, filtered back-projection is used which smoothes the data and corrects for partial ray projections. CT numbers (or Hounsfield Units) are

then assigned to each voxel based upon the relative density of water and represent the relative linear attenuation coefficient at that particular location. CT numbers are generally calculated using the following equation:

$$\text{CT number (HU)} = \frac{K\,(\mu - \mu_{water})}{\mu_{water}}$$

Where K is assigned the value of 1000 and μ the attenuation coefficient of the material represented by the voxel[32].

For traditional display, each CT number is assigned a range of gray scale color. Since the reconstructed image is based upon tissue attenuation, the resulting gray-scale image has the same radiodensity interpretations where dense bone is very radiopaque and air and fat very radiolucent. Additionally, the assigned CT numbers are characteristic for general tissue types where water is approximately zero, air and fat less than zero, soft tissue around 100, and bone and metal from 300-2000 or more depending on the species.

Variations of traditional CT scanners have been developed to investigate changes in bone both quantitatively and qualitatively. Quantitative Computed Tomography (QCT) employs either peripheral post-processing analysis of standard CT scans; or with newer machines, quantitative software is built into main scanner workstation. Using QCT one can measure and compare actual

voxel values in Hounsfield Units rather than relying on visual assessment to detect differences in tissue density.

Also, QCT is very beneficial in monitoring changes in bone mineral density over time. Typically, a standard calibration phantom containing materials with physical attenuation properties similar to bone, fat and water is scanned with the patient. The purpose of the calibration phantom is to correct for beam hardening errors and to standardize measurements for comparisons between different CT scanners. Liquid K_2HPO_4 and solid tri-calcium phosphate are the most common phantoms used. However, liquid phantoms have fallen out of favor because they generate air over time and require routine "degassing" to maintain accurate concentrations of K_2HPO_4[79].

QCT measurements are typically taken from single CT slices, and the most common example is vertebral bone density measurements to detect or monitor osteoporosis[80]. However, with newer computer technology, volumetric QCT (vQCT) is now possible. This involves "stacking" the CT slices to render a three-dimensional volume from the CT slices enabling the user to take density measurements from entire joint surfaces. The convex or concave nature of joint surfaces was initially a large source of error, but newer programs can actually determine the first voxel of the joint surface and measure a fixed distance from that voxel. This allows joint contours to be accounted for when measuring surfaces.

Peripheral QCT (pQCT) scanners are smaller versions of traditional second generation CT scanners. They are designed for bone mineral density analysis of the appendicular skeleton, and have been found to be precise and accurate in measuring BMD of the distal radius and tibia[69]. Reduced patient dose and cost are two attractive features of pQCT, particularly for serial scans to monitor changes in BMD. Another advantage to pQCT is the ease in distinction between cortical and trabecular bone as BMD of trabecular bone is desirable in monitoring osteoporosis. This is in part due to local anatomic distinction between cortical and trabecular bone in appendicular sites, but is also facilitated by the high resolution of newer pQCT scanners.

MicroCT is an extremely high resolution CT scanner with resolutions of 10-60 microns depending on the manufacturer[69]. Only small samples (a few centimeters at most) can fit in the scanner, limiting microCT to research use. Because of the high resolution, microCT can image individual trabecular architecture to determine direction and connectivity of trabeculae[33, 81] as well as degree of mineralization within trabeculae[82].

Although CT has excellent contrast resolution for bone, there are artifacts and limitations that affect data acquisition. Partial volume effects occur when more than one tissue type occupies the same voxel. It results in a false tissue density, and thus an absolute CT number scale cannot be employed. In order to minimize the partial volume effect, the slice thickness should be decreased, and

the preceding and succeeding slices must be examined to evaluate discontinuity of the density.

Beam hardening is a significant artifact in all types of imaging that utilizes ionizing radiation. This phenomenon occurs when a highly dense and homogenous structure, such as bone, preferentially absorbs lower energy photons. Effects are most dramatic in structures immediately adjacent to highly dense structures because as the x-ray beam exits a highly dense structure, the beam has a larger proportion of high energy photons. This is detected as a structure with a low attenuation coefficient, such as air. A classic example of beam hardening in humans occurs adjacent to the petrous temporal bone where brain tissue density is significantly decreased and appears artifactually black. However, beam hardening effects can be observed in the center of dense, solid object effectively decreasing CT numbers in the center of the object. Computational algorithms are built into CT scanners to correct for this artifact, and combined with special density calibration phantoms, the effect is thought to be minimal. Hounsfield Units (HU) are considered a relative density measurement because the scanning algorithm uses water as a basis for determining attenuation. Simple use of calibration phantoms[79, 83] are the preferred method to convert the relative HU values to objective mineral density units.

Clinical Applications of QCT and CTO

As computers have become less expensive, faster, and have more powerful processors, imaging programs are now able to analyze CT scan data from joint surfaces. One program, OsteoApp[5], was specifically developed to image CT data from joint surfaces, and performs detailed measurements previously unavailable on articular surfaces. The program was written using the Interactive Data Language[4], and was designed for both three-dimensional and two-dimensional analysis of Digital Imaging and Communications in Medicine (DICOM) format data. DICOM is the standard format by which CT scans can be networked, interface with other hospital systems, and implemented in databases in a variety of devices. In order to visualize a specific joint surface, a density threshold is selected, and a point is chosen within the bone of interest. The result is a three-dimensional image of a structure with specific densities. Three-dimensional rendering is generally used in relation to specific regions of interest (ROIs), but little has been done that considers the geographical nature of bony surface. OsteoApp[5] can be used to render individual bones or entire joints, but as with any imaging technology there are imperfections. As mentioned before with regards to CT imaging, partial volume and edge effects remain potential issues with computer modeling.

Although QCT has not been applied to equine joint surfaces, it has been a standard practice in human medicine to monitor vertebral bone density for

osteoporotic fracture risk[83]. Similarly, QCT has been used in horses to estimate age and exercise induced changes in bone mineral density[84] of the metacarpal diaphysis. Using CTO, different density distributions were seen in shoulder, elbow and hip joints in normal patients[6]. Also, density patterns of athletes and patients with various orthopedic diseases had different patterns of density than the same joints from normal patients. Thus they concluded that CTO can be used to determine the loading history of a joint[85] in a cross section of patients. Similarly, an increased percentage of high bone density was detected in the distal third metacarpal condyle of treadmill exercised horses in comparison to controls[86]. Currently, CTO hasn't been used clinically to study density patterns over time in either aging or diseased populations.

Osteochondral Damage and Fracture in Racehorses

Gross and histopathologic characteristics of overload arthrosis in horses have been documented[87-89], and demonstrate that subchondral bone plays a role in the development of osteochondral injuries and pathology. Pool and Meagher[88] observed that palmar osteochondral lesions ("traumatic osteochondrosis") occur in highly trained, mature racehorses and condylar fractures commonly occur in young racing Thoroughbreds. They also described focal areas of subchondral sclerosis and necrosis with surrounding bony remodeling as being characteristic of palmar osteochondral lesions.

Other common osteochondral lesions observed in racehorses include osteochondral fragmentation, and partial or complete osteochondral fracture. Catastrophic injuries, which occurs when there is total loss of limb support, can cause major economic losses, but even minor osteochondral injury can cause chronic, recurrent lameness problems in racehorses[2, 51, 90-95]. Equine forelimbs bear 60-65% of a horse's weight and 95% of all forelimb lamenesses occur from the carpus distad [59]. Catastrophic injuries commonly affect the third carpal bone, proximal sesamoid bones and distal third metacarpal condyle of the metacarpophalangeal joint. Specifically the metacarpophalangeal (MCP) joint is involved in the majority of catastrophic racehorse injuries, and injury can occur in both racing and training [2].

Condylar fractures can be classified as complete, complete non-displaced, and incomplete[96]. The distribution of condylar fractures is well documented[97] in relation to breed, gender, limb, and postoperative racing success. However, there seems to be little analysis of whether specific condylar fracture types occur at a specific age. One paper attempted to associate age with fracture configuration in 56 Thoroughbred racehorses[98], but no associations were found.

In summary, evidence exists that increased subchondral bone density is associated with pathologic disease changes as well as exercise induced changes. QCT and CTO appear to be valid imaging modalities to characterize

these changes in subchondral bone of horses in order to further define events in early joint disease. However, there is very little information supporting the accuracy of QCT to measure equine subchondral bone density or the characteristics of CTO patterns in aging and racing horses. Additionally, the objectivity of QCT to predict a specific threshold of bone density that may be associated with pathologic changes in equine joints is unknown.

Purpose of Study

The purpose of this study was to evaluate Computed Tomographic Osteoabsorptiometry (CTO) and Quantitative Computed Tomography (QCT) as a means of measuring subchondral bone density in the equine distal third metacarpal bone.

Study Goals

The goal of this study was to determine if CTO and QCT can be used to establish if a pathologic threshold of subchondral bone density exists in the equine distal third metacarpal bone.

Hypothesis

The working hypothesis for this research was: mean subchondral bone density as measured using QCT is associated with pathologic changes of early joint disease, and subchondral bone density maps assessed using CTO will establish density patterns characteristic of joint pathology in order to improve diagnostic sensitivity of equine joint disease.

Specific Aims

1. To determine the accuracy of subchondral bone density measurements obtained by QCT in the horse.

Hypothesis-QCT bone density correlates with bone mineral density obtained by ash analysis

2. To determine mean subchondral bone density differences of the distal third metacarpal bone of three different equine populations.

Hypothesis-Surface mean subchondral bone density is significantly different between racing, treadmill exercised, and aging horses

3. To determine regional variations in subchondral bone density of the distal third metacarpal bone of three different equine populations

Hypothesis-Regional subchondral bone density determined using QCT and CTO differs between specific anatomic areas and between uses

4. To determine subchondral bone density patterns of the distal third metacarpal bone of three different equine populations.

Hypothesis-CTO subchondral bone density distribution patterns are significantly different between racing, treadmill exercised, and aging horses

4. To correlate QCT subchondral bone density with gross pathologic and histologic scores in racing horses

Hypothesis- Mean subchondral bone density measured using QCT correlate with gross pathologic articular surface scores and subchondral bone histologic scores

Chapter 2

Correlation of Computed Tomographic Subchondral Bone Density and Ash Density in Horses

Introduction

Quantitative Computed Tomography (QCT), is a powerful tool for physicians and veterinarians due to the ability to noninvasively expand our knowledge of normal and abnormal joint anatomy. Several studies [76, 99-103] have been performed in humans to verify that bone mineral density measurements obtained using QCT, which measures volumetric bone density, are accurate representations of true bone mineral density. The majority of the studies focused on trabecular bone, but cortical and subchondral bone are significantly denser. Thus, the higher density of subchondral bone may influence QCT density measurements of articular surfaces due to beam hardening effects. Beam hardening occurs in areas of high density, such as subchondral bone, where the mean energy of the CT beam passing through the bone is artificially increased as the low-energy photons are filtered out by the bone material, and results in adjacent structures having falsely low measured densities[55]. This phenomenon can also occur in the center of highly dense materials. However bone reconstruction algorithms used by the CT computer aim to reduce these effects, and are thought to be adequately corrected by the CT computer[69].

One study that investigated the relationship between cortical QCT density and ash density found only a moderate correlation between the two indices[104]. In horses, research is very limited, but one study found that cylinders of equine trabecular and cortical bone correlated strongly with QCT density[105]. Another study found cross-sectional area, thought to be related to ash content, is strongly correlated to QCT bone density[106]. Other studies in dogs have found similar strong correlations of calcium content to QCT density[107]. No correlations have been reported for subchondral bone density measured using QCT and ash density in humans or animals.

With newer more powerful computer applications, three-dimensional volumes of subchondral bone surfaces can be created. Mean QCT density of reconstructed volumes of equine subchondral bone using PC-based three-dimensional modeling programs has not been published. Therefore, it is also unknown what effect three-dimensional modeling programs have on the accuracy of QCT equine subchondral bone density measurements. The accuracy of density values obtained using 3D-QCT need to be determined before applying this technology to clinical and experimental applications in the horse. In order to evaluate the accuracy of 3D-QCT, comparisons with ash density are necessary. Measuring specific regions of interest (ROI) from CT scans to correlate with ash density can be technically challenging. One way to ensure that an ROI is measured identically in the CT scan is to cut the ROI in the bone prior to CT

scanning. However, the air bone interface created when cutting ROIs could potentially increase error in 3D-QCT ROI density measurements.

Thus the goal of this study is to evaluate 3D-QCT models as a measure of subchondral bone density in distal third metacarpal bone of horses. We hypothesize that equine bone density measured using apparent ash density will correlate well with bone density measured using 3D-QCT. Additionally, we will examine the effects of cutting equine bone on 3D-QCT measures to test the hypothesis that cutting ROIs prior to CT scanning significantly changes 3D-QCT bone density measures.

Materials & Methods

Preliminary Computed Tomography (CT) Scans

In order to determine the degree of artifact error created by cutting regions of interest into the joint surface prior or to CT scanning, one left metacarpophalangeal (MCP) joint from two different horses were CT scanned three separate times. The first scan was performed on the intact MCP joint, which was removed at mid-diaphysis during necropsy. A Picker PQ[a] was used to perform the CT scans and a 512 x 512 matrix with an 18-cm field of view and 1.5-mm slice thicknesses at 140 kVp. Also, a tri-calcium density equivalent CT phantom[b] was scanned at the end of the CT scan for bone density calibration. After intact joint scanning, the MCP joint was incised and the distal third

metacarpal condyle was removed, using a band saw, approximately three centimeters proximal to the medial condyle. The removed condyle was then CT scanned using the previous scan settings, and positioned similarly using foam padding. Finally, four 1-cm^2 regions of interest (figure 2.1) were cut to a depth of 1-cm on the removed condyle using a precision cutting system[c], and the cut condyle was scanned again in approximately the same position using the same CT scan settings.

Three-dimensional modeling of the distal third metacarpal condyle CT scans was performed using a specially designed PC-based application (OsteoApp [d,e]). A voxel threshold of 500 Hounsfield Units was used to isolate the distal third metacarpal bone for rendering into a three-dimensional model (Appendix 1). The four regions of interest were placed precisely on the distal articular surface for each CT scan (figure 2.1) by determining the coordinates, in millimeters, of each corner of the square ROI in relation to the medial, dorsal, and palmar joint edges of the actual distal third metacarpal bone specimen. Coordinates, in millimeters, were then reproduced in OsteoApp on the distal third metacarpal bone articular surface of the three-dimensional model. Mean density values were calibrated using a tri-calcium phosphate density phantom and a simple linear regression for each scan. The QCT mean density for each ROI was measured to a depth of 1-cm from the surface, and area for each region of interest recorded. Comparisons between scans for mean density and area were analyzed using a Wilcoxon Signed Rank test [f].

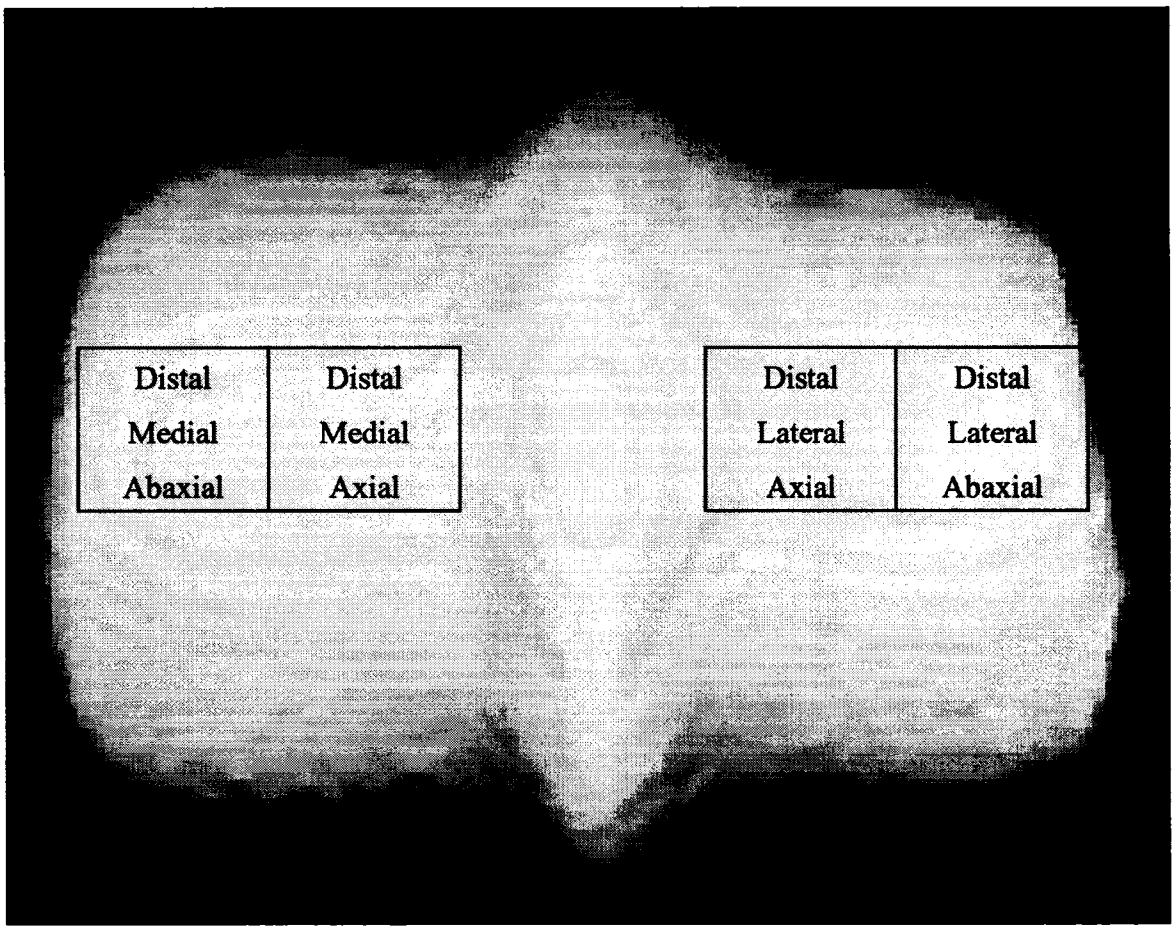

Figure 2.1: Three-dimensional model of the equine distal third metacarpal bone with the four 1-cm^2 regions of interest.

Ash Analysis & Corresponding CT Scans

Five left MCP joints from two racing and three non-racing horses were used for ash sampling. Racing horses were both two year-old female Thoroughbreds euthanized for non-musculoskeletal diseases or injuries, while non-racing horses were a 21 year-old Arabian gelding, a 10 year-old Quarter Horse female, and a 4 year-old mixed breed female euthanized for non-

musculoskeletal diseases or injuries. Intact MCP joints were removed and CT scanned as previously described for the preliminary scans. The distal third metacarpal condyle was removed approximately 3-cm proximal to the medial condyle. Four regions of interest were cut as in the preliminary scan section (Figure 2.1). The regions of interest were then removed at a depth of 1-cm from the surface of the medial condyle to create approximately 1-cm^3 bone cubes for ashing.

Bone cubes were soaked for 24 hours in physiologic saline to soften and loosen any soft tissue present. Cartilage was scraped from the surface and cubes were sonicated for ten minutes to remove residual soft tissue. Prior to ashing, samples were transferred to fresh physiologic saline and frozen at -20° C. Samples were ashed using a previously published protocol[108] where an apparent dry density (ρ_d) was obtained after placing samples in a 100° C vacuum oven for 24 hours and weighed using a precision scale. Apparent ash density (ρ_a) was measured by heating samples in a muffle furnace at 800° C for 24 hours and weighed using a precision scale. Percent mineralization was calculated by dividing apparent ash density by apparent dry density (ρ_a/ρ_d). Mean QCT bone density (mg/ml TCP) of each bone cube was obtained as described in the preliminary portion. Ash density and percent mineralization were correlated to CT mean bone density using a Pearson's correlation coefficient. A mixed-model analysis for differences in mean QCT density, mean ash density and mean percent mineralization were performed by side (medial/lateral), anatomic sector

(distal axial, distal abaxial), and specific ROI site (lateral distal abaxial, lateral distal axial, medial distal abaxial, medial distal axial) with horse as a random factor. Results were significant with $p<0.05$, and were considered a trend with $p<0.10$.

Results

Preliminary CT Scans

Area did not vary significantly between scans at each ROI location, indicating that ROIs were placed consistently between scans on each 3D-modeled articular surface. However, ROI mean QCT density measured on the pre-cut condyle was significantly less ($p=0.01$) from the removed condyle. Mean QCT density of the pre-cut condyle was less than the intact condyle ($p=0.05$), but was only a trend. Intact condyle mean QCT density was not significantly different than removed condyle mean QCT density ($p=0.25$).

Table 2.1: P-values of Signed Ranks for area and mean density values

Scan	Area	Mean Density (mg/ml TCP)
Pre-Cut vs. Condyle	p=0.18	p=0.01
Pre-Cut vs. Intact	p=0.89	p=0.05
Condyle vs. Intact	p=0.19	p=0.25

Ash Analysis

The correlation pooled for all ROIs was r=0.8176 ($p<0.0001$) for ash density and r=0.9246 ($p<0.0001$) for percent mineralization. Individual correlations for specific condylar side, anatomic sector, and ROI sites are listed in Table 2.2. All pooled correlations for condylar side and anatomic sector were significant ($p<0.05$) except lateral and medial distal axial ash density, and medial distal abaxial percent mineralization.

Mean QCT density, ash density and percent mineralization were not significantly different between lateral and medial ROIs. For axial and abaxial sites, mean QCT density, mean ash density, and mean percent mineralization of distal abaxial sites were significantly higher than distal axial sites ($p=0.02$, $p=0.01$, and $p=0.007$ respectively). No significant differences were found at each individual ROI site for mean QCT density, mean ash density, and percent mineralization.

Table 2.2: Pearson's Correlation Coefficients (r) and p-values by region and specific ROI for ash density and percent mineralization.

Region	Ash Density (r)	Percent Mineralization (r)
Lateral	0.8691 (p=0.0011)	0.9246 (p=0.0001)
Medial	0.8370 (p=0.0025)	0.8397 (p=0.0024)
Distal Axial	0.8546 (p=0.0016)	0.6345 (p=0.048)
Distal Abaxial	0.9278 (p=0.0001)	0.7901 (p=0.0065)
Lateral Distal Axial	0.7530 (p=0.14)	0.9191 (p=0.027)
Lateral Distal Abaxial	0.9665 (p=0.0073)	0.9218 (p=0.026)
Medial Distal Axial	0.6277 (p=0.26)	0.9085 (p=0.033)
Medial Distal Abaxial	0.9560 (p=0.0096)	0.7318 (p=0.16)

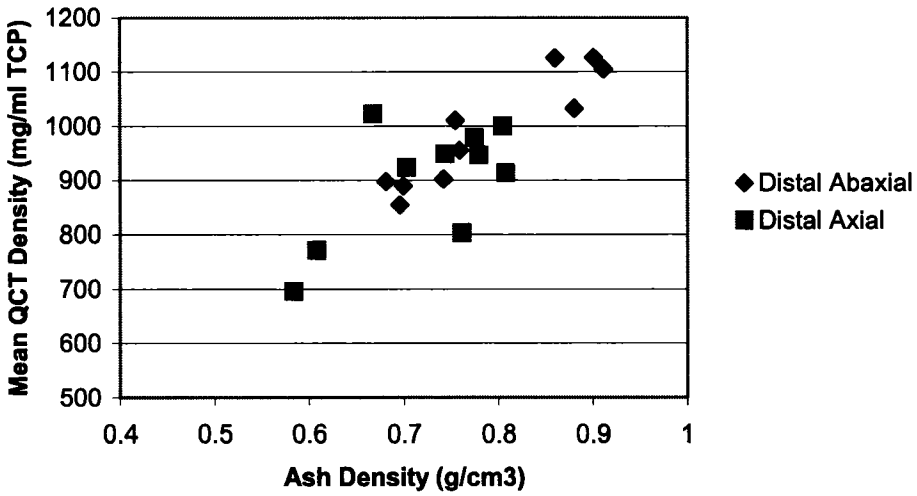

Figure 2.2: Scatter plot of ash density and mean QCT density by side.

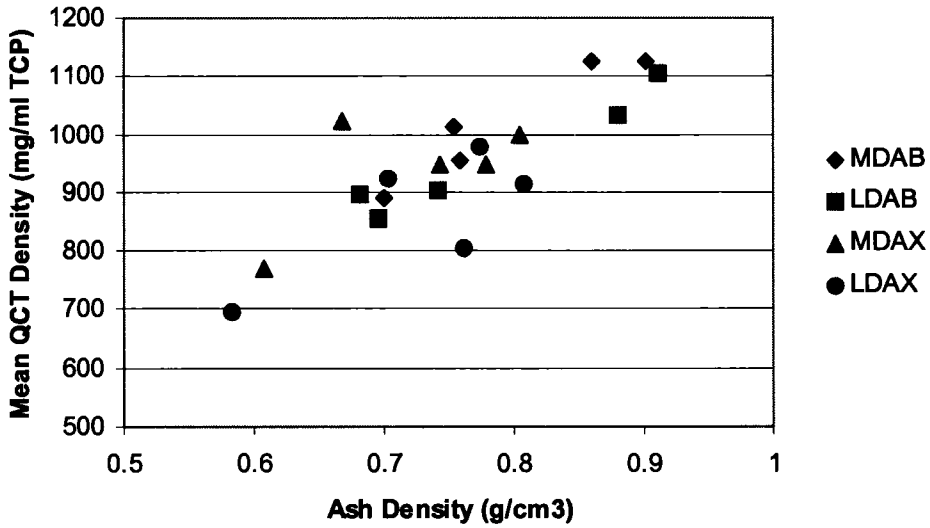

Figure 2.3: Scatter plot of ash density and mean QCT density by ROI site. LDAX=lateral distal axial, LDAB=lateral distal abaxial, MDAX=medial distal axial, MDAB=medial distal abaxial.

Mean Density **Different letters indicate significant differences at α=0.05

Side	Mean +/- SEM
Lateral	910.22 + 38.19
Medial	979.36 + 38.19

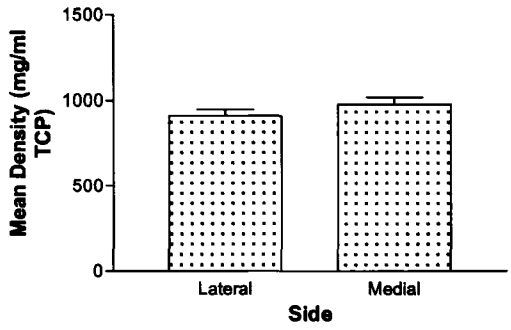

Sector	Mean +/- SEM
Distal Axial	989.55 $\pm$ 37.43[b]
Distal Abaxial	900.02 $\pm$ 37.43[a]

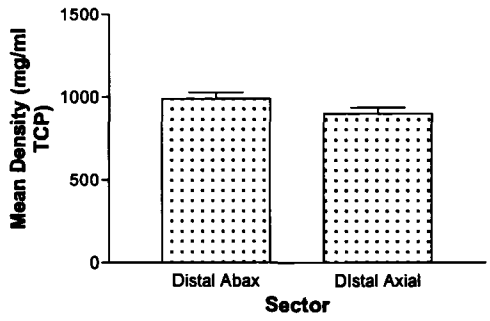

ROI Site	Mean +/- SEM
Lateral Distal Axial	862.54 $\pm$ 47.27
Lateral Distal Abax	957.89 $\pm$ 47.27
Medial Distal Axial	937.50 $\pm$ 47.27
Medial Distal Abax	1021.22 $\pm$ 47.27

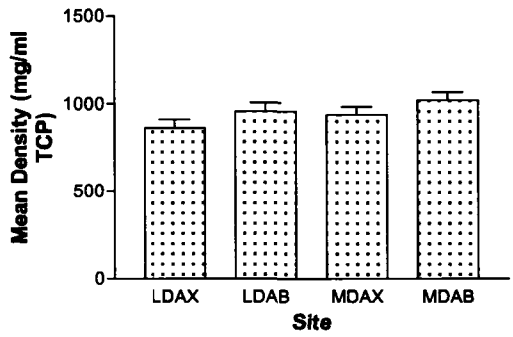

Ash Density **Different letters indicate significant differences at α=0.05

Side	Mean +/- SEM
Lateral	0.7540 + 0.037
Medial	0.7575 + 0.037

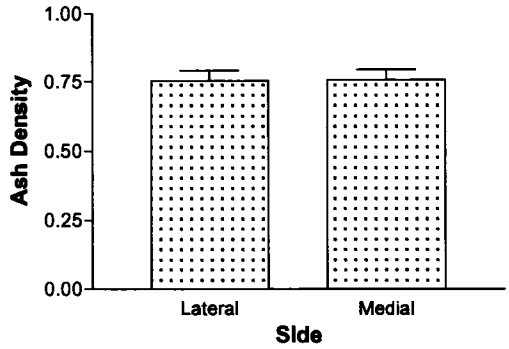

Sector	Mean +/- SEM
Distal Axial	0.7884 $\pm$ 0.36[b]
Distal Abaxial	0.7231 $\pm$ 0.036[a]

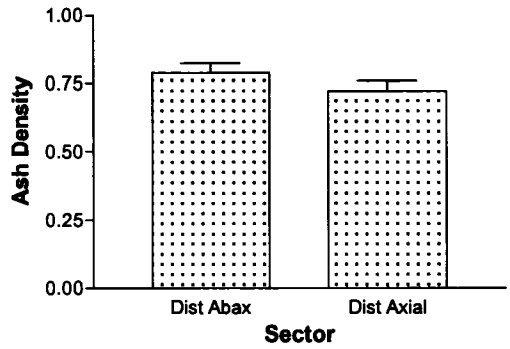

ROI Site	Mean +/- SEM
Lateral Distal Axial	0.7259 $\pm$ 0.04
Lateral Distal Abaxial	0.7821 $\pm$ 0.04
Medial Distal Axial	0.7204 $\pm$ 0.04
Medial Distal Abaxial	0.7947 $\pm$ 0.04

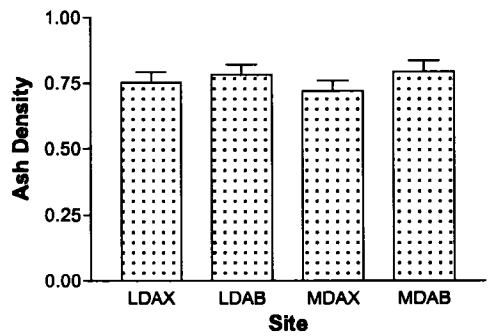

% Mineralization **Different letters indicate significant differences at α=0.05

Side	Mean +/- SEM
Lateral	56.47 + 1.70
Medial	56.56 + 1.70

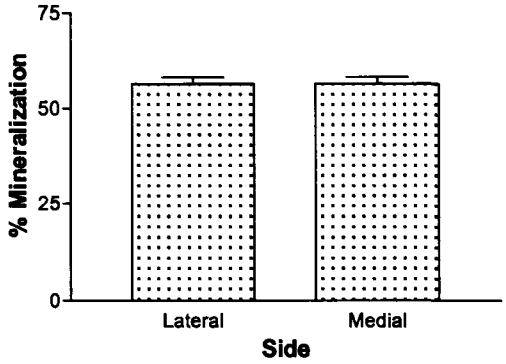

Sector	Mean +/- SEM
Distal Axial	57.90 $\pm$ 1.67[b]
Distal Abaxial	55.13 $\pm$ 1.67[a]

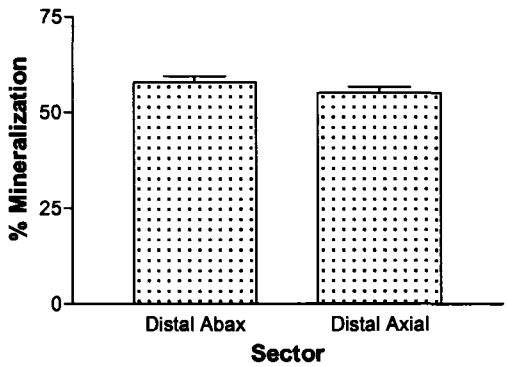

ROI Site	Mean +/- SEM
Lateral Distal Axial	55.08 $\pm$ 1.85
Lateral Distal Abaxial	57.87 $\pm$ 1.85
Medial Distal Axial	55.18 $\pm$ 1.85
Medial Distal Abaxial	57.94 $\pm$ 1.85

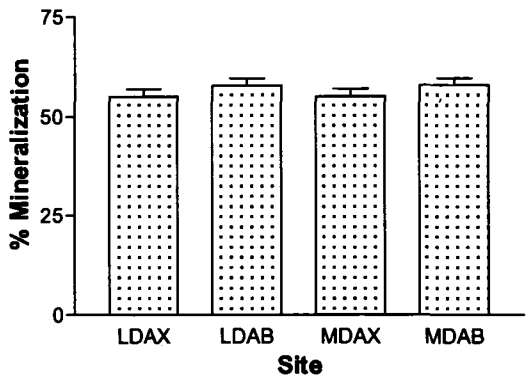

Discussion

Determining the ability of quantitative computed tomography (QCT) to measure subchondral bone density in equine whole bone cadaver specimens is crucial in determining if QCT is a valid diagnostic modality for evaluating equine subchondral bone density in clinical diseases, such as early joint disease in horses. The current study not only evaluated the relationship of QCT subchondral bone mineral density to apparent ash density and percent mineralization, but also evaluated the effect of pre-cutting regions of interests on QCT subchondral bone density and the anatomic variation of percent mineralization and ash density over the surface of the equine third metacarpal bone.

Although there has been a report of good correlations with pre-cut QCT bone density values to apparent ash density[99], it was unknown if this relationship existed with equine subchondral bone and ash density or what effect pre-cutting ROIs might have on correlations. Pre-cutting regions of interest (ROI) into the distal third metacarpal condyle (DMC) would ease placement of ROIs and improve measurement precision on three-dimensionally modeled DMCs used in comparison with ash density. However, the concern was that volume averaging of ROI edge densities would significantly influence measurements of QCT subchondral bone density. We found significantly lower ($p<0.05$) ROI mean

densities in the pre-cut condyle versus the removed condyle. No significant difference ($p<0.25$) was found between the intact and removed condyle ROI mean densities. This finding is meaningful as collaborative research often limits sample acquisition to fresh-frozen removed DMCs rather than intact MCP joints. Interestingly, a significant trend ($p=0.05$) in lower mean ROI densities of pre-cut condyles in comparison to that of intact condyles. Although this level of significance is higher than the pre-cut vs. removed condyles, it is far below the p-value for intact vs. removed condyles. Even though sample size was small, we felt that the differences were significant enough between intact and pre-cut DMC QCT density values to recommend not pre-cutting ROIs prior to sample acquisition for ash analysis or biomechanical testing so as to decrease potential erroneous QCT density measures.

The overall correlation coefficient of ash density to QCT subchondral bone density in this study was high, and fell within the range of previously reported correlations between cortical and trabecular bone[100]. R-values varied depending on condylar location, but were consistent within regions of high or low bone density. QCT subchondral bone density appears to correlate strongly with ash density and percent mineralization even in areas with significantly different densities. Abaxial areas consistently have higher densities of QCT subchondral bone density, ash density and percent mineralization. This trend of abaxial areas having higher subchondral density is in accordance with the natural density distribution found in a normal, incongruously loaded joint. Overall, QCT is a

useful and accurate tool for measuring subchondral bone density in the equine distal third metacarpal condyle from three-dimensionally created models.

Chapter 3

Computed Tomographic Characterization of Subchondral Bone Density between Racing, Treadmill Exercised, and Non-racing Horses

Introduction

A great interest is taken in the diagnosis and prevention of lameness in racehorses since the impact of musculoskeletal injury often involves economic, social and emotional consequences in addition to the pain and suffering of the animals. Musculoskeletal injuries can be devastating and even fatal, and are the most common cause of death, reduced performance and early retirement of racehorses [2, 51, 90-95]. Equine forelimbs bear 60-65% of a horse's weight and 95% of all forelimb lamenesses occur from the carpus distad [59]. Specifically the metacarpophalangeal (MCP) joint is involved in the majority of catastrophic racehorse injuries, and injury can occur in both racing and training [2]. Although a study of Australian Thoroughbreds found that shin soreness was the most common cause of injury over a two-year period, MCP joint problems caused the most weeks rested at pasture from an injury [51].

Repetitive stress to the musculoskeletal system in racehorses occurs at a greater intensity and frequency when compared to horses not in training, and induces the biomechanical changes leading to the unique injuries and lamenesses seen in racehorses, western performance horses, and other disciplines of the equine sport world[59]. In addition, age and breed may also

influence the outcome of the biomechanical changes that occur during intense exercise [87, 109]. Subchondral bone responds to physical loading by increasing in volume, but the point at which this sclerosis is detrimental instead of adaptive is yet to be determined. Sclerotic subchondral bone is also a feature of osteoarthritis[61] and has been associated with degeneration of articular cartilage[16]. Exercise can induce subchondral sclerosis and clinical lameness[86] in horses, but increases in bone density also have a protective effect biomechanically[110]. Increased bone density has been associated with stiffer bone[33], which conversely has been thought to increase fracture susceptibility[111]. This paradoxical relationship may indicate that degenerative joint disease has a different biomechanical etiology than load-induced fractures observed in racing horses, and further research is necessary to investigate this relationship.

Diagnosis of subtle joint injury can prove challenging even for the most skilled clinician. Radiographs are insensitive to changes in bone mineral[112]. Nuclear scintigraphy is extremely sensitive for detection of bony changes but cannot distinguish between stress induced changes and osteochondral damage[62]. Magnetic resonance imaging and computed tomography have been able to detect lesions when traditional diagnostics have failed[52] [66, 113]. Quantitative Computed Tomography (QCT) involves measuring a volume of bone density in a specific area . Whereas Computed Tomographic Osteoabsorptiometry (CTO) is used to map bone density distributions with

specific density ranges assigned to specific colors across an entire joint surface. Although QCT has not been applied to equine joints, it has been a standard practice in human medicine to monitor vertebral bone density for osteoporotic fracture risk[83]. Using CTO, different density distributions were seen in within individual normal joints in humans [6]. In addition, density patterns of athletes and various orthopedic conditions had different patterns of density than normal joints. Thus, it was concluded that CTO could be used to determine the loading history of a joint in humans[85]. Similarly, increased percentage of high bone density was detected in the distal third metacarpal condyle of treadmill-exercised horses in comparison to controls[86]. Although sensitivity of QCT to detect bone mineral changes in horses is unknown, CT remains the best clinical tool to identify early subchondral bone lesions in horses[68].

Thus it seems that QCT and CTO could be applied to equine joints to evaluate changes associated with use, age, breed, and gender to determine how these factors affect subchondral bone density and improve understanding of events early in joint disease. We hypothesize that a certain level of bone density is associated with pathologic changes in equine joints and that Quantitative Computed Tomography can be used to characterize bone density indicative of joint pathology.

The first aim of this study is to determine if there are significant differences in mean density or density variation between racing, exercised, and non-racing horses. The second aim is to determine if there are specific areas of the third

metacarpal condyle that have significantly different mean densities or density variation between racing, exercised, and non-racing horses. The third aim is to determine if mean density or density variation can predict gross pathologic damage. The last aim is to determine if there are visible differences in CTO maps between racing, exercised, and non-racing horses.

Materials and Methods

Sample Population

167 metacarpophalangeal (MCP) joint cadaver scans were performed over a five-year period from 1999-2004 on a total of 122 horses. Horses were classified into groups as racing, exercised, or non-racing. Racing horse MCPs were obtained from the Colorado Racehorse Necropsy program where racehorses that were euthanized or died for any reason at a Colorado racetrack were brought to the Colorado State University Veterinary Medical Center (CSU-VMC) for a survey musculoskeletal necropsy. The exercised group MCPs were obtained from 2-5 year old horses that were part of research projects where prescribed exercise was used to study osteoarthritis in a carpal joint chip model. Non-racing horse MCPs were obtained from the CSU-VMC routine necropsy service, and were euthanized for reasons other than musculoskeletal disease of the forelimbs. Non-racing horses had no CSU-VMC record of lip tattoos or previous history of race training. Draft horses, ponies and mules were excluded from the study.

CT Scans

MCP joint scans from 1999-2000 (65 scans) were performed on a GE Pace CT scanner[g] using a bone algorithm at 140 kVP with a slice thickness of 1-mm, field of view 184 mm, and a 512x512 pixel matrix which creates a 0.359mm spatial resolution. Scans from 2002-2004 (102 scans) were performed on a Picker PQ CT[a] using a bone algorithm at 140 kVP with a slice thickness of 1.5-mm, 180mm field of view, and a 512x512 pixel matrix which creates a 0.352mm spatial resolution. CT studies were exported for analysis to the customized image analysis program OsteoApp[e] that was created using the Interactive Design Language[d]. Additionally, a portion of the CT scans were scanned with a calibration phantom. However, there were 48 scans performed without a calibration phantom, 69 scans performed with a liquid K_2HPO_4 phantom[l], 29 scans performed with a solid tri-calcium phosphate (TCP) phantom[b], and 22 scans performed with both phantoms.

QCT modeling

Three-dimensional modeling of the distal third metacarpal condyle CT scans was performed using OsteoApp [d,e]. A voxel threshold of 500 Hounsfield Units was used to isolate the distal third metacarpal bone for rendering into a three-dimensional model (Appendix 1). If any extraneous bone from the proximal

phalanx or proximal sesamoid bones fell within this ROI threshold, the unwanted areas were manually removed. Mean density was measured to a depth of 3-mm, perpendicular to the distal surface of the third metacarpal condyle as a study of site-dependent subchondral bone variation of the equine third metacarpal found the thickness of radiographically apparent subchondral bone to be between 2-3 mm[114]. Additionally, measuring to a depth of 3-mm reduced potential partial voxel effects caused by the difference in slice thickness between CT scanners. Since CT scan slice thicknesses were 1-mm or 1.5-mm, voxel depth was then either 1-mm or 1.5-mm. OsteoApp measures to an exact depth from the first voxel encountered. Thus, in 1-mm thick scans three voxels were included and in 1.5-mm thick scans two voxels were included in the 3D model. If a measurement depth of 2-mm were selected, OsteoApp would have to estimate the density in ½ of the second voxel in the 1.5-mm thick scans potentially introducing additional error. Even with this strategy, the models were still affected by partial voxel artifacts as any thresholded model is subject to partial voxel artifacts. Models were measured in mean Hounsfield Units (HU), rather than calibrating to a solid density phantom. This occurred because over the study period, there were some scans without a phantom, and two different phantoms with two different scanners.

Mean voxel standard deviation (MVSD) was measured by taking the standard deviation of the mean density within the ROI. Thus, all voxel values were taken into account when calculating the MVSD, and it is a representation of

the actual variation in bone density within the ROI. MVSD was also measured to a depth of 3-mm in HU.

Since previous work has shown anatomic differences in subchondral density across joint surfaces[6, 85], [86, 115] eight individual areas were also measured for mean and standard deviation. Regional 1cm^2 ROIs were placed in the dorsal axial/abaxial, palmar axial/abaxial of the medial and lateral aspects of the distal condyle (Figure 3.1). Density maps were also created to examine subchondral density patterns across the entire joint surface (Figure 3.2a). This was done by applying colors to the individual density ranges (Figure 3.2b). Maps were created to a depth of 3-mm in accordance with the mean density analysis. Visual assessment for trends in density patterns was performed to determine if density patterns exist, to describe these density patterns, and if a particular group is represented by a specific pattern.

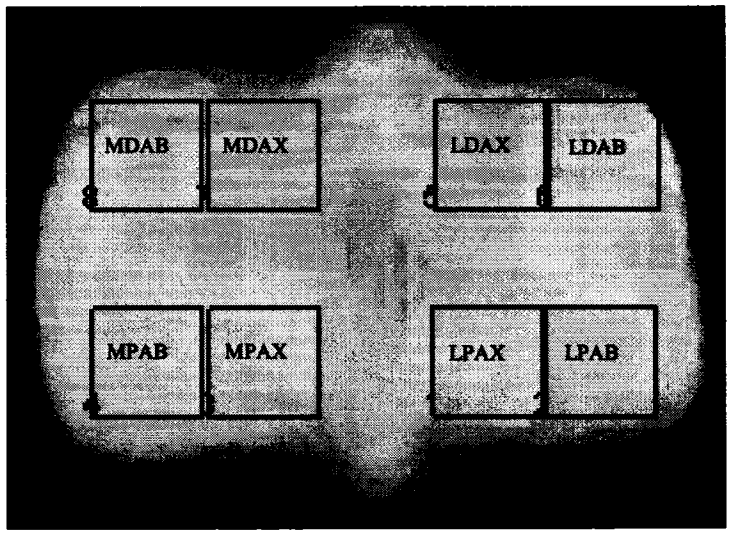

Figure 3.1: Three-dimensional model of the distal third metacarpal condyle with eight 1-cm^2 regions of interest. MDAB = medial dorsal abaxial, MDAX = medial dorsal, axial, MPAB = medial palmar abaxial, MPAX = medial palmar axial, LDAB = lateral dorsal abaxial, LDAX = lateral dorsal axial, LPAB = lateral palmar abaxial, LPAX = lateral palmar axial.

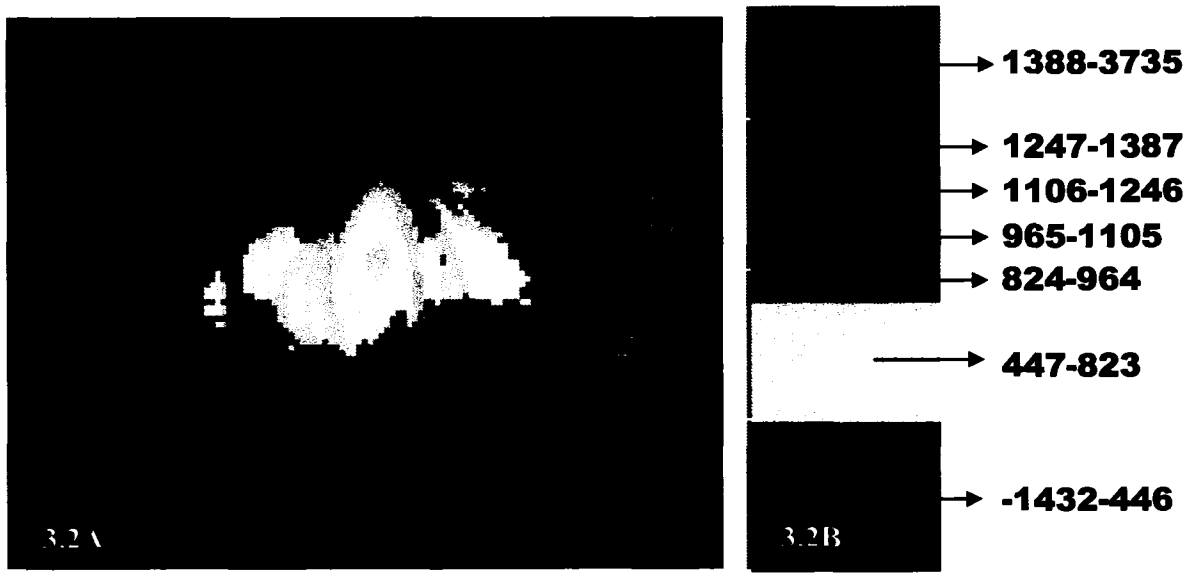

Figures 3.2A & B: Figure 3.2A is an example of the density color map applied to the distal third metacarpal condyle to assess pattern distribution. Each color corresponds to a specific density range in mg/ml tri-calcium phosphate.

Gross Pathologic Evaluation

MCP joints were disarticulated after CT scanning and the distal third metacarpal condyle (MCIII) scored for gross pathologic changes (Figure 3.3). If gross pathologic changes existed, the distal MCIII was photographed for reference, and removed with a band saw approximately 3 cm proximal to the medial condylar surface. The condyles were either wrapped in physiologic buffered saline soaked gauze and frozen at –20 C until further processing or placed in 10% formalin for use in histologic preparations.

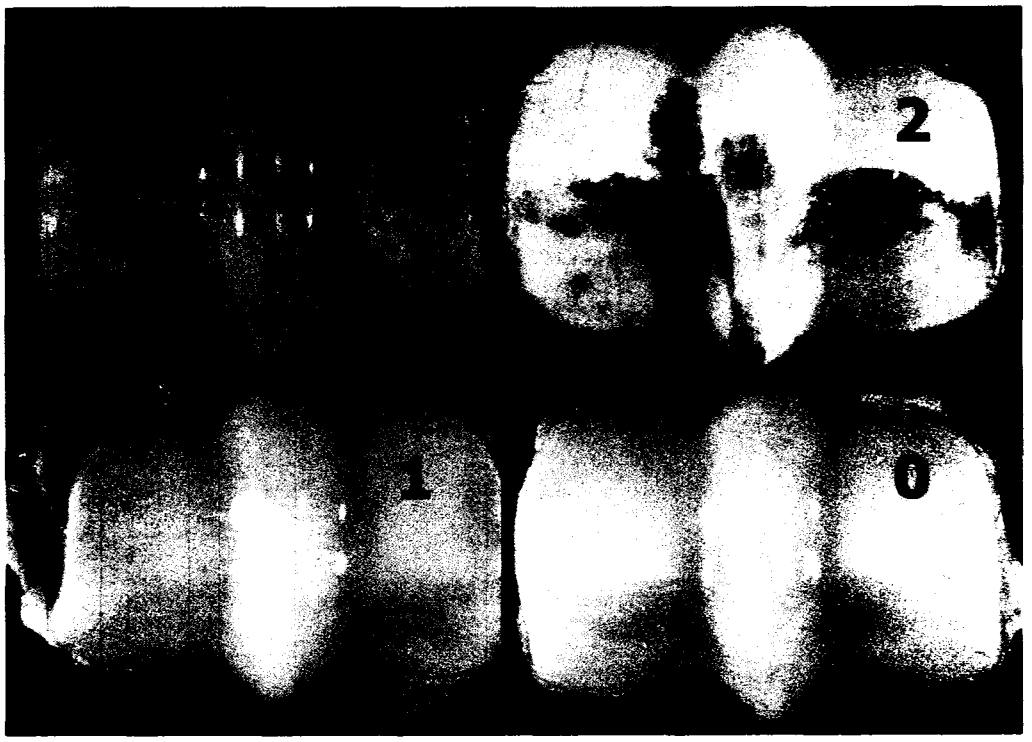

Gross Score	Description
0	No visible abnormalities or changes in cartilage or bone
1	Minimal scoring with fibrillation of cartilage
2	Mild erosion, small pits and/or more prominent fibrillation
3	Similar changes as above, but additionally focal divots or indentations of cartilage with/without focal cartilage opacities, and partial to full-thickness erosions in small (4-8mm) areas.
4	Extensive degeneration, erosion, and ulceration of cartilage with some exposure and/or loss of underlying bone, generally involving a large area (1cm or greater). **Note-only one grade 4 leasion was observed and photographed poorly

Statistical Analysis

In determining the best fitting model of mean density regressed on age without any adjustments for other factors (breed, gender, or use); a logarithmic transformation of age was a slightly better fit (R^2=0.249 age, R^2=0.357 log age). Additionally, an alternate, non-linear piecewise regression model of age against mean density was created that modeled a quadratic regression equation to age

48 months and a linear regression equation for ages > 48 months. R^2= 0.363 for this model, which although it is a slightly better fit than the simple logarithmic regression, would not account for random variation from each horse. Age versus gross score and mean voxel standard deviation were graphed to determine if a linear or logarithmic function was a better fit. In each case, the logarithmic transformation of age was a better fit, so a logarithmic term for age was selected for all statistical models.

A mixed-model analysis was performed to determine the effects of age, breed, limb, gender and group on mean surface density and mean voxel standard deviation. Horse was considered a random effect and was nested within breed, gender and group. A second mixed-model analysis was done to determine the effects of age, breed, gender, group, mean density, and mean voxel standard deviation on gross pathologic score. Again, horse was considered a random effect and was nested within breed, gender and group. Also, because not all breeds existed within each group, for example there were only Quarter horses and Thoroughbreds in the racing group, the original mixed-model analysis was reanalyzed with a combined group*breed term to further explore possible breed influences within and across groups.

The coefficient of variation (CV) for overall surface area measured (mm^2) was calculated. If a significant variance was present (CV>5%), another mixed model analysis of surface area was performed with the same model selection

protocol as mean density and mean voxel standard deviation (MVSD). The basis being first to determine if area measured is consistent between all horses, and if significant variation exists then determination if horse level factors are influencing area rather than user or program error.

For analysis by regional areas of interest, additional classification variables were added for palmar or dorsal ROI sites, medial or lateral ROI sites, and axial or abaxial ROI sites. These three regional classification terms in addition to effects of age, breed, gender, limb and group with the random effect of horse was nested within breed, gender, group, or group*breed were used to analyze mean density and standard deviation. Again, age, breed, gender, limb, medial or lateral sites, axial or abaxial sites, group or group*breed were analyzed as predictors of gross score. However, only palmar ROI site densities were included because gross pathologic scores only represent changes in the palmar aspect of the distal third metacarpal bone. Additionally, coefficient of variation was calculated for individual ROI area to determine the variability of measurement and potential user error, and if significantly high variation existed (CV>5%), a mixed model analysis was performed as described above to determine horse level factor influences on ROI area.

Effects were considered significant at $\alpha<0.05$, and effects at $\alpha<0.10$ were considered a trend in the data. Effects with p-values >0.10 were removed in order to maximize model fit. Full-order interaction terms were added for

significant fixed effects. Backwards selection of interaction terms was used with an inclusion $\alpha<0.10$. Fisher's least significant differences (LSD) were computed for model terms and interactions with p-values <0.10. However, only differences with p-values <0.05 were reported as significant. Residual versus predicted means were plotted and evaluated for normality of the final fitted model.

Furthermore, because there were many different scanner-phantom combinations, and a single unit for mean density and MVSD analysis was desirable an analysis of scanner and phantom variations were performed. A paired t-test for each density equivalent (0, 50, 100, or 200 mg/ml K_2HPO_4) of the liquid phantom was performed between the Picker and GE scanners. Coefficients of variation for each density equivalent by scanner were also calculated. Also, a regression of Hounsfield Units (HU) and K_2HPO_4 mg/ml was performed and differences in slopes and intercepts compared between scanners to evaluate how calibration equations could differ due to scanner variance. Moreover, to determine how well HU represented true density measures (apparent ash density), the data from Chapter 2 was used to compare a correlations apparent ash density and HU or TCP mg/ml.

Results

48 of the horses were racing horses with 38/48 horses having bilateral MCP scans, and ranged in age from 24 to 138 months. 28 of the horses were exercised horses with 4/28 horses having bilateral MCP scans, and ranged in

age fr7om 24 to 51 months. 46 of the horses were non-racing horses with left MCP scans, and ranged in age from 24 to 250 months. Breed breakdown is as follows: 43 Quarter Horses (14 racing, 26 non-racing, 3 exercised), 36 Thoroughbreds (34 racing, 0 exercised, 2 non-racing), and 43 all other breeds (0 racing, 25 exercised, 18 non-racing). Gender was classified as either male or female, with 75 males (32 racing, 21 exercised, 22 non-racing) and 47 females (16 racing, 9 exercised, 22 non-racing).

The following table lists the different phantom-scanner combinations for each CT scan of the racing, exercised and non-racing groups.

Scanner-Phantom Combination	Racing	Exercised	Non-Racing
None GE	8	8	32
K_2HPO_4 GE	3	5	10
K_2HPO_4 Picker	46	22**	5
TCP Picker	28	22**	0

**Denotes metacarpophalangeal joints scanned with both phantoms

Means were significantly different between GE and Picker for K_2HPO_4 0 mg/ml (p=0.0002, 95% CI {2.58, 7.56}) and K_2HPO_4 50 mg/ml (p=0.0025, 95% CI {1.83, 7.87}), but not significantly different for K_2HPO_4 100 mg/ml (p=0.31, 95% CI {-2.04, 6.32}) and K_2HPO_4 200 mg/ml (p=0.49, 95% CI {-5.64, 2.77}). The

slopes were not significantly different between GE and Picker scans ($p=0.24$, power=0.38), but intercepts were significantly different ($p<0.001$, power=0.99). The r-value for TCP correlated with ash density was $r=0.82$ and for HU correlated with ash density was $r=0.81$. The following table lists the coefficients of variance for each K_2HPO_4 density equivalent by scanner.

Scanner	0 mg/ml K_2HPO_4	50 mg/ml K_2HPO_4	100 mg/ml K_2HPO_4	200 mg/ml K_2HPO_4
GE	0.72	0.05	0.05	0.03
Picker	0.51	0.09	0.07	0.03

Surface Analysis-Mean Density and Mean Voxel Standard Deviation (MVSD)

In the full first-order model, gender was not significant for either mean density ($p=0.46$) or MVSD ($p=0.58$). Group was significant for mean density ($p<0.05$) and standard deviation ($p<0.001$). Age was significant for both mean density ($p<0.0001$) and MVSD ($p<0.0001$). Breed was not significant for mean density ($p=0.57$), but was significant for MVSD ($p<0.05$). Limb was not significant for mean density ($p=0.98$) or MVSD ($p=0.67$). Age*Group was not significant ($p=0.10$) for mean density, so pairwise comparisons for group were performed in the first order model.

Again, since not all breeds occurred in every group, breed and group were removed from the model and the term group*breed was added instead. The new

group*breed term was significant for mean density ($p<0.01$), and all other terms were non-significant ($p>0.10$) except age ($p<0.01$). The interaction of group*breed and age was highly significant ($p<0.001$). Pairwise comparisons for group*breed were performed with the interaction in the model. Group*breed was also significant for MVSD ($p<0.01$), and all other terms were non-significant ($p>0.10$) except age ($p<0.03$). There was a trend for the age by group*breed interaction for MVSD ($p<0.10$), so pairwise comparisons were done with the interaction in the model. Residuals plots of both models appeared normal.

Racehorses did not have significantly different mean densities than exercised horses ($p=0.28$), and were significantly lower than mean densities of non-racing horses ($p<0.0001$). Non-racing horses also had significantly higher mean densities than exercised horses ($p<0.05$). For group*breed differences in mean density, non-racing other breeds were significantly higher than exercised other breeds ($p<0.05$). Non-racing Quarter horses had higher mean densities than racing Quarter Horses ($p<0.02$), and exercised other breeds ($p<0.03$). Exercised Quarter horses had higher mean densities than non-racing Quarter Horses ($p<0.01$), racing Quarter Horses ($p<0.001$), racing Thoroughbreds ($p<0.001$), non-racing other breeds ($p<0.01$), and exercised other breeds ($p<0.001$). Racing Thoroughbreds had significantly lower mean densities than non-racing other breeds ($p<0.001$) and non-racing Quarter Horses. All other differences were non-significant, including no significant difference in mean density between racing Quarter Horses and racing Thoroughbreds.

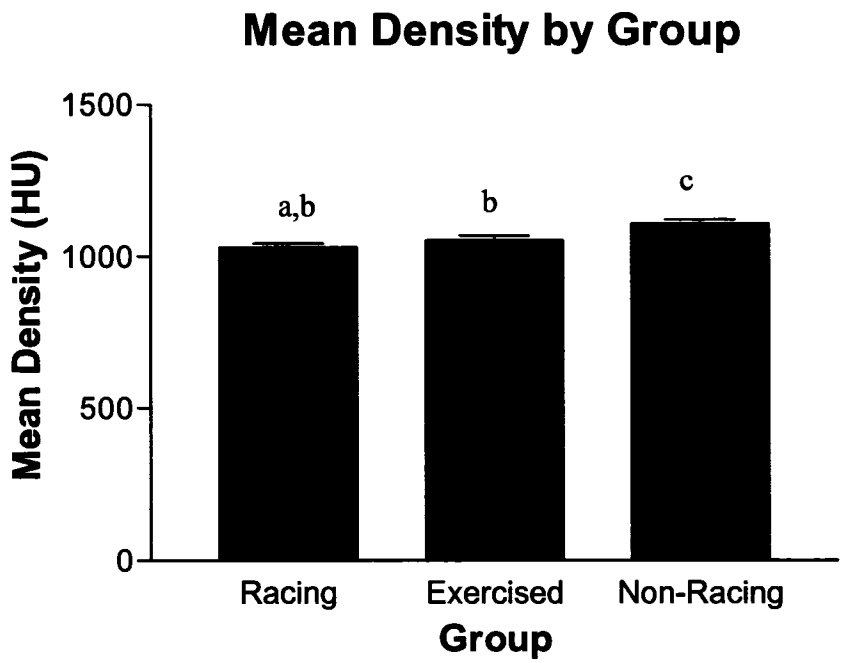

Figure 3.4: Mean density by group. Error bars represent one standard error of the mean. Different letters represent significant differences at α=0.05.

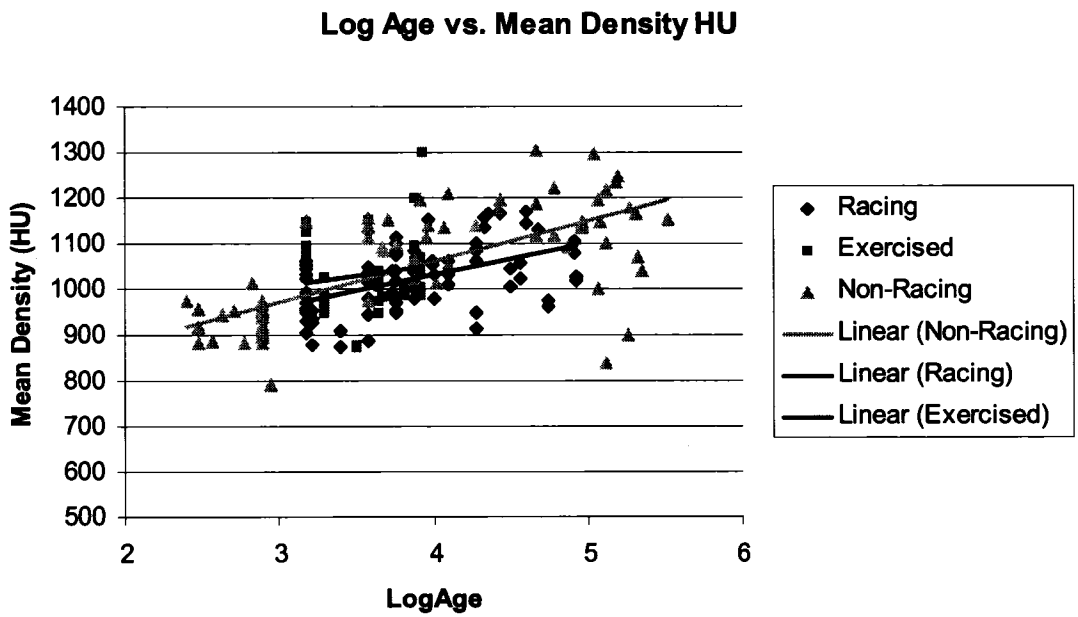

Figure 3.5: Scatter plot of mean density by group and age. Again, racing and exercised horses had significantly lower mean densities than non-racing horses

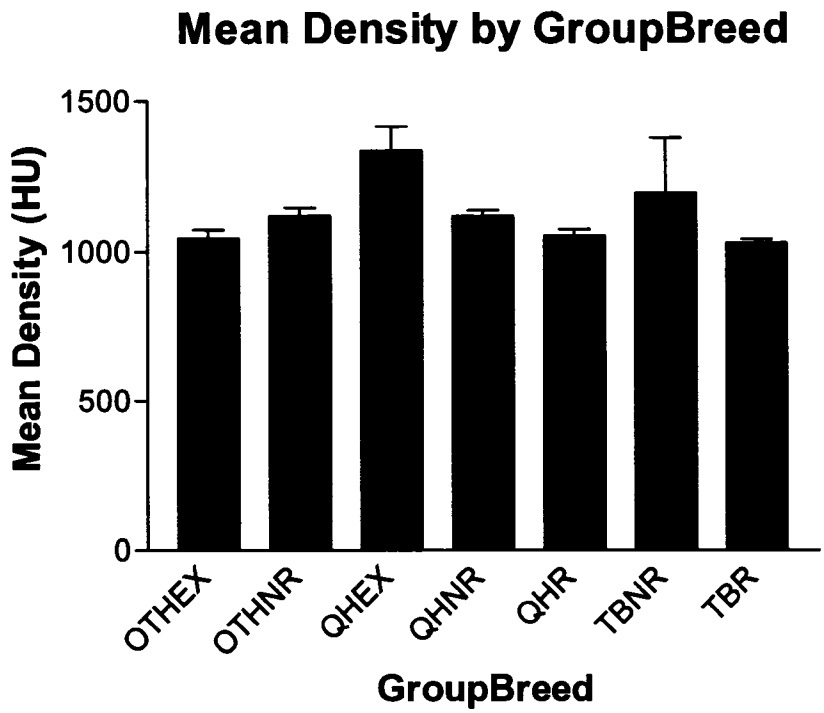

Figure 3.6: Mean density by group and breed. Error bars represent one standard error of the mean.

Thoroughbreds had significantly higher MVSD than Quarter Horses ($p<0.001$) and other breeds ($p<0.003$). There was no significant difference in MVSD between Quarter Horses and other breeds ($p=0.48$). Significantly higher group*breed MVSD differences existed for racing Thoroughbreds compared to non-racing other breeds ($p<0.05$), exercised other breeds ($p<0.01$) non-racing Quarter horses ($p<0.05$), exercised Quarter horses ($p<0.01$), and racing Quarter horses ($p<0.001$). No other comparisons were significant.

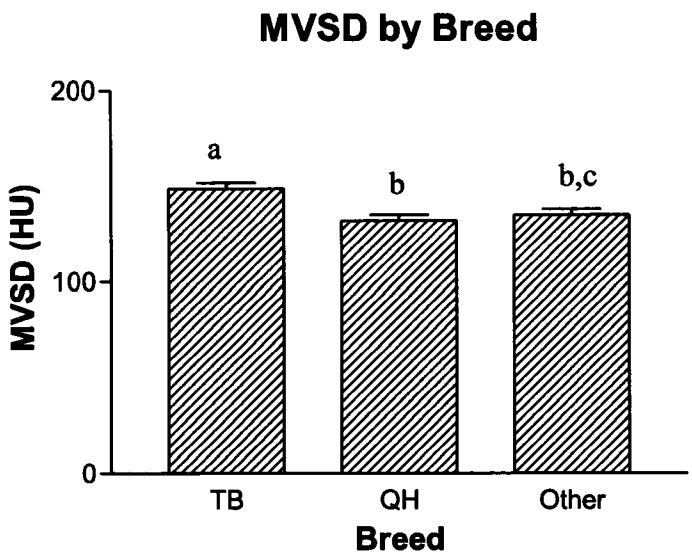

Figure 3.7: Mean voxel standard deviation by breed. Error bars represent one standard error of the mean. Different letters represent significant differences at α=0.05.

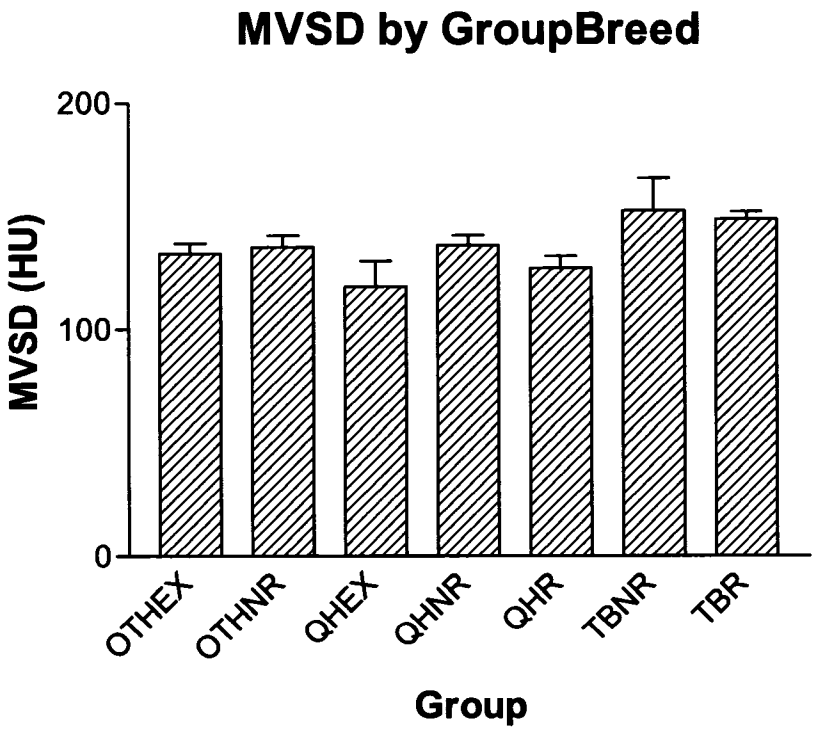

Figure 3.8: Mean voxel standard deviation by group and breed. Error bars represent one standard error of the mean.

With gross score analyzed as the response variable, only group*breed ($p<0.01$) and log age ($p<0.0001$) were significant, but there was a trend for group ($p<0.10$). However, the interaction between age and group was significant ($p<0.05$), but the interaction between age and group*breed was not significant ($p=0.19$). Racehorses had higher gross scores than exercised ($p<0.002$) and non-racing ($p<0.001$). There was no significant difference in gross scores between non-racing and exercised horses ($p=0.39$). Racing Thoroughbreds had higher gross scores than non-racing other breeds ($p<0.001$), exercised other breeds ($p<0.03$), non-racing Quarter Horses ($p<0.01$), and non-racing Thoroughbreds ($p<0.03$). Racing Quarter Horses had significantly higher gross scores than non-racing other breeds ($p<0.03$) only. All other comparisons were non-significant ($p>0.05$).

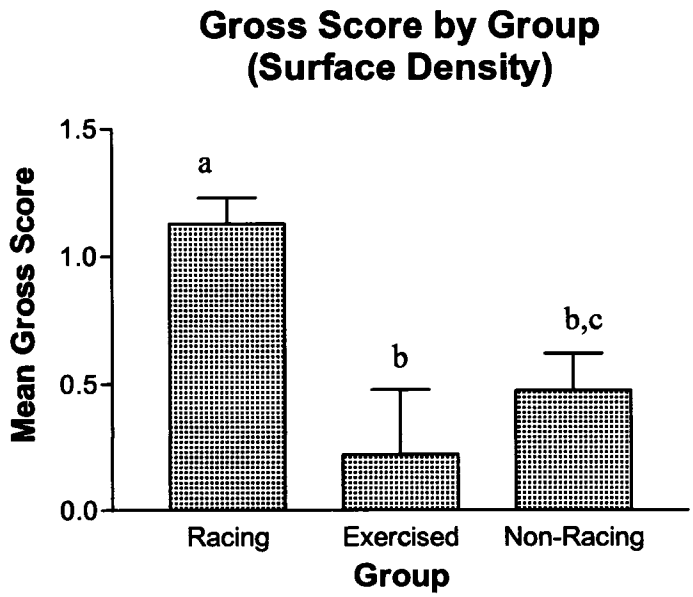

Figure 3.9: Gross score by group. Error bars represent one standard error of the mean. Different letters represent significant differences at α=0.05.

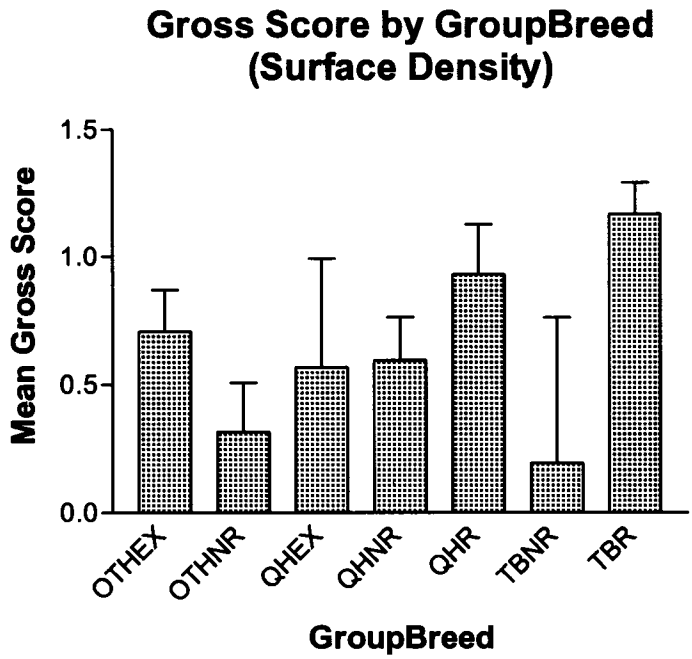

Figure 3.10: Gross score by group and breed. Error bars represent one standard error of the mean. Different letters represent significant differences at α=0.05.

Analysis of ROI Mean Density and Mean Voxel Standard Deviation

In the first order model, age ($p<0.001$), dorsal/palmar sites ($p<0.0001$), medial/lateral sites ($p<0.05$), axial/abaxial sites ($p<0.0001$), and group ($p<0.0001$) were all significant for mean density. Limb ($p=0.67$), breed ($p=0.92$) and gender ($p=063$) were not significant for mean density. The five-way interaction of significant terms was not significant ($p=0.98$). The four-way

interaction between group, dorsal/palmar sites, medial/lateral sites and axial abaxial site was significant ($p<0.006$), and the interaction between age, dorsal/palmar sites, medial/lateral sites and axial abaxial sites was significant ($p<0.05$). In the first order model with group*breed as a term, age ($p<0.0001$), dorsal/palmar sites ($p<0.0001$), medial/lateral sites ($p<0.04$), axial/abaxial sites ($p<0.0001$), and group*breed ($p<0.0001$) were all significant for mean density. Limb ($p=0.68$) and gender ($p=0.82$) were still not significant for mean density. The five-way interaction of significant terms was not significant ($p=0.72$). A four-way interaction between group* breed, dorsal/palmar sites, medial/lateral sites, and axial/abaxial sites was significant ($p<0.05$), and the interaction between age, dorsal/palmar sites, medial/lateral sites and axial abaxial sites was significant ($p<0.05$). Multiple significant differences existed and are by ROI site within groups and breeds listed in Figures 3.11-3.38.

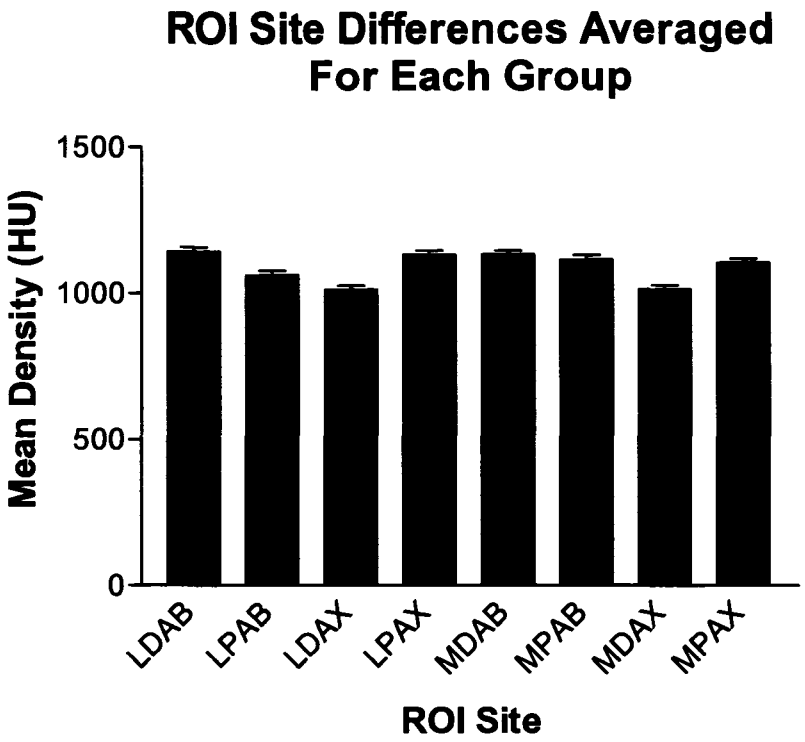

Figure 3.11 : Least significant differences and p-values for each ROI site averaged over all groups

Location	LSD	P-Value
LDAB-LDAX	128.68	<0.0001
LDAB-LPAB	79.39	<0.0001
LDAB-MDAB	9.80	0.38
LDAX-LPAX	-118.40	0.0002
LDAX-MDAX	-2.19	0.85
LPAB-LPAX	-69.22	<0.0001
LPAB-MPAB	-52.50	0.0001
LPAX-MPAX	25.96	0.02
MDAB-MDAX	116.69	<0.0001
MDAB-MPAB	17.10	0.13
MDAX-MPAX	-90.26	<0.0001
MPAB-MPAX	9.33	0.41

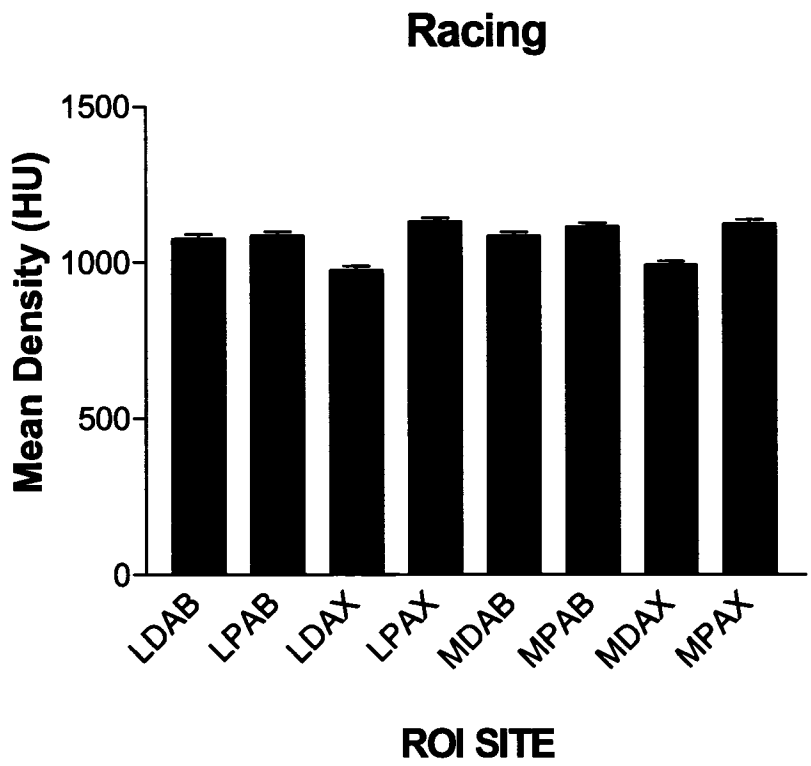

Figure 3.12: Least significant differences and p-values for each ROI site within racing horses

LOCATION	LSD	P-VALUE
LDAB-LDAX	102.13	< 0.0001
LDAB-LPAB	-9.73	0.31
LDAB-MDAB	-7.84	0.41
LDAX-LPAX	-155.41	< 0.0001
LDAX-MDAX	-16.80	0.08
LPAB-LPAX	-43.54	< 0.0001
LPAB-MPAB	-27.52	0.004
LPAX-MPAX	7.10	0.46
MDAB-MDAX	93.18	< 0.0001
MDAB-MPAB	-93.03	< 0.0001
MDAX-MPAX	-131.51	< 0.0001
MPAB-MPAX	-8.92	0.35

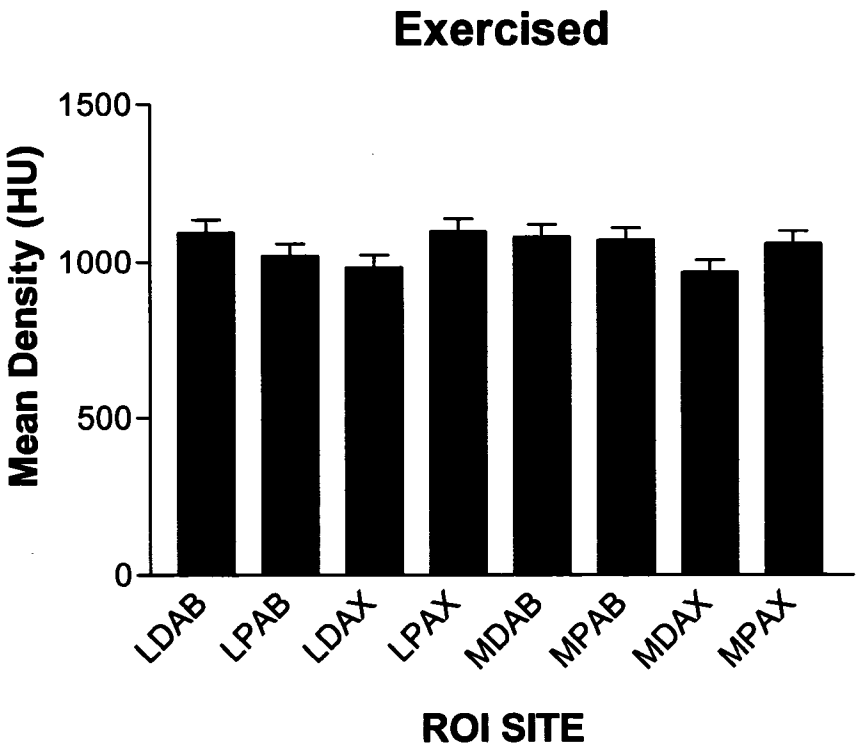

Figure 3.13: Least significant differences and p-values for each ROI site within exercised horses

LOCATION	LSD	P-VALUE
LDAB-LDAX	111.05	0.0002
LDAB-LPAB	75.15	0.01
LDAB-MDAB	14.28	0.64
LDAX-LPAX	-115.39	0.0001
LDAX-MDAX	16.73	0.58
LPAB-LPAX	-79.50	0.008
LPAB-MPAB	-49.80	0.10
LPAX-MPAX	38.91	0.20
MDAB-MDAX	113.49	0.0002
MDAB-MPAB	11.06	0.71
MDAX-MPAX	-93.21	0.002
MPAB-MPAX	9.21	0.76

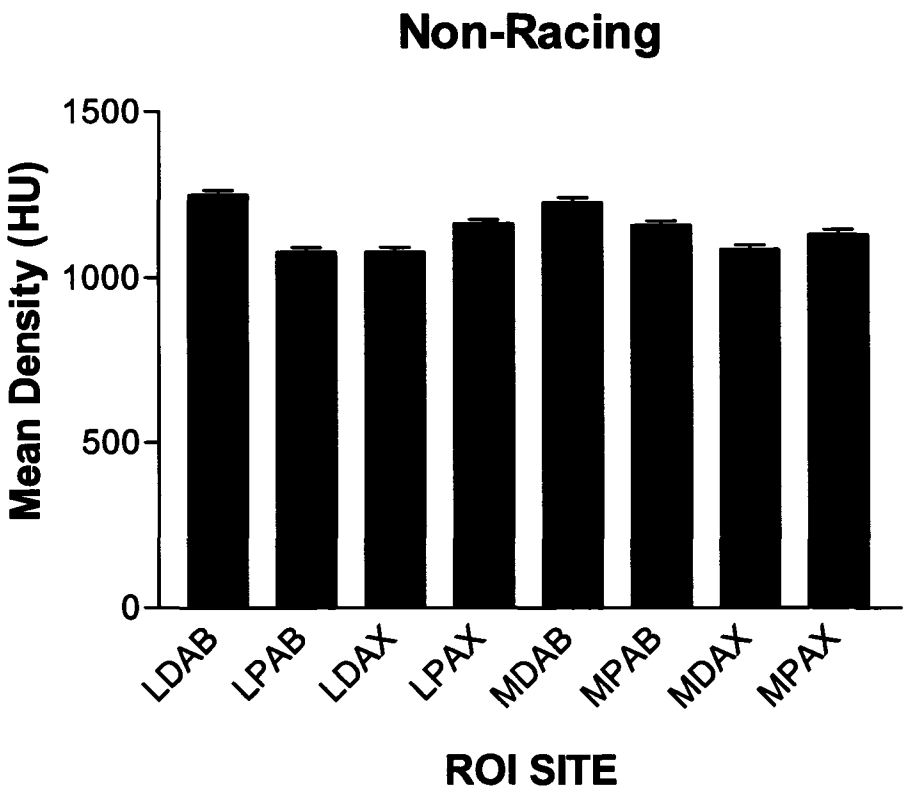

Figure 3.14: Least significant differences and p-values for each ROI site within non-racing horses

LOCATION	LSD	P-VALUE
LDAB-LDAX	172.86	< 0.0001
LDAB-LPAB	172.78	<0.0001
LDAB-MDAB	22.98	0.05
LDAX-MDAX	-6.49	0.59
LDAX-LPAX	-84.41	<0.0001
LPAB-LPAX	-84.33	< 0.0001
LPAB-MPAB	-80.17	<0.0001
LPAX-MPAX	31.87	0.007
MDAB-MDAX	143.18	< 0.0001
MDAB-MPAB	69.65	< 0.0001
MDAX-MPAX	-46.05	0.0001
MPAB-MPAX	27.70	0.02

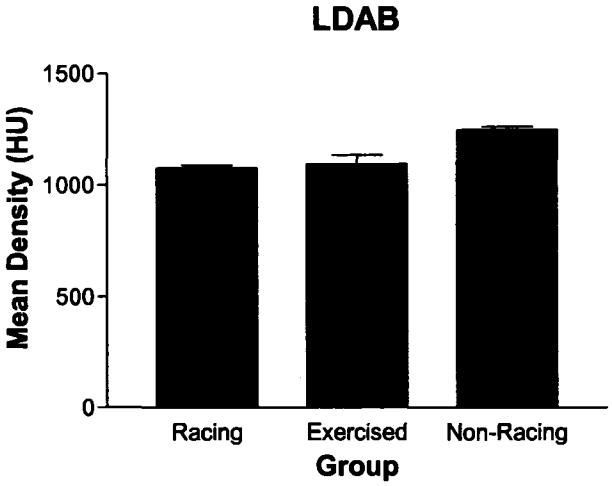

Figure 3.15: Group differences at lateral dorsal abaxial sites

LDAB	LSD	P-Value
RACE-EX	-16.78	0.69
RACE-NR	-174.92	<0.0001
EX-NR	-158.14	0.0002

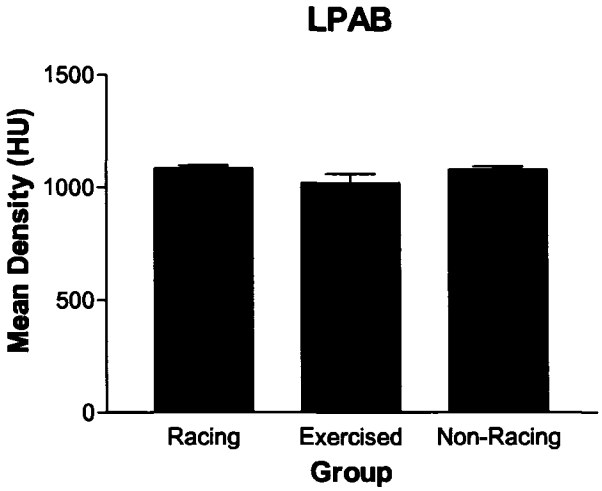

Figure 3.16: Group differences at lateral palmar axial sites

LPAB	LSD	P-Value
RACE-EX	68.10	0.11
RACE-NR	7.60	0.68
EX-NR	-60.51	0.15

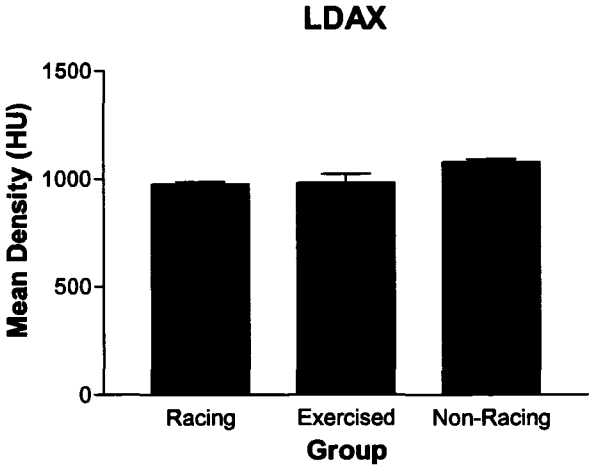

Figure 3.17: Group differences at lateral dorsal axial sites

LDAX	LSD	P-Value
RACE-EX	-7.87	0.85
RACE-NR	-104.20	<0.0001
EX-NR	-115.39	0.0001

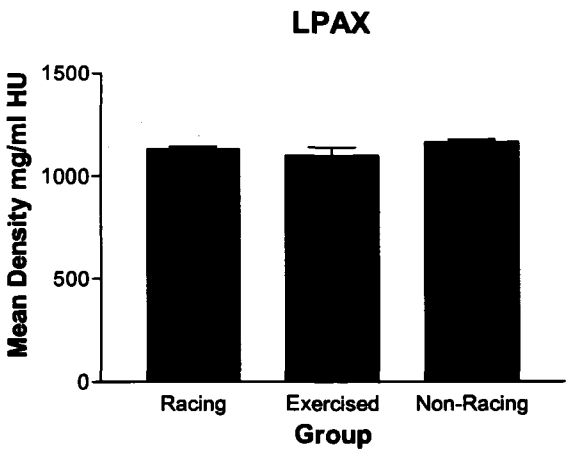

Figure 3.18: Group differences at lateral palmar abaxial sites

LPAX	LSD	P-Value
RACE-EX	32.15	0.44
RACE-NR	-33.20	0.07
EX-NR	-65.34	0.12

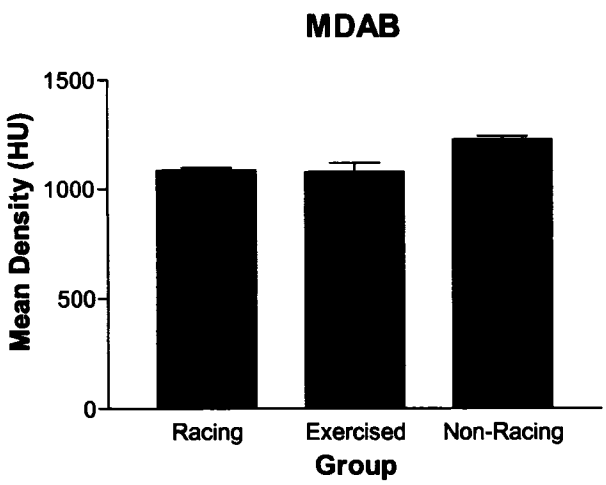

Figure 3.19: Group differences at medial dorsal abaxial sites

MDAB	LSD	P-Value
RACE-EX	5.35	0.90
RACE-NR	-144.10	<0.0001
EX-NR	-149.45	0.005

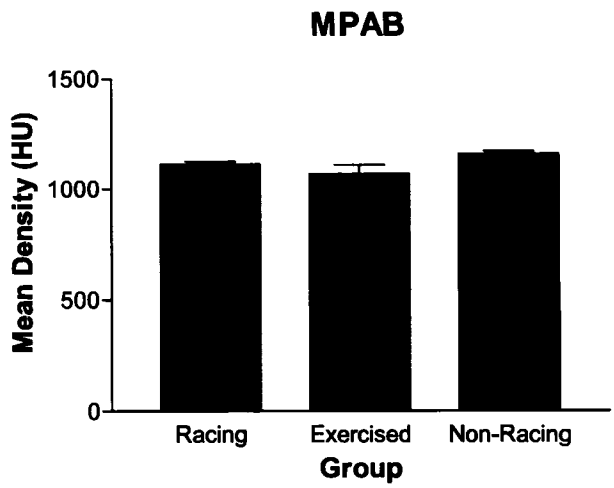

Figure 3.20: Group differences at medial palmar abaxial sites

MPAB	LSD	P-Value
RACE-EX	45.82	0.28
RACE-NR	-45.06	0.02
EX-NR	-90.67	0.03

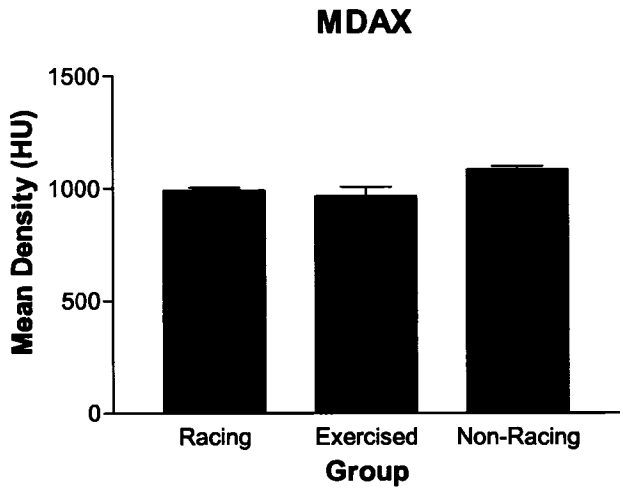

Figure 3.21: Group differences at medial dorsal axial sites

MDAX	LSD	P-Value
RACE-EX	25.66	0.54
RACE-NR	-93.89	<0/0001
EX-NR	-119.55	0.0049

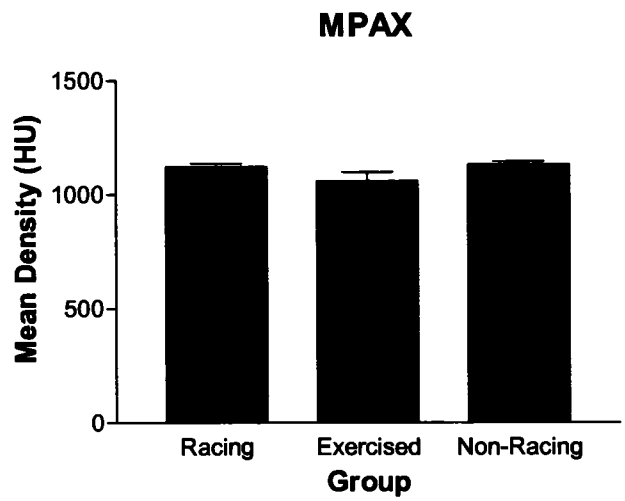

Figure 3.22: Group differences at medial palmar axial sites

MPAX	LSD	P-Value
RACE-EX	63.95	0.13
RACE-NR	-8.43	0.65
EX-NR	-72.38	0.09

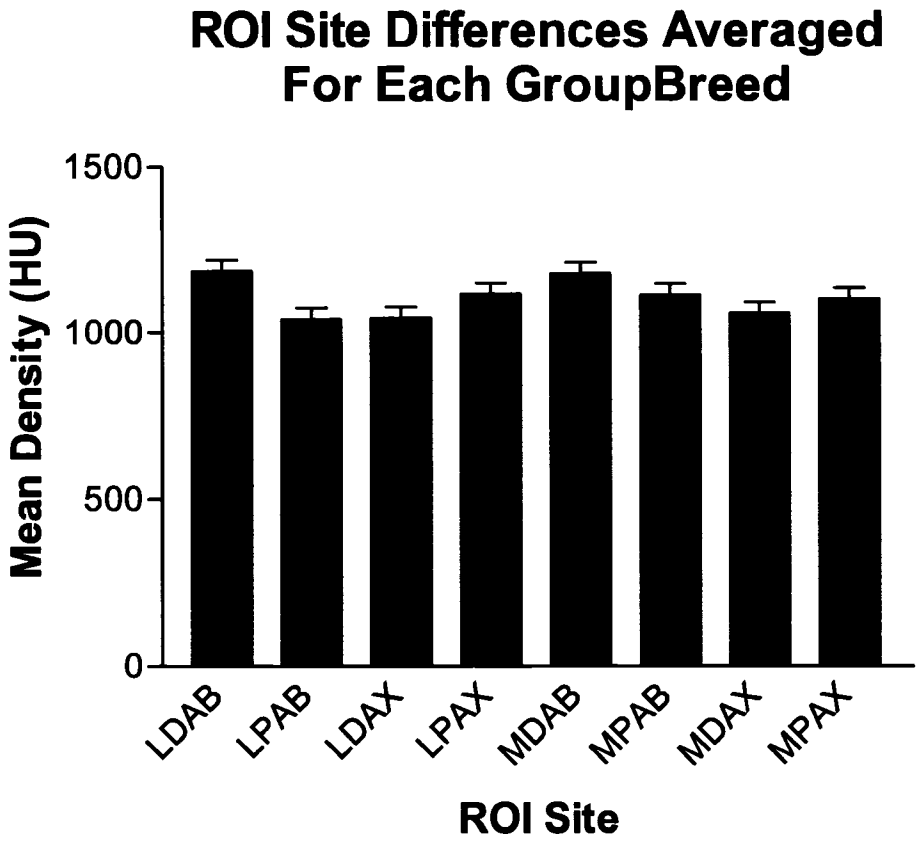

Figure 3.23: Least significant differences and p-values for each ROI site averaged over all groupbreed combinations

LOCATION	LSD	P-VALUE
LDAB-LDAX	142.00	<0.0001
LDAB-LPAB	145.34	<0.0001
LDAB-MDAB	7.68	0.69
LDAX-LPAX	-72.83	0.0002
LDAX-MDAX	-14.20	0.46
LPAB-LPAX	-76.17	<0.0001
LPAB-MPAB	-73.34	0.0001
LPAX-MPAX	15.25	0.43
MDAB-MDAX	120.12	<0.0001
MDAB-MPAB	64.31	0.0009
MDAX-MPAX	-43.39	0.02
MPAB-MPAX	12.42	0.52

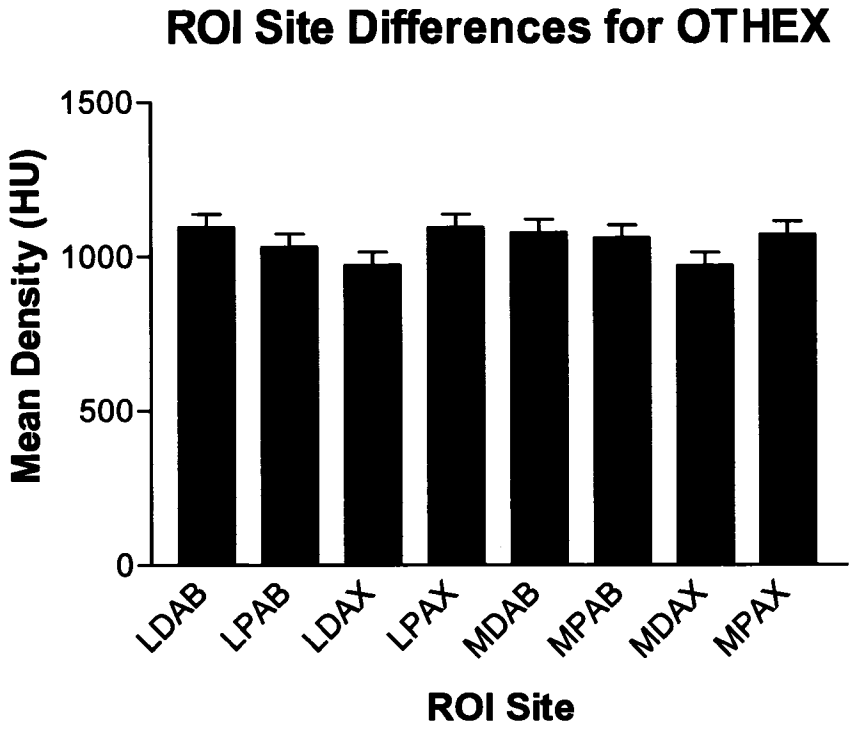

Figure 3.24: Least significant differences and p-values for each ROI site within exercised other breeds.

LOCATION	LSD	P-VALUE
LDAB-LDAX	122.27	<0.0001
LDAB-LPAB	64.08	0.01
LDAB-MDAB	18.25	0.47
LDAX-LPAX	-120.60	<0.0001
LDAX-MDAX	2.057	0.93
LPAB-LPAX	-62.41	0.01
LPAB-MPAB	-28.03	0.27
LPAX-MPAX	22.74	0.43
MDAB-MDAX	106.08	<0.0001
MDAB-MPAB	17.80	0.48
MDAX-MPAX	-99.93	<0.0001
MPAB-MPAX	-11.65	0.64

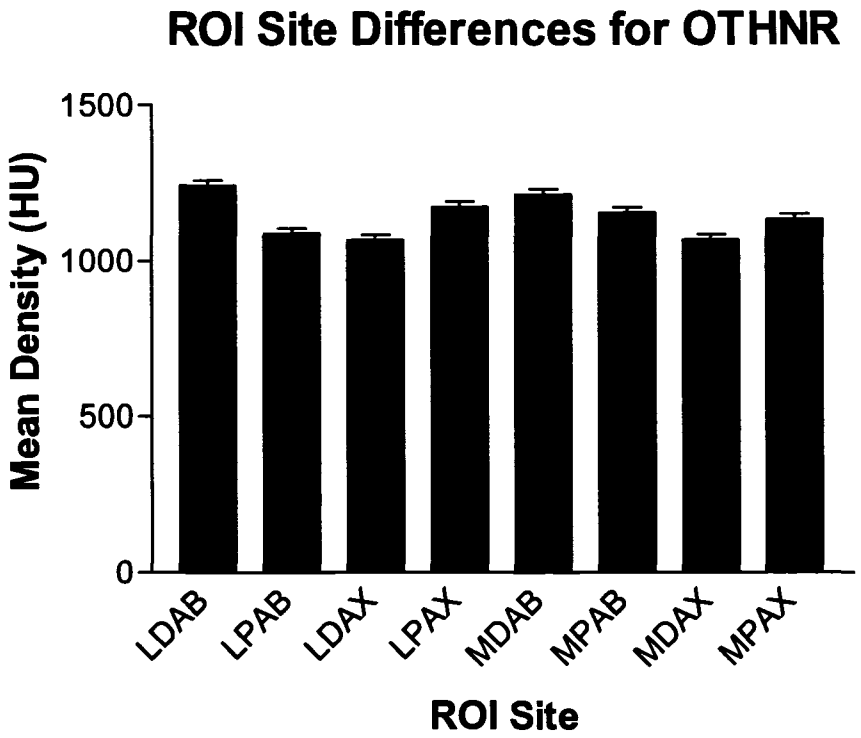

Figure 3.25: Least significant differences and p-values for each ROI site within non-racing other breeds

LOCATION	LSD	P-VALUE
LDAB-LDAX	174.36	<0.0001
LDAB-LPAB	153.71	<0.0001
LDAB-MDAB	26.31	0.09
LDAX-LPAX	-120.60	<0.0001
LDAX-MDAX	2.06	0.93
LPAB-LPAX	-85.80	<0.0001
LPAB-MPAB	-68.29	<0.0001
LPAX-MPAX	38.83	0.01
MDAB-MDAX	146.62	<0.0001
MDAB-MPAB	59.11	0.0001
MDAX-MPAX	-66.19	<0.0001
MPAB-MPAX	21.32	0.17

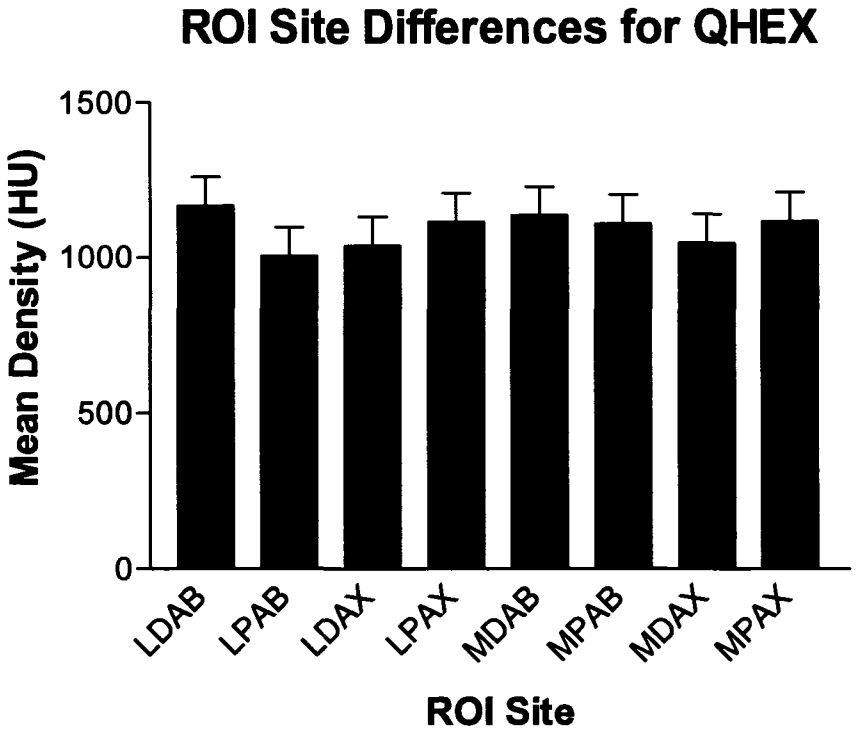

Figure 3.26: Least significant differences and p-values for each ROI site within exercised Quarter Horses.

LOCATION	LSD	P-VALUE
LDAB-LDAX	130.18	0.02
LDAB-LPAB	163.83	0.003
LDAB-MDAB	32.17	0.56
LDAX-LPAX	-78.52	0.15
LDAX-MDAX	-9.20	0.87
LPAB-LPAX	-112.17	0.04
LPAB-MPAB	-105.20	0.06
LPAX-MPAX	-2.35	0.97
MDAB-MDAX	88.80	0.11
MDAB-MPAB	26.46	0.63
MDAX-MPAX	-71.66	0.19
MPAB-MPAX	-9.32	0.87

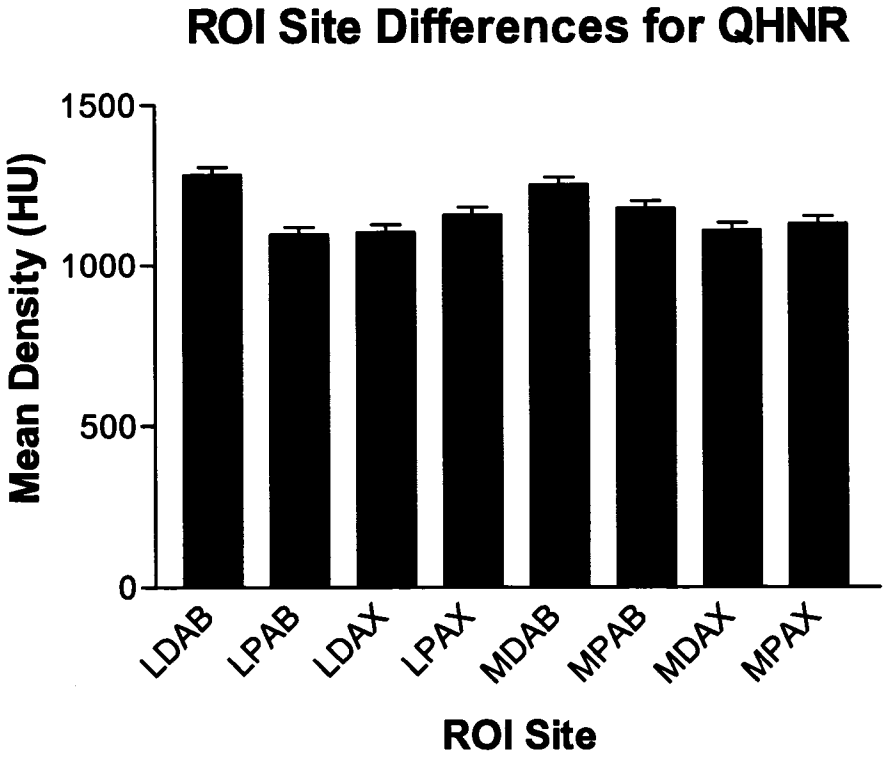

Figure 3.27: Least significant differences and p-values for each ROI site within non-racing Quarter Horses

LOCATION	LSD	P-VALUE
LDAB-LDAX	178.26	<0.0001
LDAB-LPAB	186.06	<0.0001
LDAB-MDAB	32.44	0.08
LDAX-LPAX	-53.70	0.004
LDAX-MDAX	-4.56	0.81
LPAB-LPAX	-61.50	0.001
LPAB-MPAB	-80.72	<0.0001
LPAX-MPAX	29.14	0.12
MDAB-MDAX	141.26	<0.0001
MDAB-MPAB	72.91	<0.0001
MDAX-MPAX	-19.99	0.28
MPAB-MPAX	48.36	0.009

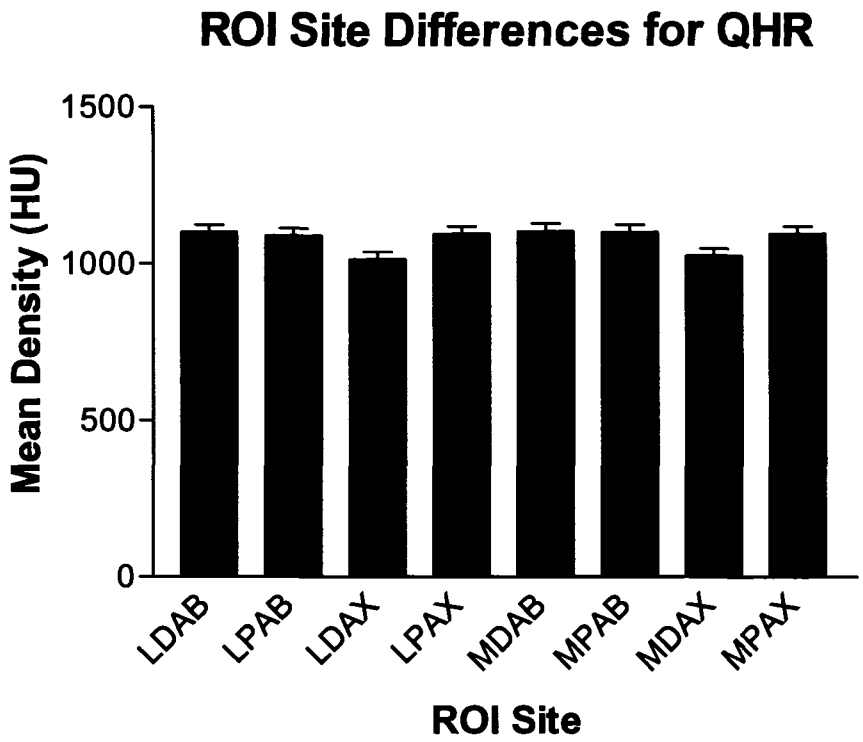

Figure 3.28: Least significant differences and p-values for each ROI site within racing Quarter Horses

LOCATION	LSD	P-VALUE
LDAB-LDAX	87.72	<0.0001
LDAB-LPAB	11.53	0.51
LDAB-MDAB	-3.66	0.83
LDAX-LPAX	-82.18	<0.0001
LDAX-MDAX	-10.96	0.53
LPAB-LPAX	-5.98	0.73
LPAB-MPAB	-10.72	0.54
LPAX-MPAX	-0.41	0.98
MDAB-MDAX	80.42	<0.0001
MDAB-MPAB	4.47	0.80
MDAX-MPAX	-71.63	<0.0001
MPAB-MPAX	4.32	0.81

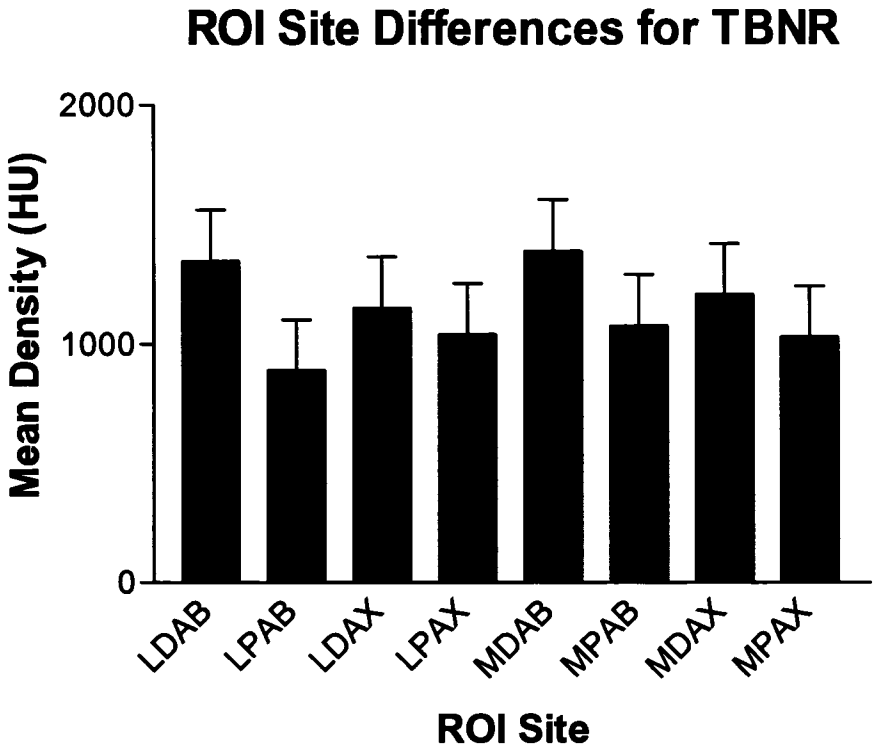

Figure 3.29: Least significant differences and p-values for each ROI site within non-racing Thoroughbreds

LOCATION	LSD	P-VALUE
LDAB-LDAX	194.52	0.10
LDAB-LPAB	455.32	<0.0001
LDAB-MDAB	-41.59	0.72
LDAX-LPAX	111.61	0.34
LDAX-MDAX	-54.81	0.64
LPAB-LPAX	-149.19	<0.0001
LPAB-MPAB	-185.93	0.11
LPAX-MPAX	9.42	0.94
MDAB-MDAX	181.31	0.12
MDAB-MPAB	310.98	0.008
MDAX-MPAX	175.84	0.13
MPAB-MPAX	46.17	0.69

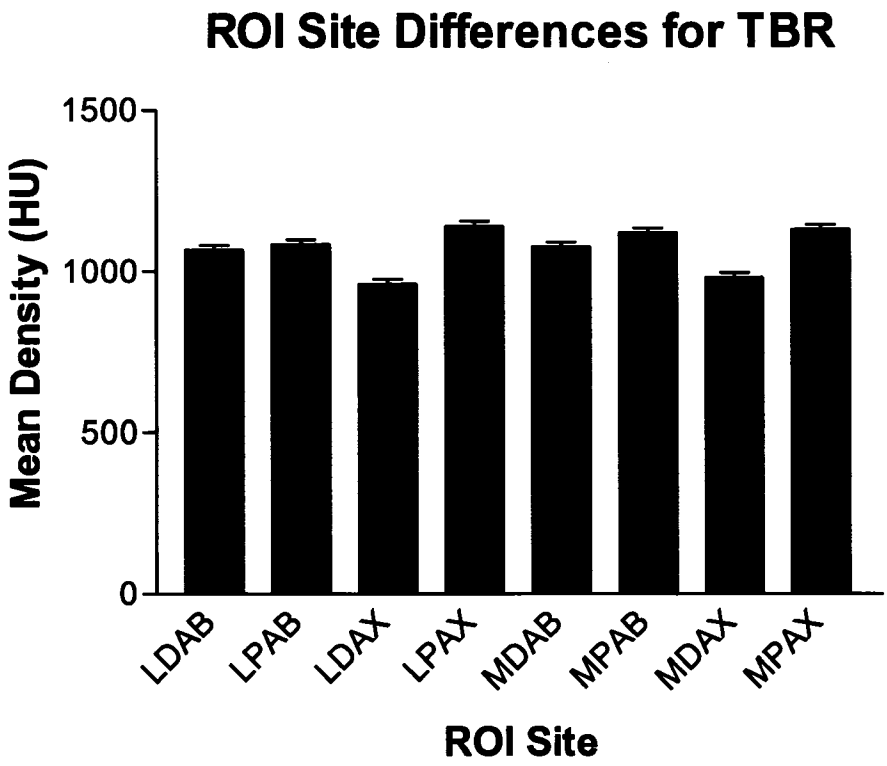

Figure 3.30: Least significant differences and p-values for each ROI site within racing Thoroughbreds

LOCATION	LSD	P-VALUE
LDAB-LDAX	106.67	<0.0001
LDAB-LPAB	-17.18	0.12
LDAB-MDAB	-10.51	0.35
LDAX-LPAX	-179.99	<0.0001
LDAX-MDAX	-20.46	0.06
LPAB-LPAX	-56.14	<0.0001
LPAB-MPAB	-34.50	0.002
LPAX-MPAX	9.35	0.39
MDAB-MDAX	96.36	<0.0001
MDAB-MPAB	-41.53	0.0001
MDAX-MPAX	-150.18	<0.0001
MPAB-MPAX	-12.29	0.26

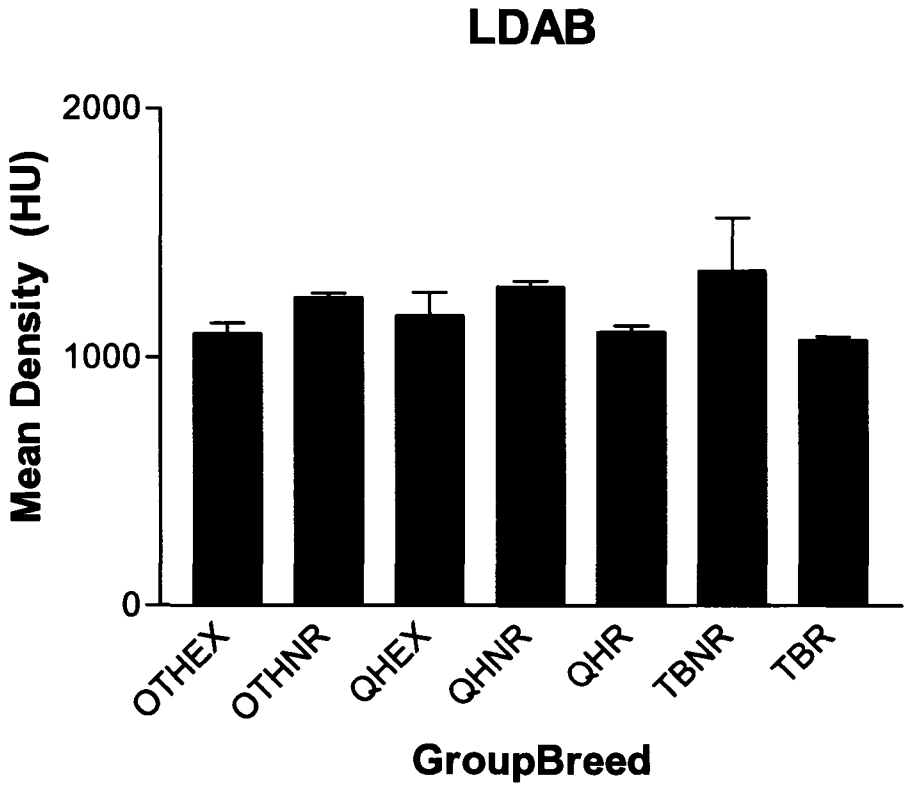

Figure 3.31a: Differences within breeds between groups for lateral dorsal axial sites.

Figure 3.31b: Differences within groups between breeds for lateral dorsal abaxial sites.

LDAB

TB	LSD	P-VALUE
TBNR-TBR	279.72	0.19
QH		
QHEX-QHNR	-114.21	0.24
QHEX-QHR	66.44	0.49
QHNR-QHR	180.64	<0.0001
Other		
OTHEX-OTHNR	-146.05	0.0018

LDAB

Racing	LSD	P-VALUE
QHR-TBR	34.15	0.24
Exercised		
OTHEX-QHEX	-72.1794	0.48
Non-racing		
OTHNR-QHNR	-10.52	0.75
OTHNR-TBNR	-105.26	0.62
QHNR-TBNR	-64.30	0.76

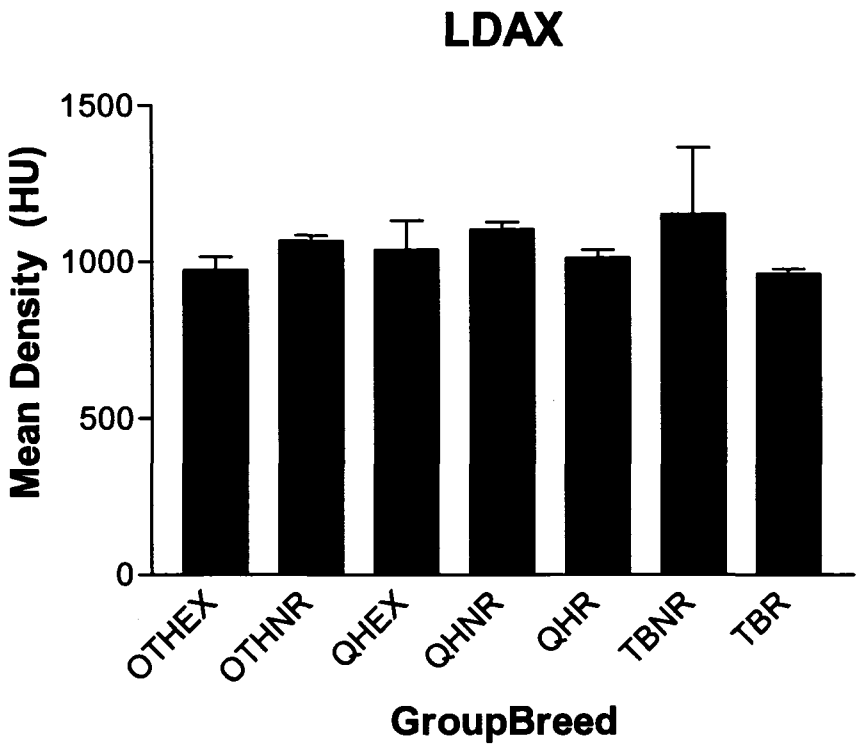

Figure 3.32a: Differences within breeds between groups for lateral dorsal axial sites.

LDAX

TB	LSD	P-VALUE
TBNR-TBR	191.87	0.37
QH		
QHEX-QHNR	-66.13	0.49
QHEX-QHR	23.98	0.80
QHNR-QHR	90.11	0.009
OTH		
OTHEX-OTHNR	-93.97	0.04

Figure 3.32b: Differences within groups between breeds for lateral dorsal axial sites.

LDAX

Racing	LSD	P-VALUE
QHR-TBR	53.10	0.07
Exercised		
OTHEX-QHEX	-64.27	0.53
Non-racing		
OTHNR-QHNR	-36.43	0.21
OTHNR-TBNR	-85.09	0.69
QHNR-TBNR	-48.67	0.82

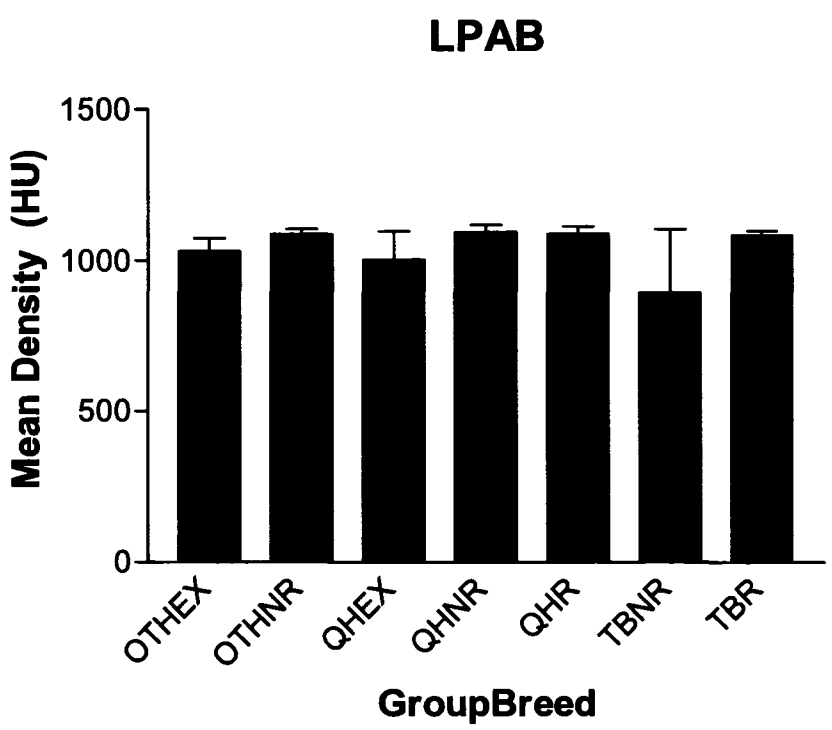

Figure 3.33a: Differences within breeds between groups for lateral palmar abaxial sites.

Figure 3.33b: Differences within groups between breeds for lateral palmar abaxial sites.

LPAB

TB	LSD	P-VALUE
TBNR-TBR	-192.78	0.37
QH		
QHEX-QHNR	-91.97	0.34
QHEX-QHR	96.90	0.34
QHNR-QHR	6.11	086
OTH		
OTHEX-OTHNR	-56.42	0.22

LPAB

Racing	LSD	P-VALUE
QHR-TBR	5.44	0.85
Exercised		
OTHEX-QHEX	27.57	0.79
Non-racing		
OTHNR-QHNR	-7.98	0.78
OTHNR-TBNR	196.35	0.36
QHNR-TBNR	204.33	0.34

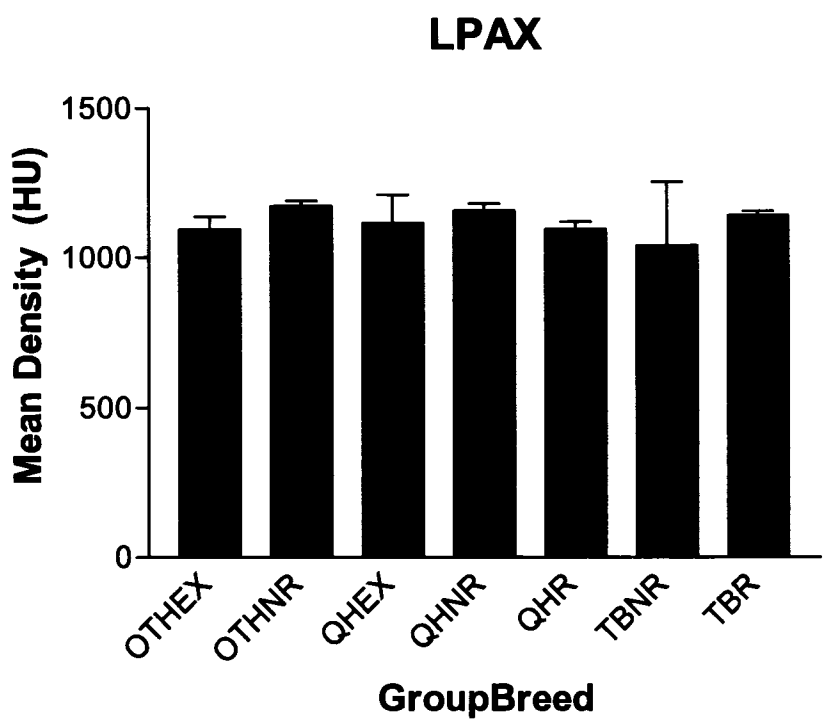

Figure 3.34a: Differences within breeds between groups for lateral palmar axial sites.

LPAX

TB	LSD	P-VALUE
TBNR-TBR	-99.73	0.64
QH		
QHEX-QHNR	-41.31	0.67
QHEX-QHR	20.33	0.83
QHNR-QHR	61.63	0.07
OTH		
OTHEX-OTHNR	-79.82	0.08

Figure 3.34b: Differences within groups between breeds for lateral palmar axial sites.

LPAX

Racing	LSD	P-VALUE
QHR-TBR	-44.18	0.12
Exercised		
OTHEX-QHEX	-22.19	0.83
Non-racing		
OTHNR-QHNR	16.32	0.58
OTHNR-TBNR	132.97	0.53
QHNR-TBNR	116.65	0.59

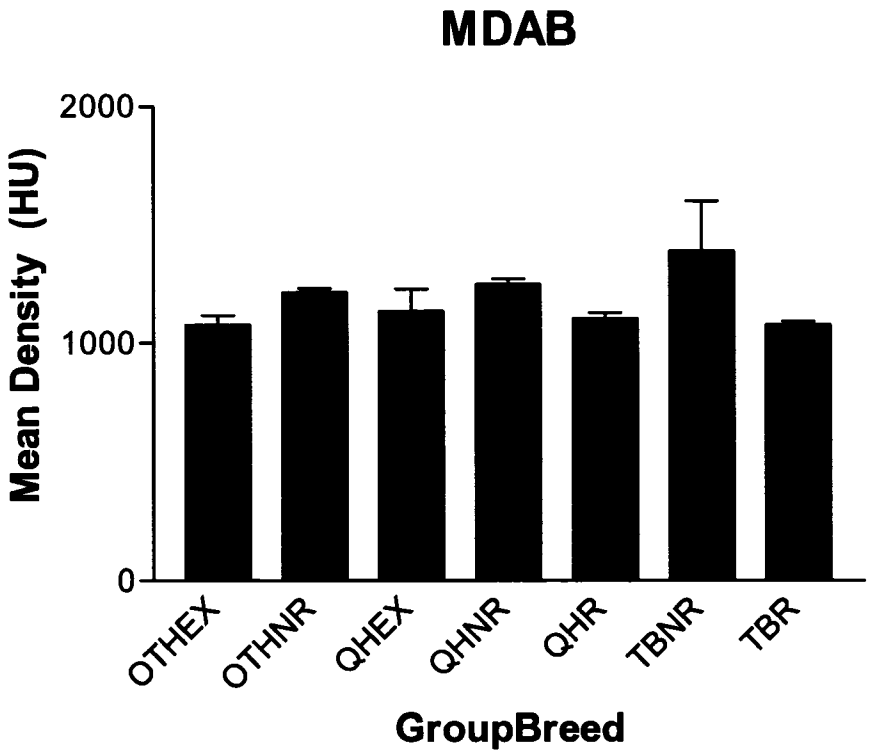

Figure 3.35a: Differences within breeds between groups for medial dorsal abaxial sites.

MDAB

TB	LSD	P-VALUE
TBNR-TBR	311.16	0.14
QH		
QHEX-QHNR	-113.94	0.24
QHEX-QHR	30.60	0.75
QHNR-QHR	144.55	<0.0001
OTH		
OTHEX-OTHNR	-137.99	0.0031

Figure 3.35b: Differences within groups between breeds for medial dorsal abaxial sites.

MDAB

Racing	LSD	P-VALUE
QHR-TBR	27.66	0.34
Exercised		
OTHEX-QHEX	-58.26	0.57
Non-racing		
OTHNR-QHNR	-34.21	0.24
OTHNR-TBNR	-173.16	0.42
QHNR-TBNR	-138.96	0.52

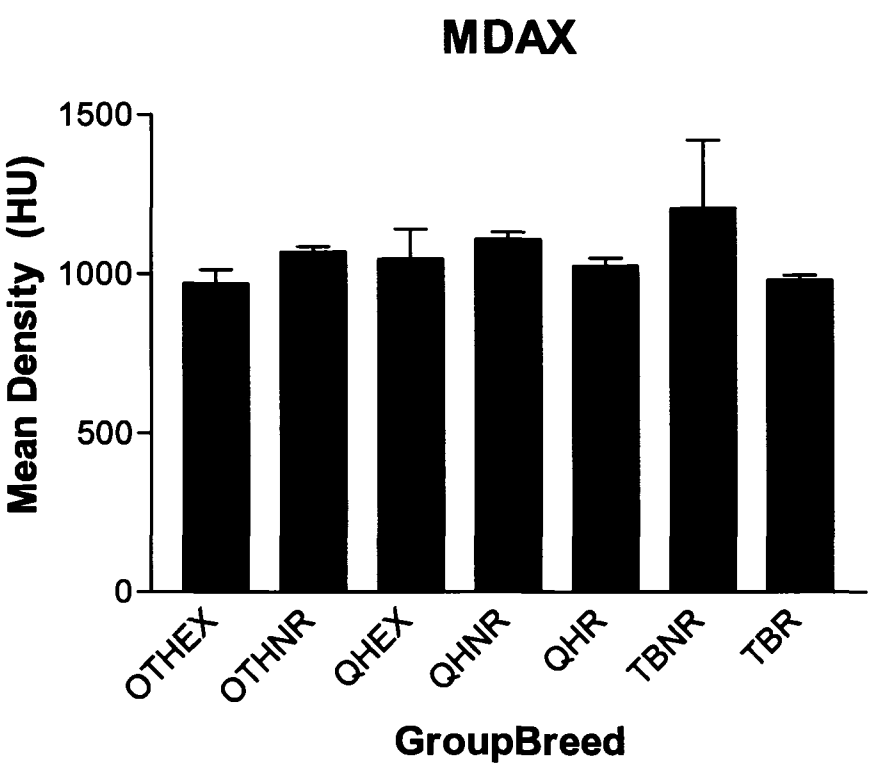

Figure 3.36a: Differences within breeds between groups for medial dorsal axial sites.

MDAX

TB	LSD	P-VALUE
TBNR-TBR	226.22	0.29
QH		
QHEX-QHNR	-61.48	0.52
QHEX-QHR	22.23	0.81
QHNR-QHR	83.71	0.02
OTH		
OTHEX-OTHNR	-39.56	0.18

Figure 3.36b: Differences within groups between breeds for medial dorsal axial sites.

MDAX

Racing	LSD	P-VALUE
QHR-TBR	43.59	0.13
Exercised		
OTHEX-QHEX	-75.54	0.46
Non-racing		
OTHNR-QHNR	16.05	0.68
OTHNR-TBNR	44.48	0.34
QHNR-TBNR	-98.91	0.64

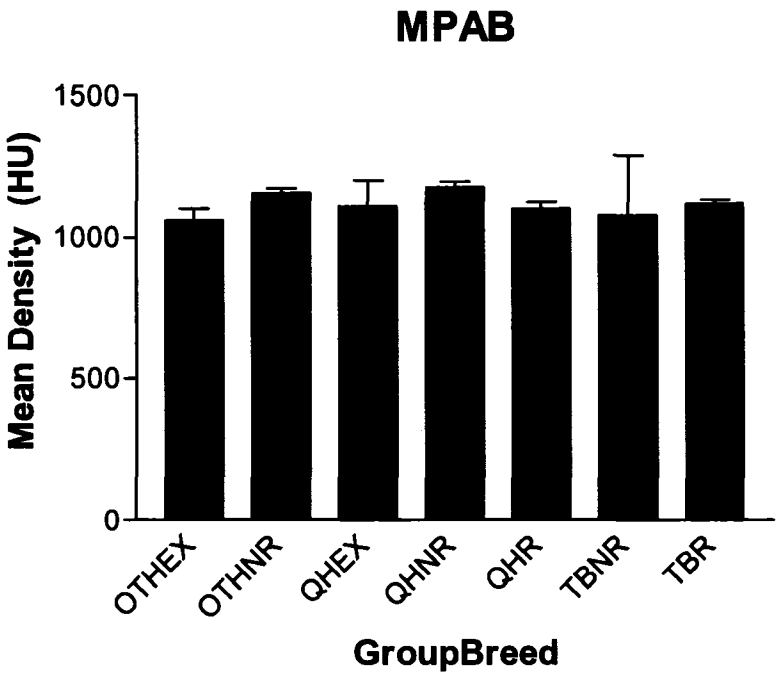

Figure 3.37a: Differences within breeds between groups for medial palmar abaxial sites.

Figure 3.37b: Differences within groups between breeds for medial palmar abaxial sites.

MPAB

TB	LSD	P-VALUE
TBNR-TBR	-41.35	0.85
QH		
QHEX-QHNR	-67.49	0.49
QHEX-QHR	8.63	0.93
QHNR-QHR	76.12	0.03
OTH		
OTHEX-OTHNR	-96.69	0.04

MPAB

Racing	LSD	P-VALUE
QHR-TBR	-18.35	0.53
Exercised		
OTHEX-QHEX	-49.60	0.63
Non-racing		
OTHNR-QHNR	-20.41	0.48
OTHNR-TBNR	78.70	0.71
QHNR-TBNR	99.11	0.64

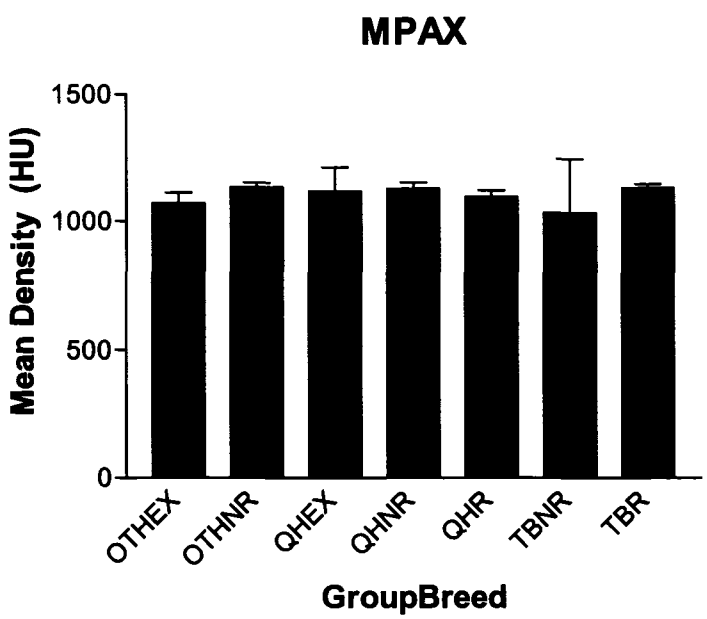

Figure 3.38a: Differences within breeds between groups for medial palmar axial sites.

Figure 3.38b: Differences within groups between breeds medial palmar axial sites.

MPAX

TB	LSD	P-VALUE
TBNR-TBR	-99.81	0.64
QH		
QHEX-QHNR	-9.82	0.92
QHEX-QHR	22.26	0.82
QHNR-QHR	32.07	0.35
OTH		
OTHEX-OTHNR	-63.72	0.17

MPAX

Racing	LSD	P-VALUE
QHR-TBR	-34.96	0.24
Exercised		
OTHEX-QHEX	-47.27	0.65
Non-racing		
OTHNR-QHNR	6.63	0.82
OTHNR-TBNR	44.48	0.34
QHNR-TBNR	96.92	0.65

For MVSD, only group ($p<0.001$), gender ($p<0.05$), and medial/lateral sites ($p<0.0001$) were significant (Figures 3.39-41). The three-way interaction was not significant ($p=0.22$), and only the group*gender two-way interaction was significant ($p<0.03$). In the group*breed model, again group*breed ($p<0.01$) and medial/lateral sites ($p<0.0001$) were significant, but gender ($p<0.07$) was only a trend. The three-way interaction was not significant ($p=0.61$), and the only significant two-way interaction was group*breed and gender ($p<0.01$).

Lateral sites had higher MVSDs than medial sites in either model ($p<0.0001$). Female racehorses had significantly higher MVSDs than males ($p<0.001$). No other gender differences were seen. Within males, racehorses had higher MVSDs than exercised ($p<0.02$) and non-racing ($p<0.0001$) male horses. Within females, exercised females had higher MVSDs than non-racing females ($p<0.05$). No other significant differences were found. Female Thoroughbred racehorses had higher MVSDs than male Thoroughbred racehorses ($p<0.0001$). No other significant gender differences were noted. Within males, non-racing Quarter Horses had significantly higher MVSDs than racing Quarter Horses ($p<0.001$). Within females, non-racing Quarter Horses had significantly higher MVSDs than racing Quarter Horses ($p<0.01$). Female racing Quarter Horses had significantly lower MVSDs than female racing Thoroughbreds ($p<0.01$).

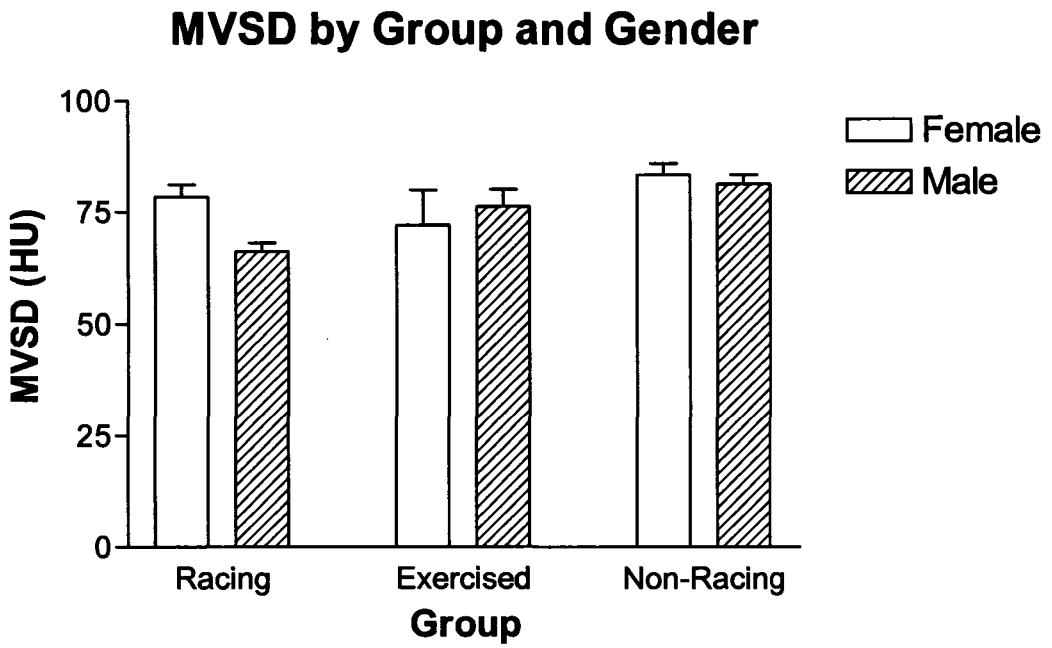

Figure 3.39: Graph of MVSD by group and gender.

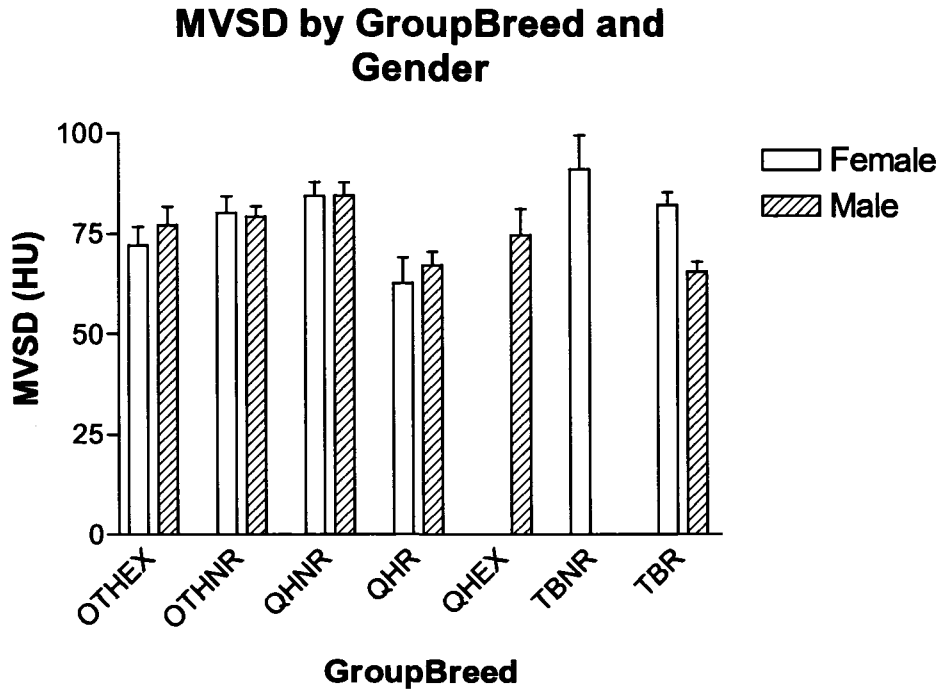

Figure 3.40: Graph of MVSD by group, breed and gender.

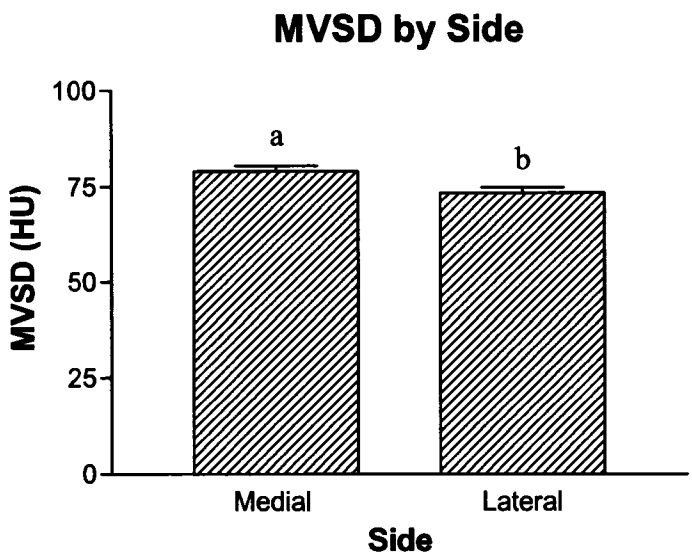

Figure 3.41: Graph of MVSD by side. Different letters indicate significant differences at $\alpha=0.05$.

Again, with gross score analyzed as the response variable for palmar ROIs, only group*breed ($p<0.01$) and log age ($p<0.0001$) were significant, but there was a trend for group ($p<0.10$). However, the interaction between age and group was significant ($p<0.05$), but the interaction between age and group*breed was not significant ($p=0.19$). Racehorses had higher gross scores than exercised ($p<0.002$) and non-racing ($p<0.001$). There was no significant difference in gross scores between non-racing and exercised horses ($p=0.39$). Racing Thoroughbreds had higher gross scores than non-racing other breeds ($p<0.001$), exercised other breeds ($p<0.03$), non-racing Quarter Horses ($p<0.01$), and non-racing Thoroughbreds ($p<0.03$). Racing Quarter Horses had significantly higher gross scores than non-racing other breeds ($p<0.03$) only. All other comparisons were non-significant ($p>0.05$).

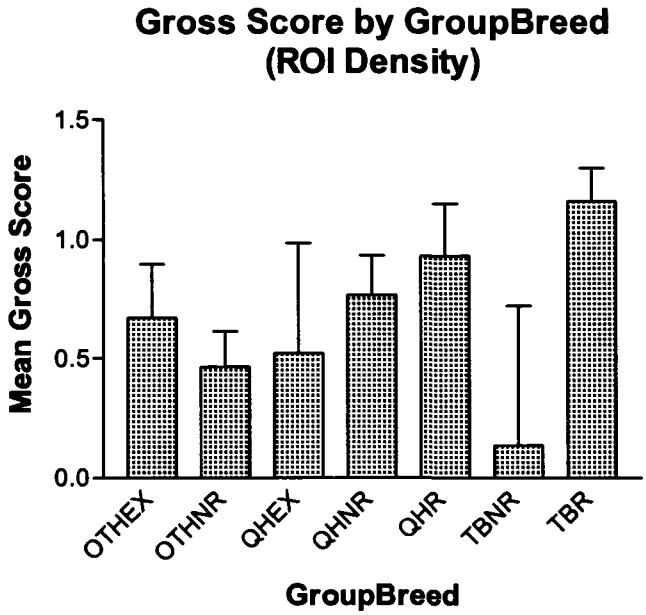

Figure 3.42: Graph of gross score by group and breed.

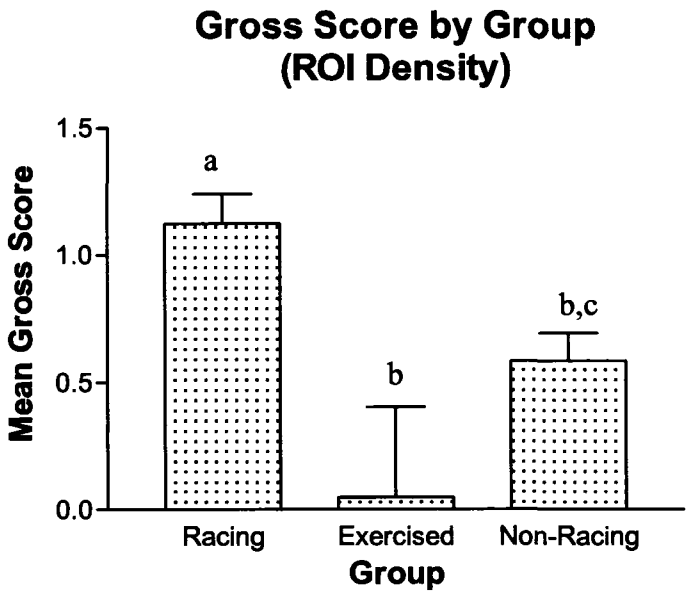

Figure 3.43: Graph of gross score by group. Different letters indicate significant differences at α=0.05.

Discussion

Subchondral bone mean density as determined by quantitative computed tomography (QCT) is significantly affected by age, use and breed but not by limb and gender. Non-racing horses had significantly higher mean densities than racing horses and exercised horses. Racing horses also had significantly higher mean densities than exercised horses. The third metacarpal condyle of racing and exercising horses were both encountering physical loading capable of inducing increased bone remodeling and formation[84, 86, 116, 117], whereas the unknown exercise histories of the non-racing group preclude us from drawing any conclusions about occurrence of activated remodeling. Therefore, we cannot definitively explain the difference in mean density between groups as a result of intense exercise, but intuitively this is the most plausible explanation.

Initiation of exercise induces a demineralization phase[77, 116] in bone due to the delay between bone resorption and formation as bone remodels and mechanically adapts to applied loads[9]. Since nearly all exercised horses and a significant number of racehorses were skeletally immature, bone modeling was likely occurring in conjunction with remodeling in these groups[37]. Bone modeling is the process in which gross bone shape is altered, and has been associated with lowered bone density[118]. This occurs because of the increased amount of newly formed bone has not fully mineralized and thus is

lower in density. Both of these reasons serve to explain why the non-racing group had significantly higher mean bone density. Amount and type of exercise did vary within the exercised group, which is a source of variability of mean density in this group. Similarly, the unknown training histories of the racehorses subjected this group to additional variability in mean density as well. Thus, this source of variability is unexplained by our model and could affect the relationship of mean bone density between groups. However, it is reasonable to assume that the amount of exercise is greater in the racing and exercised groups than the non-racing group.

Alternately, subchondral bone mineralization may not respond as quickly to remodeling as other areas, such as trabecular bone, of the distal third metacarpal bone, thus creating the impression that QCT is insensitive to early bone mineral change. It is possible to have decreased mineralization with increased bone volume, which would falsely lower radiographic measures of bone mass[118] due to the abundance of unmineralized bone matrix and insufficient density resolution of clinical QCT for trabecular level mineral changes[69]. In humans, QCT correlated poorly with osteomalacic bone, which has increased amounts of unmineralized bone[119]. The validity of these studies as models for equine bone turnover and formation is questionable as one study used end-stage renal failure patients and the other 19th century skeletons with no soft tissue covering and no mineral density measurements. More recent work[120] suggests QCT is highly correlated with normal bone formation in mice

with human bone marrow transplants, and slightly less correlated with mineralized matrix in osteomalacic transplants. Unfortunately, only mineralized matrix was measured and no comments were made about unmineralized matrix in osteomalacic transplants in these studies.

Bone density and mineralization increase with age[121]. In humans, adult bone mineralization depends upon the rate of remodeling as increased bone remodeling results in a shortened lifespan of the basic bone unit such that full mineralization of newer bone is never achieved[122]. Assuming this paradigm holds true for horses, the lower mean density of racehorses versus non-racehorses could be due to higher levels of remodeling in the distal metacarpal bone of racehorses. The results from the analysis of subchondral bone density of the entire distal metacarpal condyle can be used to demonstrate that as age increases, mean density increases at the same rate between groups, but that level of mean density is different for each age. Thus, in determining an overall pathologic threshold of subchondral bone sclerosis using QCT, references should account for age and use.

Limb differences were not observed in any of the groups. However, left limb injuries occur more commonly in racehorses[2, 123, 124], and surface strains are different between right and left metacarpophalangeal joints in racehorses[125]. It is reasonable to presume that differences in mean bone density between limbs should occur because if strain magnitude determines

bone adaptation (and subsequent bone formation) [126, 127], and strain magnitude is higher in left limbs (for North American racehorses)[128] it is logical that an increase in mean density could be seen in left limbs. The major limitation of this study that may have precluded us from observing limb differences in racehorses is that the effects of training regime were not accounted for in the racehorse group and this may offer additional statistical explanation that would determine if clinical differences in left and right limbs also occur with mean bone density.

MVSD was significantly different for group, gender and breed. Age and limb were not affected by MVSD. Thoroughbred racehorses had significantly higher mean standard deviations most other breed and group combinations, and no other breed and group comparisons were significant. Specifically, the highest significant difference was between female Thoroughbred and female Quarter horse racehorses. This is interesting to note since condylar fractures occur more often in Thoroughbred racehorses than in Quarter Horse racehorses. MVSD of subchondral bone density in Thoroughbred racehorses could represent density gradients occurring across the surface of the distal third metacarpal bone. Since MVSD represents voxel variation about the mean surface density, a larger standard deviation means there is a wider variation in the surface density. It is unknown where this variation is occurring on the surface of the third metacarpal condyle, but it is plausible that areas of low bone density are adjacent to areas of very high bone density creating a density gradient. Riggs et al[111], noted that

steep density gradients occur along the surface of the distal third metacarpal condyle in a dorsal plane of Thoroughbred horses. They suggested that this density gradient concentrates stress at the condylar groove, which is a common site for condylar fractures in Thoroughbred racehorses.

Condylar fractures occur more frequently in Thoroughbred racehorses in comparison to Standard bred and Quarter Horse racehorses, and a genetic predisposition to these fractures has been suggested[129] but not yet investigated. The strong association of mean voxel standard deviation in Thoroughbred racehorses suggest that something is occurring unique to this breed, but whether it is due to genetics, race training practices[130], or yet some other unidentified factor, is unknown without exercise or genetic background on the Thoroughbred racehorses in this study. Clearly, further work into this interesting relationship is needed, and may yield valuable information on causative factors of condylar fractures in Thoroughbred racehorses.

Mean gross score was highest for racing horses, which is expected. Racehorses are susceptible to osteochondral lesions of the palmar metacarpus not seen in other horses[87]. Trauma is the proposed etiology, and focal areas of subchondral bone sclerosis and necrosis with surrounding bony remodeling are characteristic of palmar osteochondral lesions in racehorses[39, 88]. However, no density measure was predictive of gross score. One limiting issue

is that there were very few severe lesions and an abundance of condyles without any gross pathologic change.

CTO density distribution

In general, there seemed to be a "V" shaped pattern to density distribution across the condyle from dorsal to palmar in non-racing horses (Figure 3.44). That is, higher density across the width of the dorsal aspect that narrowed towards the palmar aspect of the condyle. This pattern could be representative of the dorsal articulation of the proximal phalanx and the palmar articulation of the proximal sesamoid bones with the third metacarpal bone. In stark contrast, racehorses had a "box" like appearance to the density distribution (Figure 3.44). That is, increased bone density spanning the same width of each condylar side and coursing from dorsal to palmar. This indicates loss of joint incongruity and altered biomechanical function[115]. One possible cause for this pattern is abaxial movement of the proximal sesamoids during hyperextension of the metacarpophalangeal joint. Exercised horses appeared to vary somewhere in between these two patterns, but seemed to be in a transition state between incongruous and congruous surface density patterns. This study demonstrates that CTO subchondral bone density patterns assessed visually indicate specific patterns are associated with use in horses.

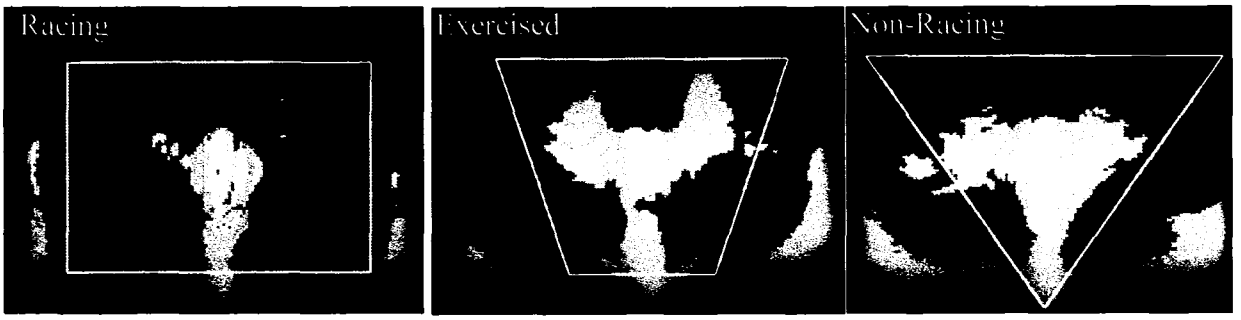

Figure 3.44: CTO maps of racing, exercised and non-racing horses. Lighter shades of gray representslow density, whereas darker areas are higher density. Note the change in density patterns between the three groups of horses with similar ages.

Individual ROI mean density seemed to approximate the density distribution changes observed in three-dimensional models. A noticeable trend representing a loss of joint incongruity, that is areas of high density subchondral bone predominantly located at the periphery of the condyle, was observed in racehorses and most exercised horses whereas non-racing horses appeared to have very consistent and peripherally loaded (incongruous) joint mineralization patterns. Variations in mineralization patterns of racing and exercised horses may be due to the strong age effect seen and unmeasured exercise or training effects.

Objectively, the density pattern change between groups is supported by the ROI site differences within groups. Mean density of dorsal ROIs in non-racing horses were consistently significantly higher than exercised or non-racing horses. Most importantly, the palmar abaxial ROI sites were significantly higher in racing and exercised horses compared to non-racing horses. This seems to be an area where the degree of joint congruency could be measured. In the normal horse, the proximal sesamoids would not exert force in this area, but the

contact between proximal sesamoids and the third metacarpal bone would increase as cyclic load trauma increases. These differences support the visually assessed pattern differences between groups.

Again, Thoroughbreds had an association with mean voxel standard deviation. Interestingly, male Thoroughbreds had significantly lower MVSD than females. Historically, studies of condylar fractures have been reported more in males than females, and have been attributed to greater bodyweight and speed[131], reluctance to refer females with condylar fractures[132], and sex predisposition in training[97]. Condylar fractures appear to originate from the palmar aspect of the distal third metacarpal bone[133]. Since there is not solid evidence as to whether condylar fractures occur more frequently in males or females, it is difficult to determine if a higher MVSD actually predisposes females to condylar fractures due to sharp density gradients or if a lower MVSD in males predisposes them to condylar fractures due to homogenization of bone mineral density.

Calibration considerations

The analysis of phantom variation demonstrates that there were some significant differences between CT scanners. However, it this study demonstrated that water is most significantly affected as variance decreased with increasing K_2HPO_4 concentrations and the lower equivalent concentrations were

significantly different while the higher concentrations were not. This is consistent with systematic errors previously identified in the literature[134], and further supports the use of solid phantoms for calibration or only using liquid equivalents of low water concentrations. One must also point out that the power was relatively low in these analyses. However, the confidence intervals did include zero for the 100 mg/ml and 200 mg/ml equivalent concentrations, so a larger sample size would be needed to further determine the effect of scanner. Although the slopes of the calibration between scanners using the K_2HPO_4 phantom were not signficantly different, the intercepts were significantly different. Still, the high correlations between HU or TCP and ash density suggest that HU is still a good estimate of true bone density.

Scanner variation has been identified previously as an issue in comparing CT numbers between machines[135, 136]. However, it has also been demonstrated that every scanner has a linear response to increasing densities such that objects of similar density can be compared given similar scanner settings[137]. In the study by Levi, et al, several tubes of water were used to evaluate variation between scanners. As has already been mentioned, water is significantly affected by scanner variation, which is a considerable issue when measuring trabecular bone due to marrow fat. Subchondral bone has very little marrow in comparison to cancellous bone, and thus it may be possible that machine variation would affect the measurement of subchondral bone less than that of trabecular bone[138].

The use of HU as an absolute value of density measure in this study was necessitated in order to evaluate population effects over many CT scans. Reducing the datasets within each scanner-phantom combination would help reduce the potential machine variation, but would significantly reduce sample size. Given the nature of the study (ie, evaluating breed, age, gender and exercise effects), a large sample size is essential to determining differences. An alternative to unify the data would be to perform a cross-calibration between phantoms as has been previously described[139-141]. However, the question still remains whether variation due to scanner effects were large enough to influence the group and ROI differences observed in this study. In future studies, it is highly recommended that scans be performed on the same CT scanner with the same phantom to eliminate the problems encountered in this study.

In conclusion, differences in subchondral bone density were observed between racing or exercised horses and non-racing horses as assessed using QCT and CTO. Horses undergoing experimentally controlled exercise appear to be a good a model of subchondral mineralization changes in racehorses as the subchondral density changes were more characteristic of racing than non-racing horses. MVSD is significantly different in Thoroughbred racehorses, but it is unclear whether this is a factor of breeding genetics, training differences or a true factor in condylar fracture risk. Gross pathologic lesions were not associated with subchondral bone density or density variation in any group of horses.

Chapter 4

Comparison of Gross Pathologic, Histologic, and Subchondral Density Changes in Racing Horses

Introduction

Musculoskeletal injury and disease are responsible for significant morbidity and mortality in racing horses[2]. A model of 'overload arthrosis' has been suggested as the primary etiology of osteochondral pathology in racehorses[39]. In overload arthrosis, subchondral bone becomes thickened and sclerotic, altering the biomechanics and normal shock absorbing capabilities of bone. This stiffening is thought to increase overlying cartilage degeneration, and incites irreversible degenerative joint disease[16].

Gross and histopathologic characteristics of overload arthrosis in horses have been documented[87-89], and demonstrate that subchondral bone plays a role in the development of osteochondral injuries and pathology. Computed tomographic osteoabsorptiometry has been used to measure bone mineral density[80] and more recently to map the changes in bone density under articular surfaces[6]. However, no direct comparison of quantitated subchondral bone density obtained using CT and histologic or gross pathologic changes have been made in horses. It would be useful to reliably predict gross pathologic change of articular cartilage non-invasively in order to help diagnose early joint disease.

The goal of this study was to determine if subchondral bone density is associated with gross and histopathologic lesions of the distal third metacarpal condyle in racing horses.

Materials and Methods

Experimental Design

Metacarpophalangeal (MCP) joints were collected from 9 horses euthanized during the 2003 Colorado racing season for a variety of reasons (Figure 4.1).

Figure 4.1: Colorado racing demographics 2003

TB=Thoroughbred, QH=Quarter Horse, RF=right forelimb, LF=left forelimb, fx=fracture

Horse#	Gender	Age(mos)	Breed	Cause of Death
1	M	138	TB	Sudden collapse, acute subdural hem.
2	F	90	TB	Cecal rupture
3	M	30	TB	RF scapular fx
4	M	55	TB	RF 3rd carpal bone slab fx
5	M	115	QH	Streptococcal pneumonia
6	M	43	TB	RH proximal phalanx fx
7	F	43	QH	Pulmonary hemorrhage
8	M	43	TB	Biaxial LF sesamoid fx
9	F	43	TB	RF proximal interphalangeal luxation

Scans were performed on a Picker PQ CT[a] at 140 kVP with a slice thickness of 1.5-mm, 180mm field of view, and a 512x512 voxel matrix, which creates a 0.352mm spatial resolution. CT studies were exported for analysis to the customized image analysis program OsteoApp[e] that was designed using the Interactive Design Language[d]. Additionally, each joint was scanned with a tri-calcium phosphate (TCP) density phantom[b] to convert bone mineral density from Hounsfield Units to mg/ml TCP using a simple linear regression.

Gross Evaluation

MCP joints were disarticulated after CT scanning and scored for superficial palmar gross pathologic changes on a scale of 0-4 (Figure 4.2). After assigning a gross score, the entire MCP joint was photographed for reference. The distal third metacarpal condyle was removed with a band saw approximately 3-cm proximal to the medial condylar surface. Again, the removed condyle was photographed for reference. The condyles were wrapped in physiologic buffered saline soaked gauze and frozen at –20° C until further processing.

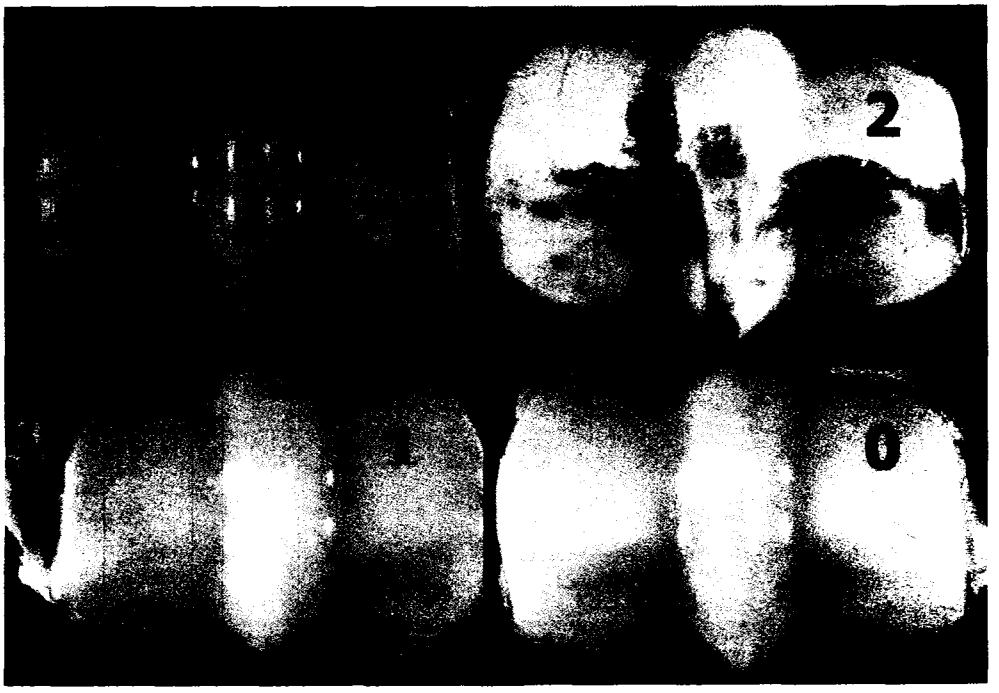

Gross Score	Description
0	No visible abnormalities or changes in cartilage or bone
1	Minimal scoring with fibrillation of cartilage
2	Mild erosion, small pits and/or more prominent fibrillation
3	Similar changes as above, but additionally focal divots or indentations of cartilage with/without focal cartilage opacities, and partial to full-thickness erosions in small (4-8mm) areas.
4	Extensive degeneration, erosion, and ulceration of cartilage with some exposure and/or loss of underlying bone, generally involving a large area (1cm or greater). **Note-no grade 4 lesions were observed

Figure 4.2: Superficial palmar gross scoring scheme with photographic examples of each score.

Histologic preparation

Each condyle was cut 2-cm proximal to the medial condyle measured at the central axis of rotation. Next, sagittal and dorsal plane sections were obtained, respectively, using a precision cutting system[c] in 4mm thick sections. Additionally, the dorsal plane sections were cut using a specialized jig such that the dorsal plane was taken 30° palmar to the central axis of rotation (Figure 4.3). The sections were then fixed in 10% buffered formalin for 72 hours. Samples were rinsed with tap water and placed in ethylenediaminetetraacetic acid (EDTA) decalcifying solution[h] at a volume of 10:1 for three weeks. Although the EDTA solution was changed every 2-3 days, the samples were not adequately decalcified for sectioning, so samples were rinsed in tap water, radiographed, and placed in 10% formic acid with polyacrimide resin beads[i]. Repeat radiographs suggested decalcification was complete in 2 days. Additionally, the samples tested free of calcium using an aluminum hydroxide decalcification endpoint assay[j]. Samples were then embedded in paraffin and sectioned for staining with hematoxylin and eosin (H&E).

Histologic Grading

Osteochondral lesions apparent on H&E sections were graded for severity on a scale of 0-4 (Figure 4.4). Subchondral remodeling was scored on a scale of 0-3 (Figure 4.5). Subchondral bone volume was measured using a software

package[k] that measures percent bone as a function of bone volume/total volume. Since horses could potentially have multiple lesions within the same limb, additional variables were created to represent the total number of lesion sites observed and severity of lesions. Lesion severity was calculated by adding the individual lesion scores to create an overall score.

Quantitative Computed Tomography

CT scans were imported to a PC workstation for three-dimensional modeling using OsteoApp[e]. CT scans were cropped to 4-mm thick sections in the dorsal plane 30° palmar to the central axis of rotation or at specific sites in the sagittal plane in accordance with histologic sections (Figure 4.6 A). Voxel thresholding at 500 Hounsfield Units (Appendix 1) was used to create a three-dimensional volume of the cropped section (Figure 4.6 B). A region of interest was drawn by physically measuring the size of the histologic section and creating the same size area as the histologic section (Figure 4.6 C). Mean and standard deviation values were recorded in mg/ml TCP.

Lesion Grade	Features
Grade 1	Minor disruption of subchondral bone matrix. Lesion occupies <25% of histologic condylar surface, and extends no more than 1-2mm deep to the normal osteochondral junction. Some of the matrix within the lesion is pale staining and occasional marrow spaces contain debris. Tidemark is reduplicated. Fibrin may be present in the subchondral bone layer. No apparent superficial cartilage fibrillation.
Grade 2	More severe disruption of subchondral bone matrix. Areas of matrix are fragmented to comminuted. Lesion occupies 25-50% of histologic condylar surface and extends approximately 2-4 mm deep to the normal osteochondral junction. A significant amount of the subchondral matrix is pale staining, and there is significant debris within lesional marrow spaces. The tidemark is reduplicated and often disrupted. Moderate fibrin present in the subchondral bone layer. Cartilage overlying lesion is thickened with superficial cartilage erosion and fibrillation. Reparative fibrocartilage is also apparent in the superficial cartilage layers.
Grade 3	Complete collapse of osteochondral tissue. Lesion occupies >50% of histologic condylar surface and extends >3 mm deep to the normal osteochondral junction. Pale staining subchondral matrix and fibrin are abundant. The tidemark is reduplicated and often disrupted. Superficial thickened cartilage/fibrocartilage present and may be completely detached from thickened deeper cartilage.
Grade 4 *not observed	Obvious loss of osteochondral tissue leaving an ulcer.

Figure 4.3: Osteochondral lesion histologic grading scale

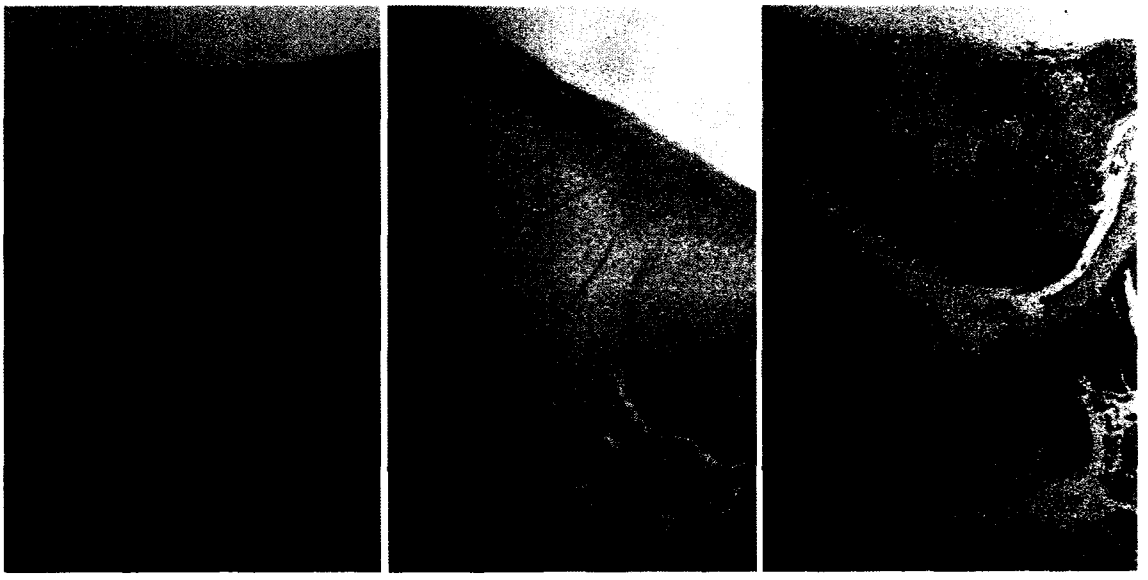

Figure 4.4: Grade 1-3 osteochondral lesion appearance on H&E staining. Far left is an photograph of grade 1 lesion, middle photograph a grade 2 lesion and far right photograph a grade 3 lesion.

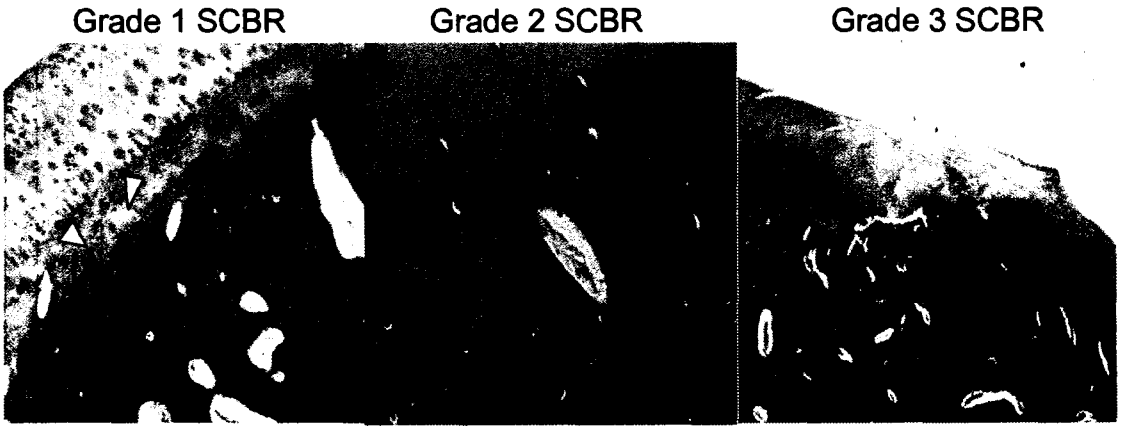

Figure 4.5: Severity of subchondral remodeling (SCBR) from 1-3. Grade 1 SCBR is advancement of the subchondral bone into the calcified cartilage layer with scalloped subchondral bone margins (arrowheads), but not crossing any tidemarks. Grade 2 SCBR is subchondral advancement through the calcified cartilage layer, crossing one or more tidemarks, but stopping at the tidemark front. Grade 3 SCBR is subchondral advancement through both the calcified cartilage layer and tidemark front (block arrow).

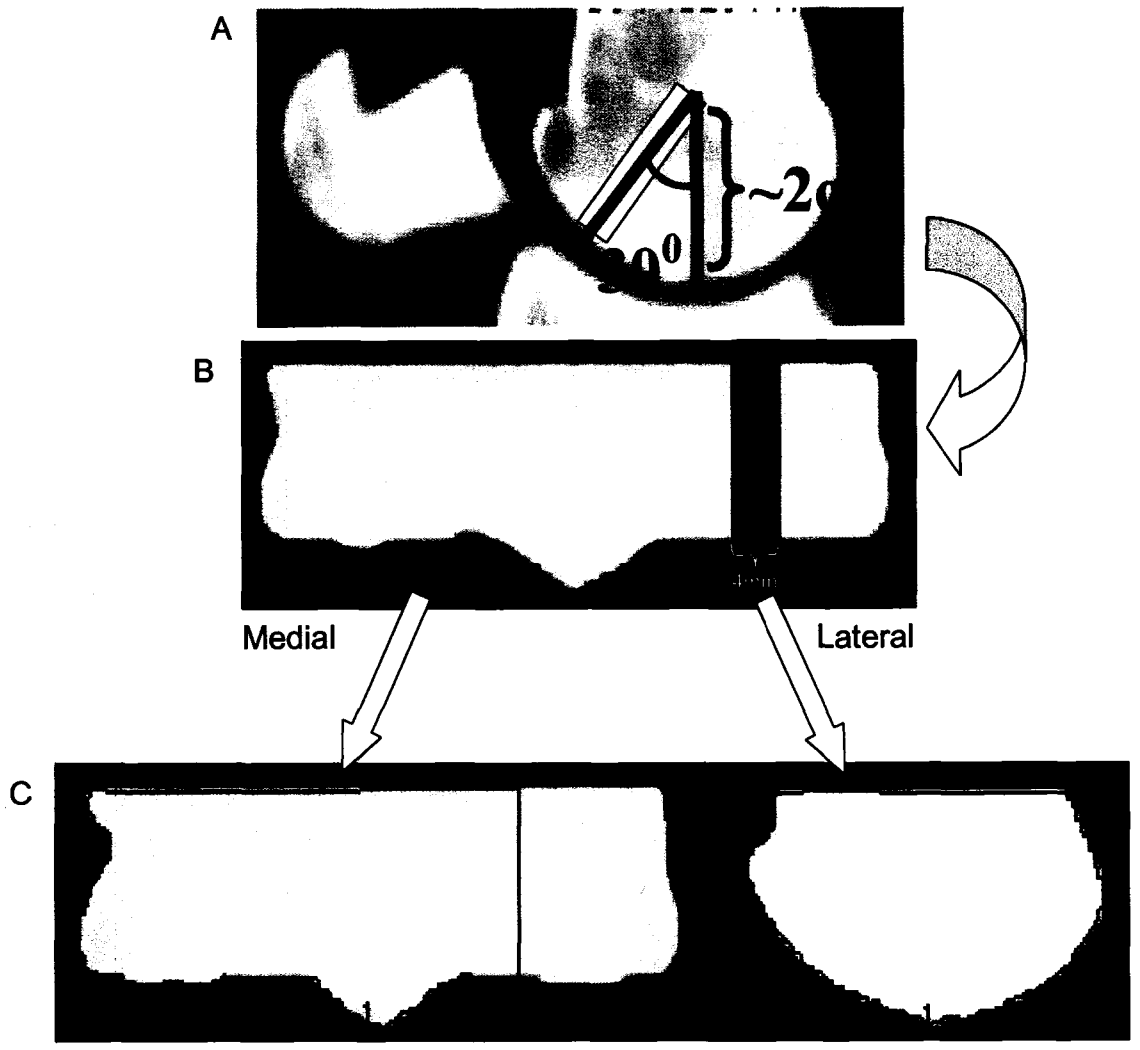

Figure 4.6: Flowchart of slice rendering. A) Measurement techniques to create a 30° palmar 4-mm thick section B) 3D representation of a palmar slice with sagittal slice previously removed as was done in cutting histologic sections C) Palmar and sagittal slices with ROIs drawn over areas of interest in accordance with histologic sections.

Statistical Analysis

Probability plots for lesion severity, number of lesions, mean density, mean voxel standard deviation, gross score, and age were examined for normality. Again, a logarithmic transformation of age was used (see Chapter 3 methods). Pearson's correlation coefficients were calculated for mean density, mean voxel standard deviation, age, subchondral remodeling score, percent subchondral bone, number of lesions, lesion severity score, and gross score for each histologic plane (sagittal or dorsal) and pooled data for both section planes. Terms were considered significant at $\alpha<0.05$, and a data trend was considered at $\alpha<0.10$.

A split-split plot analysis was performed with a backwards selection method ($\alpha=0.10$) for gross score, lesion severity and number of lesions as response variables and subchondral remodeling score, mean density, mean voxel standard deviation, section, limb and age as independent variables. Pairwise comparisons for significant categorical predictors was performed using Fisher's least significant differences. Subchondral remodeling score was also analyzed using a backward elimination method with mean density, mean voxel standard deviation, section, limb and age as predictors. Additionally, a logistic regression for each lesion grade was modeled with a backwards selection method ($\alpha=0.10$) for mean density, mean voxel standard deviation, and age.

Results

Only 13 of 18 possible dorsal slices were able to be graded, as sectioning of dorsal slices proved difficult (Figure 4.4) due to the large section size (3-5 cm in width). However, the objective was to evaluate architecture across the entire length of the dorsal slice hence the large section size. Horses 7 and 9 did not have any readable dorsal slices, and the right dorsal section of horse 6 was not cuttable. 17 of 18 sagittal slices were cut, with the left section of horse 4 being unreadable. In general, overdecalcification was a problem (Figure 4.7), but since staining characteristics were not graded, did not influence any subjective scoring.

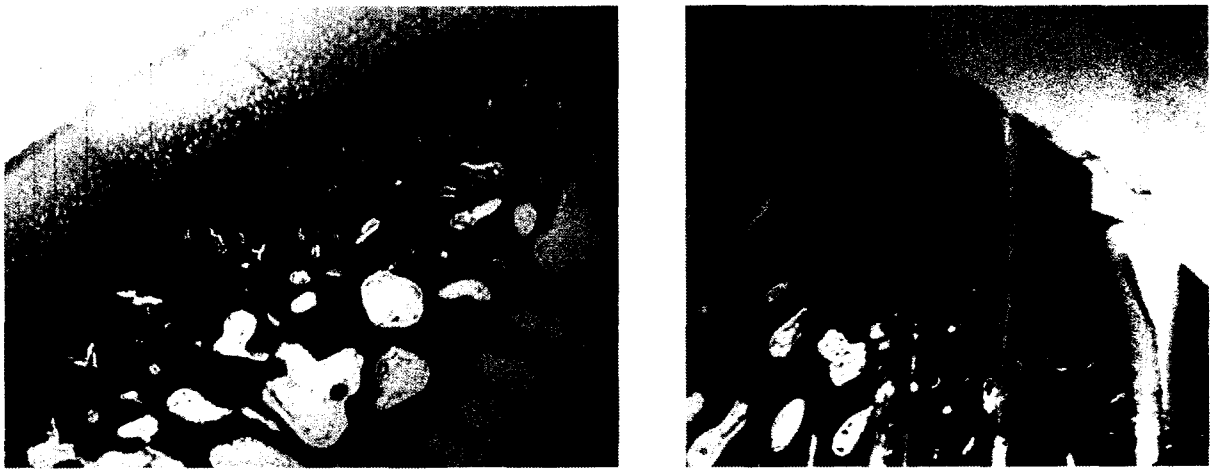

Figure 4.7: The left image is an example of a poorly staining section because of over decalcification. The cartilage should stain basophilic (purple). The right image is an example of an uncuttable section. The chatter marks from the microtome are so severe in areas that architecture cannot be graded, and in other sections caused loss of tissue over large areas.

Probability plots were acceptable, that is plots appeared linear, for all parameters except lesion severity (Figure 4.8b). A square-root transformation

was performed for lesion severity to normalize values (Figure 4.9) for split-split plot analysis.

Results

A total of eight grade one lesions (6/8 in left limbs, 2/8 in right limbs), six grade two lesions (3/6 in left limbs, 3/6 in right limbs), and one grade three lesion (left limb) were identified. Two grade one lesions were observed in the dorsal plane (both in left limbs) and four horses had grade one lesions in the sagittal plane (one horse with bilateral lesions, remaining three lesions were only in the right limb). Grade two lesions were observed in dorsal sections of two horses (one horse bilaterally, one horse right limb only), and in sagittal sections two horses had grade two lesions (one horse bilaterally, one horse right limb only). The only observed grade 3 lesion was found in the right dorsal slice (lateral condyle). This horse also had a grade two lesion in the medial condyle of the same dorsal section. Two other horses also had more than one lesion in a single section. One horse had a right sagittal section with a grade one lesion adjacent to the transverse ridge and a grade two lesion in the palmar aspect of the condyle. The other horse had two grade one lesions in the left medial condyle from a dorsal section.

Figure 4.8a: Normal probability plots of measured variables

Age

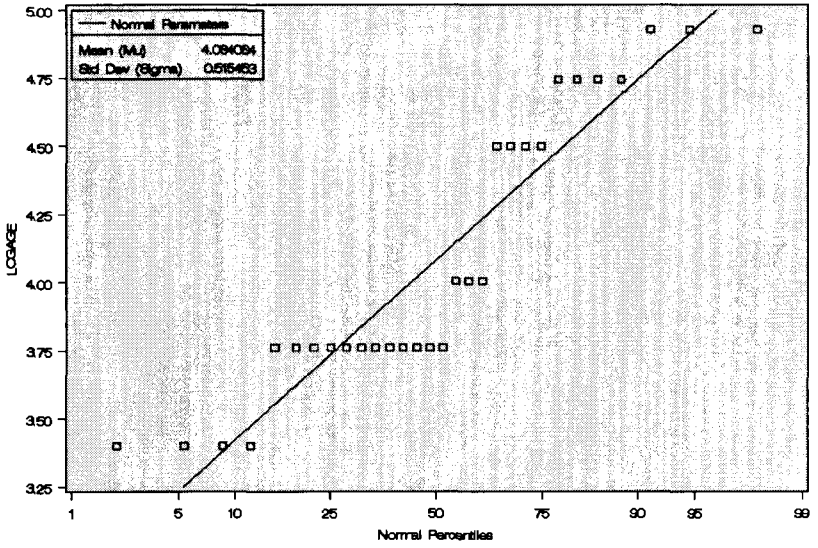

Gross Score

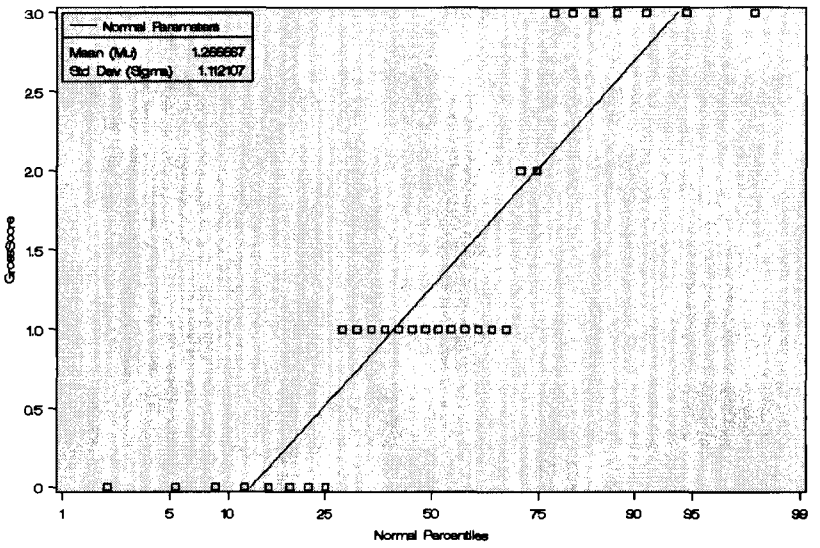

Mean Density (mg/ml TCP)

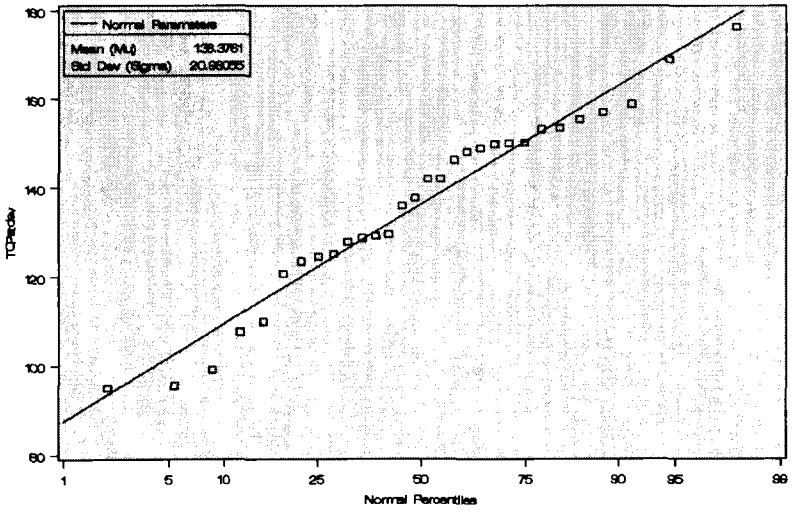

Mean Voxel Standard Deviation (mg/ml TCP)

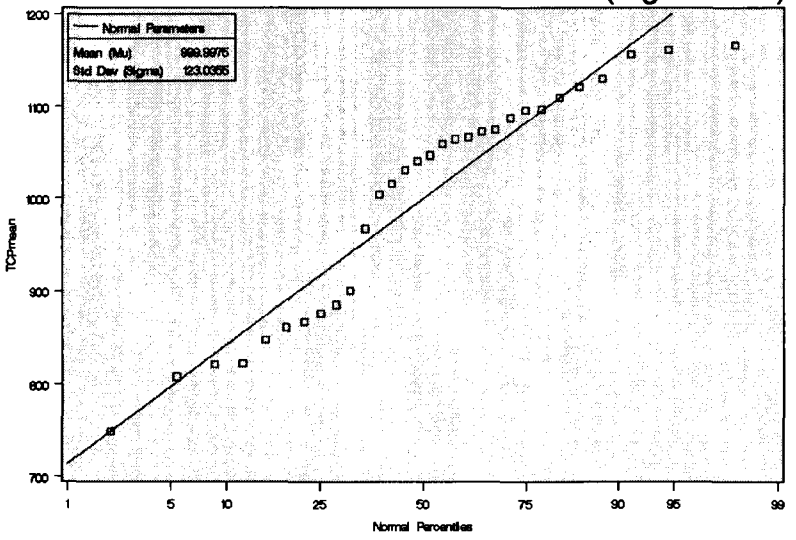

Figure 4.8b: Normal probability plots of measured variables

Subchondral Remodeling Score

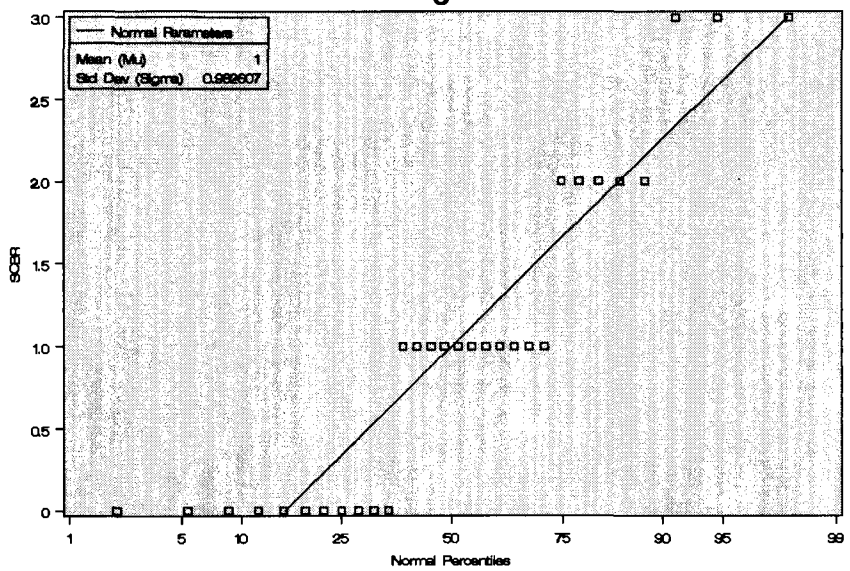

Subchondral Bone Percent

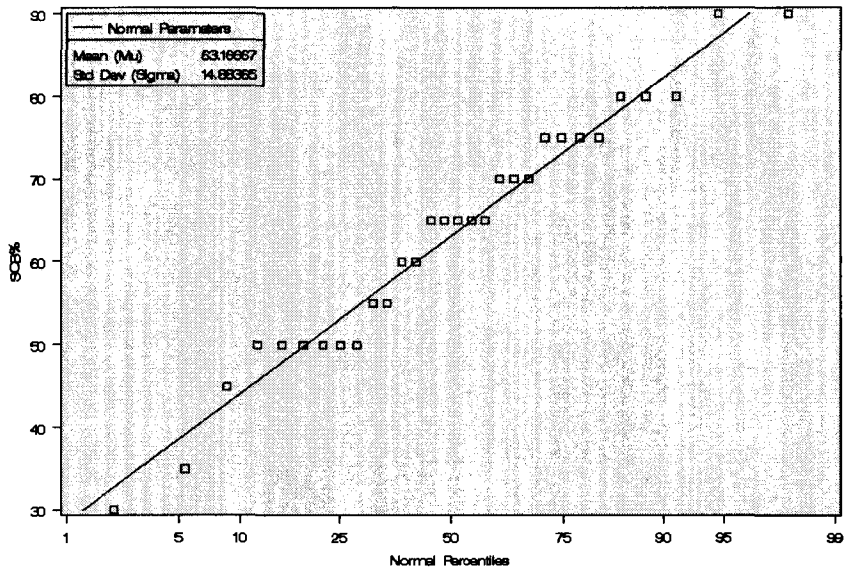

Number of Lesions

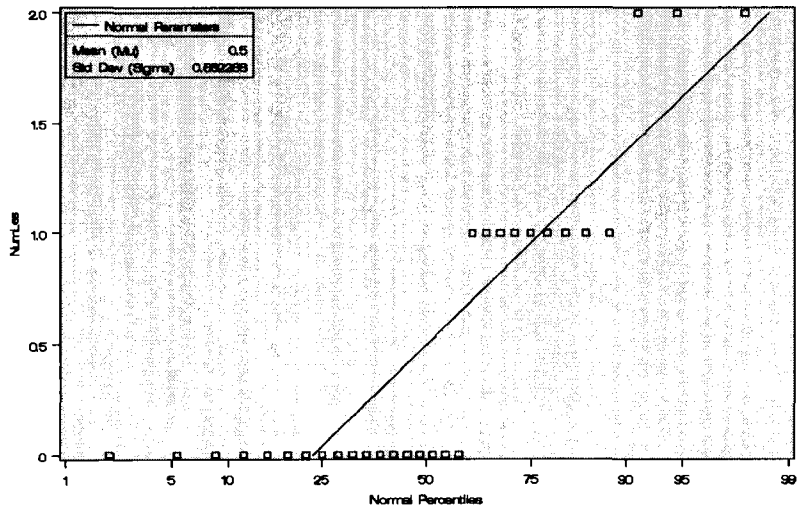

Figure 4.9: Normal probability plot of Lesion Severity (left graph) and the square-root transformation of lesion severity (right graph). The square-root transformation brings the values closer together and brings the line closer to normal, thus an appropriate transformation

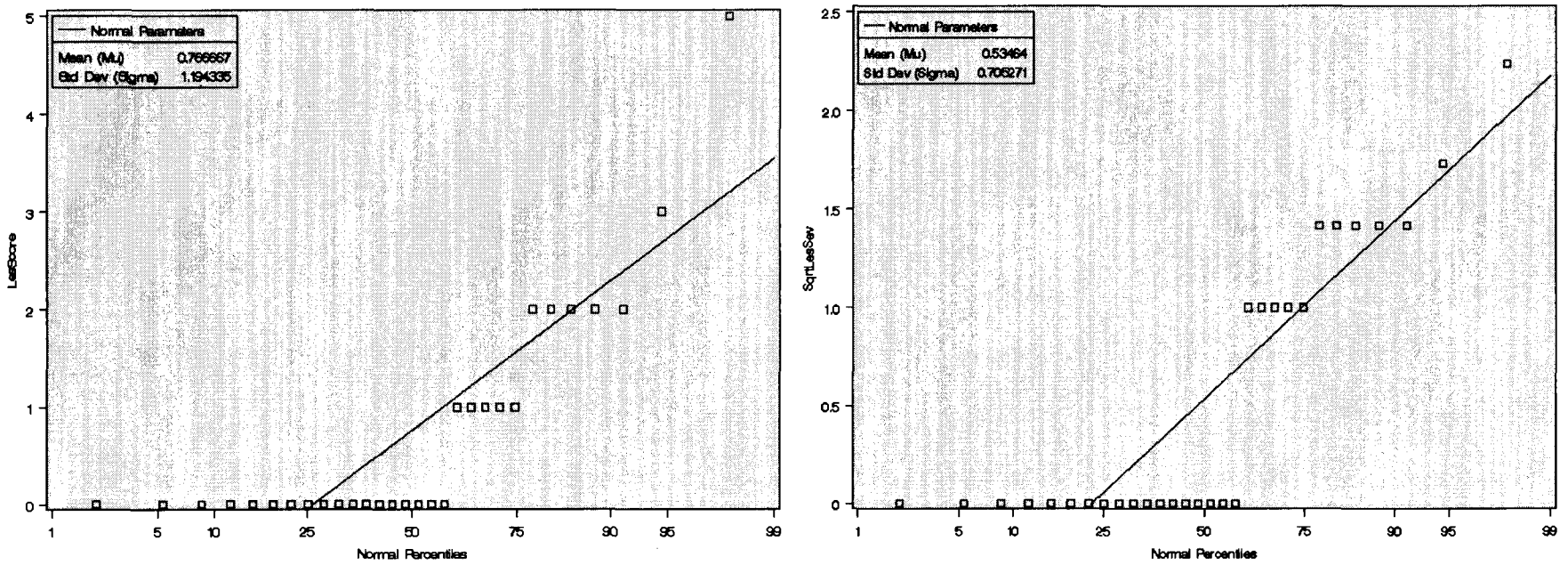

Raw data are listed in Figure 4.11. Average overall gross score was 1.29, with average gross score of left limbs being 1.5, and right limbs 1.11. Mean, standard deviation and standard error of the mean for measured variables for each section are listed below:

Section	N	Variable	Mean	SD	SEM
Dorsal	13	Mean (TCP)	986	131	36.5
		MVSD (TCP)	144	21.4	5.94
		LesScore	0.923	1.50	0.415
		NumLes	0.538	0.776	0.215
		GrossScore	1.23	1.17	0.323
		SCB%	70.8	12.4	3.43
		SCBR	0.692	0.947	0.263
Sagittal	17	Mean (TCP)	1010	119	28.9
		MVSD (TCP)	131	19.2	4.66
		LesScore	0.647	0.931	0.226
		NumLes	0.471	0.624	0.151
		GrossScore	1.29	1.10	0.268
		SCB%	57.4	14.2	3.46
		SCBR	1.24	0.970	0.235

Figure 4.11: Mean density, mean voxel standard deviation, presence of grade 1, 2, or 3 lesions (1=yes, 0=no), lesion severity, number of lesions, subchondral bone percentage, subchondral remodeling score and gross score for all viable sections

Horse	Limb	AGE	Section	Mean Den	MVSD	GR1Les	GR2Les	GR3Les	LesSeverity	#Lesions	SCB%	SCBR	GrossScore
1	Left	138	FR	1095.59	148.11	0	0	0	0	0	75	1	3
1	Right	138	FR	1065.92	149.80	0	1	0	2	1	80	2	3
2	Left	90	FR	1040.03	176.47	0	0	0	0	0	70	0	1
2	Right	90	FR	1003.92	169.02	0	0	0	0	0	90	1	1
3	Left	30	FR	821.38	155.50	0	0	0	0	0	60	0	0
3	Right	30	FR	748.79	142.00	0	0	0	0	0	65	0	0
4	Left	55	FR	1030.62	158.85	0	0	0	0	0	70	0	1
4	Right	55	FR	967.30	156.98	0	0	0	0	0	75	0	0
5	Left	115	FR	867.02	129.56	1	0	0	2	2	60	0	1
5	Right	115	FR	821.92	137.83	0	0	0	0	0	45	1	1
7	Left	43	FR	1166.40	95.07	1	0	0	1	1	90	0	0
9	Left	43	FR	1129.96	124.54	0	1	1	5	2	75	3	3
9	Right	43	FR	1064.00	128.74	0	1	0	2	1	65	1	2

Mean Den=mean density (mg/ml TCP), MVSD=mean voxel standard deviation (mg/ml TCP), GR1=grade one, GR2=grade two, GR3=grade three, LesSeverity=lesion severity, SCBR=subchondral remodeling score, FR=dorsal, SAG=sagittal

Figure 4.12: Mean density, mean voxel standard deviation, presence of grade 1, 2, or 3 lesions (1=yes, 0=no), lesion severity, number of lesions, subchondral bone percentage, subchondral remodeling score and gross score for all viable sections

Horse	Limb	AGE	Section	TCPmean	TCPstdev	GR1Les	GR2Les	GR3Les	LesSeverity	#Lesions	SCB%	SCBR	GrossScore
1	Left	138	SAG	1161.26	150.23	0	1	0	2	1	80	2	3
1	Right	138	SAG	1074.33	150.05	1	1	0	3	2	70	2	3
2	Left	90	SAG	1087.53	148.91	0	0	0	0	0	65	1	1
2	Right	90	SAG	1072.36	153.53	1	0	0	1	1	50	1	1
3	Left	30	SAG	847.59	153.26	0	0	0	0	0	35	0	0
3	Right	30	SAG	807.91	125.22	0	0	0	0	0	30	0	0
4	Right	55	SAG	1015.96	142.01	0	0	0	0	0	50	1	0
5	Left	115	SAG	860.53	109.90	0	0	0	0	0	50	1	1
5	Right	115	SAG	900.39	129.18	1	0	0	1	1	50	1	1
6	Left	43	SAG	1096.44	107.58	0	0	0	0	0	55	0	1
6	Right	43	SAG	1046.47	127.86	0	0	0	0	0	55	0	1
7	Left	43	SAG	1156.34	95.50	1	0	0	1	1	50	3	0
7	Right	43	SAG	1120.92	123.50	1	0	0	1	1	80	2	1
8	Left	43	SAG	875.71	146.25	0	0	0	0	0	50	1	3
8	Right	43	SAG	885.13	136.03	0	1	0	2	1	65	3	1
9	Left	43	SAG	1058.50	120.65	0	0	0	0	0	65	1	3
9	Right	43	SAG	1109.69	99.15	0	0	0	0	0	75	2	2

Mean Den=mean density (mg/ml TCP), Mean SD=mean voxel standard deviation (mg/ml TCP), GR1=grade one, GR2=grade two, GR3=grade three, LesSeverity=lesion severity, SCBR=subchondral remodeling score, FR=dorsal, SAG=sagittal

Interestingly, a unique lesion of the calcified cartilage was observed when samples were being subjectively evaluated for osteochondral lesions. The calcified cartilage had vertically oriented splits. These splits appeared to range in severity (Figure 4.13) from mild to severe and were localized to the condylar groove. Although some splitting of the calcified cartilage matrix can be attributed to artifact, the vertically oriented splits seen here were thought to be actual representations of matrix defects because debris and fibrin were seen within the splits.

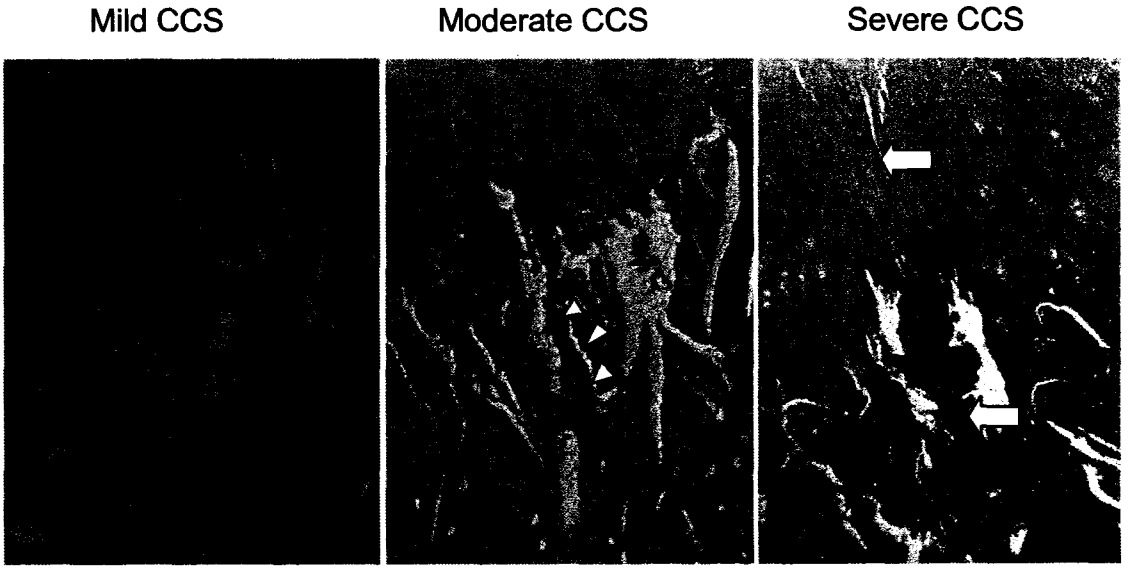

Figure 4.13: Severity of calcified cartilage splitting (CCS) from mild to severe. Mild splits involve the tidemark and subchondral bone, but are simple linear defects. Moderate splits have debris (arrowheads) within the split and connection of several splits. Severe splits involve articular cartilage and proximal displacement of the calcified cartilage layer into the underlying subchondral bone (block arrows).

Pearson's correlation coefficients for dorsal slices, sagittal slices, and pooled slices are listed in Figure 4.16. Mean density correlated well with subchondral bone percent for pooled ($r=0.84$, $p<0.001$), dorsal ($r=0.90$, $p<0.0001$), and sagittal ($r=0.80$, $p=0.001$) slices. Weak, but significant correlations were found between mean density and SCBR score ($r=0.38$, $p=0.04$) and gross score ($r=0.36$, $p=0.04$) for pooled slice data. A trend in correlations of mean density and lesion severity of pooled slices ($r=0.34$, $p=0.07$), and mean density and gross score of dorsal slices ($r=0.36$, $p=0.05$) was observed. Age and number of lesions ($r=0.52$, $p=0.03$) and lesion severity ($r=0.50$, $p=0.04$) in sagittal sections were significantly correlated. In pooled slices, age and gross score had a significant correlation ($r=0.43$, $p=0.02$), but sagittal slices were non-significant ($r=0.39$, $p=0.13$) and only a data trend existed in dorsal slices ($r=0.49$, 0.09).

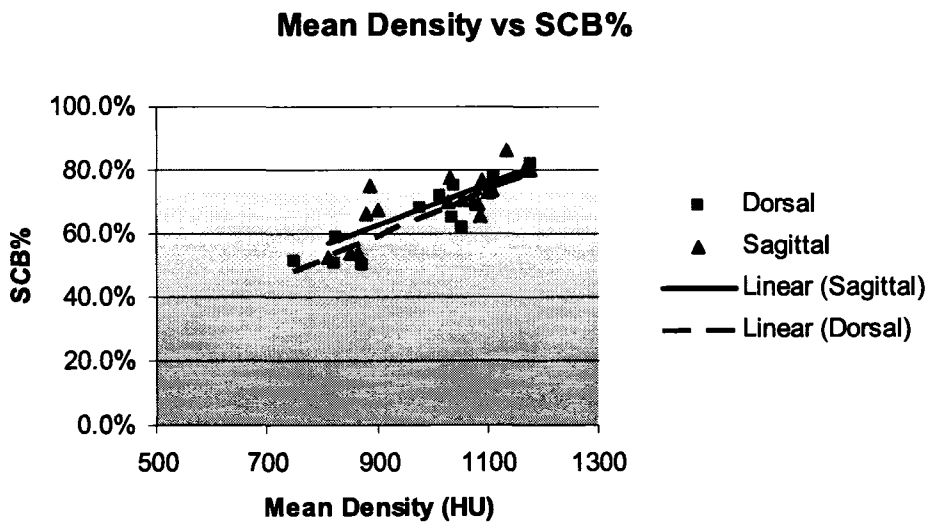

Figure 4.14: Mean density vs. subchondral bone percent with linear regression lines for each histologic plane (dorsal or sagittal).

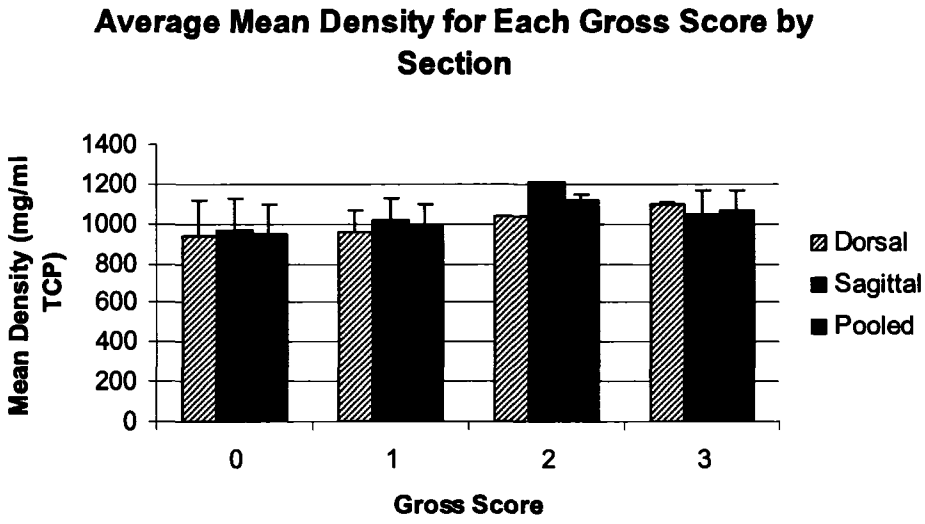

Figure 4.15: Average mean density by section for each superficial palmar gross score.

Mean standard voxel deviation did not correlate with any parameters. Number of lesions correlated significantly with subchondral remodeling score for pooled (r=0.51, p=0.0036) and sagittal (r=0.63, p=0.0007) slices but not for dorsal slices (r=0.47, p=0.11). Lesion severity correlations with subchondral remodeling were highly significant and correlated well for all slices (r=0.62, p=0.0003 pooled, r=0.63, p=0.02 dorsal, r=0.69, p=0.002 sagittal). Finally, gross score and subchondral remodeling score were highly correlated in dorsal slices (r=0.82, p=0.0005), and marginally correlated to pooled slices (r=0.47, p=0.008).

Subchondral bone percent only correlated significantly with sagittal slice gross score (r=0.61, p=0.01) in addition to the previously mentioned mean density correlations. Trends existed with correlations of subchondral bone

percent and sagittal slice lesion severity (r=0.51, p=0.03), and pooled slice gross score (r=0.36, p=0.05). A trend was observed between gross score and lesion severity for dorsal slices (r=0.53, p=0.06).

Figure 4.16: Pearson's correlation coefficients (r) for histologic grading parameters, gross score, age, mean density, mean and standard deviation. P-values of coefficients are in parentheses.

EFFECT	SECTION	# LESIONS	LESION SEV.	SCB%	SCBR	GROSS SCORE
AGE	BOTH	0.27 (0.14)	0.24 (0.20)	0.05 (0.80)	0.18 (0.34)	0.43 (0.02)
	FR	0.03 (0.93)	-0.08 (0.79)	0.0023 (0.99)	0.22 (0.48)	0.49 (0.09)
	SAG	0.52 (0.03)	0.50 (0.04)	0.16 (0.55)	0.22 (0.39)	0.39 (0.13)
MEAN (mg/ml TCP)	BOTH	0.29 (0.12)	0.34 (0.07)	0.84 (0.001)	0.39 (0.04)	0.36 (0.05)
	FR	0.31 (0.30)	0.41 (0.16)	0.90 (<0.001)	0.42 (0.15)	0.50 (0.08)
	SAG	0.30 (0.24)	0.25 (0.32)	0.69 (0.002)	0.38 (0.13)	0.27 (0.30)
MVSD (mg/ml TCP)	BOTH	-0.13 (0.49)	-0.09 (0.62)	-0.10 (0.59)	-0.11 (0.56)	0.28 (0.12)
	FR	-0.41 (0.17)	-0.33 (0.28)	-0.12 (0.68)	0.06 (0.85)	0.23 (0.44)
	SAG	0.23 (0.38)	0.31 (0.23)	-0.04 (0.89)	-0.17 (0.52)	0.19 (0.46)
LIMB	BOTH	0.05 (0.79)	0.03 (0.88)	-0.011 (0.95)	0.14 (0.47)	-0.12 (0.52)
	FR	-0.25 (0.40)	-0.16 (0.59)	-0.28 (0.34)	0.14 (0.64)	-0.05 (0.87)
	SAG	0.34 (0.17)	0.28 (0.27)	0.08 (0.77)	0.11 (0.67)	-0.18 (0.49)

Figure 4.16 (Cont.)

	SECTION	SCB%	SCBR	GROSS SCORE
# LESIONS	BOTH	0.25 (0.19)	0.51 (0.0036)	0.32 (0.09)
	FR	0.04 (0.88)	0.47 (0.11)	0.40 (0.17)
	SAG	0.49 (0.05)	0.63 (0.007)	0.24 (0.35)
LESION SEVERITY	BOTH	0.32 (0.09)	0.62 (0.0003)	0.38 (0.04)
	FR	0.16 (0.59)	0.63 (0.02)	0.53 (0.06)
	SAG	0.51 (0.03)	0.69 (0.002)	0.24 (0.35)
GROSS SCORE	BOTH	0.35 (0.06)	0.47 (0.008)	1.0
	FR	0.33 (0.27)	0.82 (0.0005)	1.0
	SAG	0.38 (0.13)	0.22 (0.39)	1.0

Using the backward elimination method, gross score significantly associated with limb (p=0.03) with left limbs having higher gross scores than right limbs. A trend for gross score and MVSD (p=0.08), and no interactions were significant. Lesion severity was only predicted significantly by subchondral remodeling score (p=0.003). Significant differences are depicted in Figure 4.8. Grade 2 SCBR had significantly higher lesion severity scores than grade 0 and grade 1 SCBR. Grade 3 SCBR had significantly higher lesion severity scores than grade 0 and 1 SCBR but not grade 2 SCBR. Lesion severity between grade 1 SCBR was not significantly different than grade 0 SCBR. Number of lesions was also predicted significantly by subchondral remodeling score (p=0.008), but age was a trend in association (p=0.05). The interaction of age and subchondral remodeling score was not significant (p=0.18). Significant differences are depicted in Figure 4.9. In contrast to lesion severity scores, grade 2 SCBR had significantly higher number of lesions that grade 1 (p=0.03) but not grade 0. Grade 3 SCBR had significantly higher number of lesions than grade 0 (p=0.008) and 1 (p=0.002). SCBR was significantly associated with SCB% (p=0.04), but no other terms were significant.

There was a negative trend in probability of having a grade one lesion for mean voxel standard deviation (p=0.05). The odds ratio for mean voxel standard deviation and grade 1 lesions was OR=0.951 (CI:0.905-0.998). However, no terms were significant for grade 2 or grade 3 lesions.

Figure 4.17: Number of lesions for each subchondral remodeling score adjusted for age. Grade three subchondral remodeling score is significantly greater from grade one and zero ($p<0.007$), but not grade two ($p=0.15$). Grade two subchondral remodeling score is significantly greater than grade zero ($p=0.03$), but not for grade one ($p=0.23$)

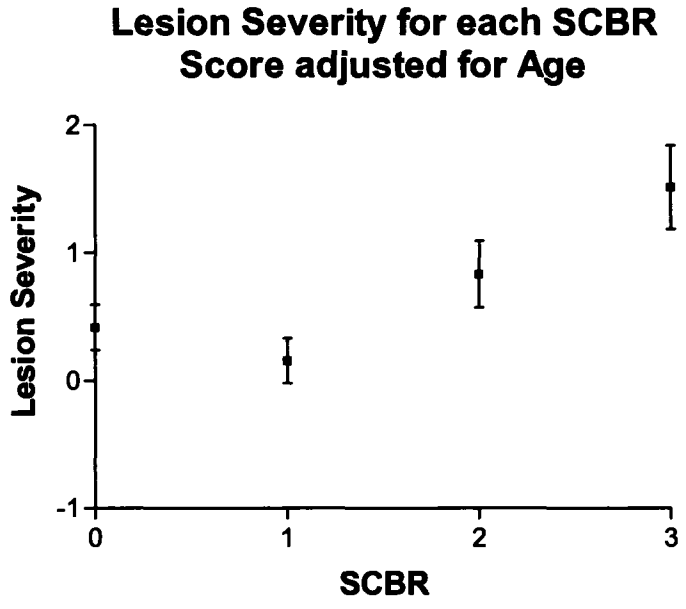

Figure 4.18: Graph of lesion severity for each subchondral remodeling score adjusted for age. Grade three subchondral remodeling score is significantly greater from grade one and zero ($p<0.003$), but not grade two ($p=0.37$). Grade two subchondral remodeling score is significantly greater than grade one and grade zero ($p=0.02$).

Discussion

Mean CT density predicted and correlated well with subchondral bone percent as determined by BV/TV measurement. This relationship is somewhat intuitive since both are measures of density. Although no direct comparisons of CT density and histologic measures or observations have been done in horses, previous studies in humans, mice and dogs have found good to excellent correlations of CT density with cortical porosity [142, 143] and amount of mineralized matrix[144, 145]. Furthermore, there has been no published work correlating CT density with subchondral bone density.

Mean CT density was not a good predictor of lesion severity or number of lesions, nor was there a good correlation with lesion severity or number of lesions. A weak correlation between mean CT density and gross score existed, but mean density was not associated with gross score when analyzed in a mixed-model regression. These results could be due to the small sample size and subsequently limited number of lesions, but the results from Chapter 3 also found that surface or palmar mean CT density is not a good predictor of superficial palmar gross pathologic score. Another possible reason for the weak relationship of mean CT density and gross pathologic score is if there is a biphasic distribution of osteochondral lesions in racehorses, as is evident by the break in distribution of the mean density probability plots. Thus, statistically your correlation would be weakened as you try to relate to two different populations

with two different variations. Also, there may truly be a lack of correlation between subchondral bone density and lesion severity.

The presence of a bimodal distribution, represented by a gap in data points of the mean CT density normality plots (Figure 4.8), suggest some lesions could be occurring during times of intense bone remodeling, which could reduce bone density, while other lesions may be occurring at a later stage of disease where increased bone density may predominate. The lower bone density could be a result of activated remodeling due to intense exercise. Currently, there is no published research linking a lower density, poor quality bone with condylar fractures of racehorses. However, Pool and Meagher observed that palmar osteochondral lesions ("traumatic osteochondrosis") occur in highly trained, mature racehorses and that condylar fractures commonly occur in young racing Thoroughbreds[88]. This supports the theory that condylar fractures may occur in horses with reduced subchondral bone density.

Focal areas of subchondral sclerosis and necrosis with surrounding bony remodeling are characteristic of palmar osteochondral lesions. This is seen as an increase in radiodensity[89, 111], and radiographic subchondral sclerosis has been found to be the most reliable index of damage to articular cartilage of the palmar third metacarpal bone[146]. Therefore, this supports the observation that there is a subset of racehorses with highly dense bone, and these horses are predisposed to palmar osteochondral lesions.

Although several studies[131, 132, 147, 148] have classified condylar fractures in racehorses, both radiographically and morphologically, none have evaluated subchondral sclerosis in association with condylar fractures. Also, the epidemiological distribution of condylar fractures is well documented[97] in relation to breed, gender, limb, and postoperative racing success. However, there seems to be little analysis of whether specific condylar fracture types (complete, complete non-displaced, incomplete[96]) occur at a particular age. One paper attempted to associate age with fracture configuration in 56 Thoroughbred racehorses[98], but no associations were found. Ages were classified as groups by year, and some groups lacked any fractures. This may have diminished any significant differences. Also, as was demonstrated in Chapter 3, outcomes may be a logarithmic function of age, so linear analysis may underestimate differences. Nonetheless, there appeared to be a weak correlation of age and mean density to gross pathologic score in this study.

The variability in condylar fracture incidence and prevalence may be related to the bimodal distribution seen in mean CT density in this study, warranting a different approach to the analysis of causality in condylar fractures and osteochondral damage in racehorses. Additionally, a significant relationship may exist between mean CT density and lesion if a larger sample of lesions could be obtained and stratified under these assumptions. In general, mean CT density proved to be a poor indicator of osteochondral lesions, but given the

small sample size and lack of previous studies further investigation is needed before the absence of a predictive relationship can be definitively established.

Although mean voxel standard deviation was associated with grade one lesions, but the associated risk was slight. This suggests that as bone density becomes more homogenous, amount and severity of subchondral lesions increase. In horses exercised for six months on a high-speed treadmill, a loss of incongruity in subchondral bone density was noted in the distal third metacarpal condyle in comparisons to controls as indicated by a significantly higher percentage of highly dense bone occupying the surface of the distal metacarpal condyle[86]. Also, palmar arthoses were higher in exercised horses[86] as well as an increase of microdamage index[39]. Thus, osteochondral damage was associated with horses predominated by a specific range of subchondral bone density, which supports the findings in this study that a decreased mean voxel standard deviation is associated with a greater number and severity of subchondral bone lesions. However, the odds ratio was not large enough to indicate a substantial increased risk. Again, given the small number of lesions in this study, this relationship is tenuous at best, particularly since the previous findings from Chapter three demonstrated a strong increase in MVSD in racing horses compared to exercised and non-racing horses. One possibility for this difference is that MVSD across a deeper, single section of bone may have a different relationship to osteochondral lesions than that of MVSD over a large

surface area of bone. Nonetheless, larger studies are warranted to determine if MVSD is more valuable than mean density in predicting osteochondral damage.

The vertical splitting of calcified cartilage has been observed in horses previously[32]. In that study, cracks (splits) were observed to extend into the subchondral bone as well as the articular cartilage of the third metacarpal condyle, as was seen in the present study. However, the location along the condyle of these calcified cartilage cracks was not given. In another study examination of pathologic lesions of equine distal third metacarpal bones[111], vertical cracks were found in the calcified cartilage and were associated with fracture lines in the palmar condylar groove of the distal third metacarpal bone. Splitting of the calcified cartilage layer has also been observed in spontaneous osteoarthritis hamster models, but splits were of a horizontal orientation in the plane of the tidemark[149]. Thus, calcified cartilage splitting may play a significant role in the development of fractures in racehorses and a further study to determine if calcified cartilage splitting is associated with condylar fractures is warranted.

The present study supported the association that subchondral remodeling plays a significant role in the development of palmar osteochondral lesions in racing horses. There were good correlations of subchondral remodeling score with number of lesions and lesion severity. Subchondral remodeling score was also significantly associated with lesion severity and number of lesions in a mixed

model analysis. While mean density was not associated with histologic lesions, it was mildly correlated with subchondral remodeling score indicating that increased density may be indirectly associated with lesion pathology. Limb differences in gross pathologic score suggest that left limbs are more susceptible to gross damage than right limbs. This supports reports that condylar fractures and catastrophic injuries are more common in the left limbs of racing horses[2, 97].

The subchondral remodeling scoring system used in this study is previously undocumented. Riggs et al[111], described similar differences in the severity of subchondral remodeling in pathologic distal third metacarpal condyles, but no direct comparisons were made with lesion outcome. The scoring system described here proved useful and predictive of osteochondral lesions but not necessarily gross pathologic change in racing horses. Thus, amount of subchondral remodeling should be considered in future histopathologic studies to further understand in the pathogenesis and determine predictability of these lesions.

In conclusion, mean CT density cannot be used to predict osteochondral lesions typical of racing horses. Mean voxel standard deviation had a slight association with mild osteochondral lesions in racing horses, and should be investigated in future studies as a potential predictor of osteochondral damage. Subchondral remodeling was observed in osteochondral lesions of racing horses

and the proposed subchondral remodeling scoring system was a good measure of osteochondral lesions in racing horses.

Chapter 5

Summary and Conclusions to Dissertation

Non-invasive measurement of bone density is well reported in humans and horses, but few studies specifically target subchondral bone density measurements using Quantitative Computed Tomography (QCT). Subchondral bone density mineralization patterns have been documented in humans, dogs, and horses, but no studies have examined the predictive relationship of subchondral bone density with gross pathologic osteochondral damage. Furthermore, no documentation exists of different subchondral mineralization patterns in joints as it pertains to age and use.

This study found that 3D-QCT accurately measures subchondral bone density in the distal third metacarpal bone of horses. Validity of 3D-QCT measures is important for the study of subchondral density characteristics in the equine population as well as predictive applications for fracture risk or osteochondral damage using 3D-QCT.

Secondly, it was determined that the mean density of the distal third metacarpal bone is significantly lower in racing as compared to exercised and non-racing horses. Mean density also increases with age in all three groups.

This finding is important as it emphasizes use and age should be accounted for with clinical applications of 3D-QCT.

Interestingly, Thoroughbred racehorses had overall increased density variations that may represent an objective measure of the steep density gradients previously observed in these horses. Also, male Thoroughbred racehorses had lower density distributions in comparison to female Thoroughbred racehorses. Thus, genetic influences, particularly in Thoroughbred racehorses, need to be examined to determine if catastrophic injuries are a heritable disease.

Contrary to our hypothesis, gross pathologic changes in the articular cartilage were not predicted by mean density or variations in density distributions. However, since there is no previous work quantitatively examining this relationship in horses using 3D-QCT, future studies with higher prevalences of gross pathologic changes are needed to determine if a lack of significant differences truly exists or was a result of overrepresentation of normal joints.

This study also demonstrated that CTO subchondral bone density patterns assessed visually indicate specific patterns are associated with use in horses. The pattern differences are related to the differences in load applied to the joint. However, we were not able to objectively measure the observable differences.

More advanced statistical programs are necessary to analyze the density maps, and hopefully will be available in the near future.

Future applications for CT modeling of subchondral bone density in racehorses should focus on possible breed and gender influences and include larger numbers of diseased bones or joints to further evaluate the effect of subchondral density variation as a possible fracture risk predictor.

Appendices

Appendix 1: Hounsfield Unit (HU) Threshold Determination

Several histograms were created from randomly selected horses within each group (racing, non-racing, and exercised) to subjectively determine where the HU threshold for bone exists. The following histogram plots, demonstrate that 500 HU is a suitable threshold for bone to create a region of interest (ROI). However, it must be noted that in some graphs subchondral bone values began below or above 500 HU. In the final models, small areas that appeared obviously as artifact were either added or removed manually to be included or excluded in the ROI. In relation to the total area, these subjective areas typically compromised a very small area, consistently less than 1% of the total area.

Histograms of Voxel Populations in Representative Horses

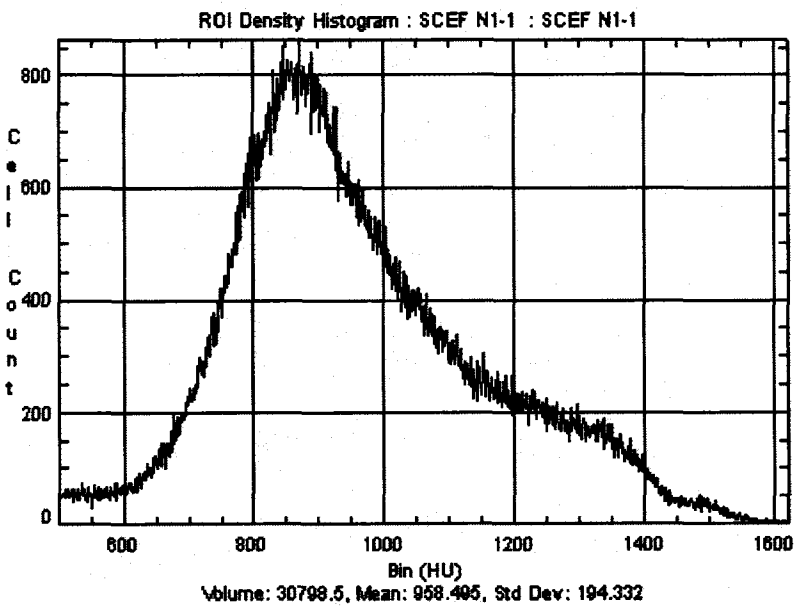

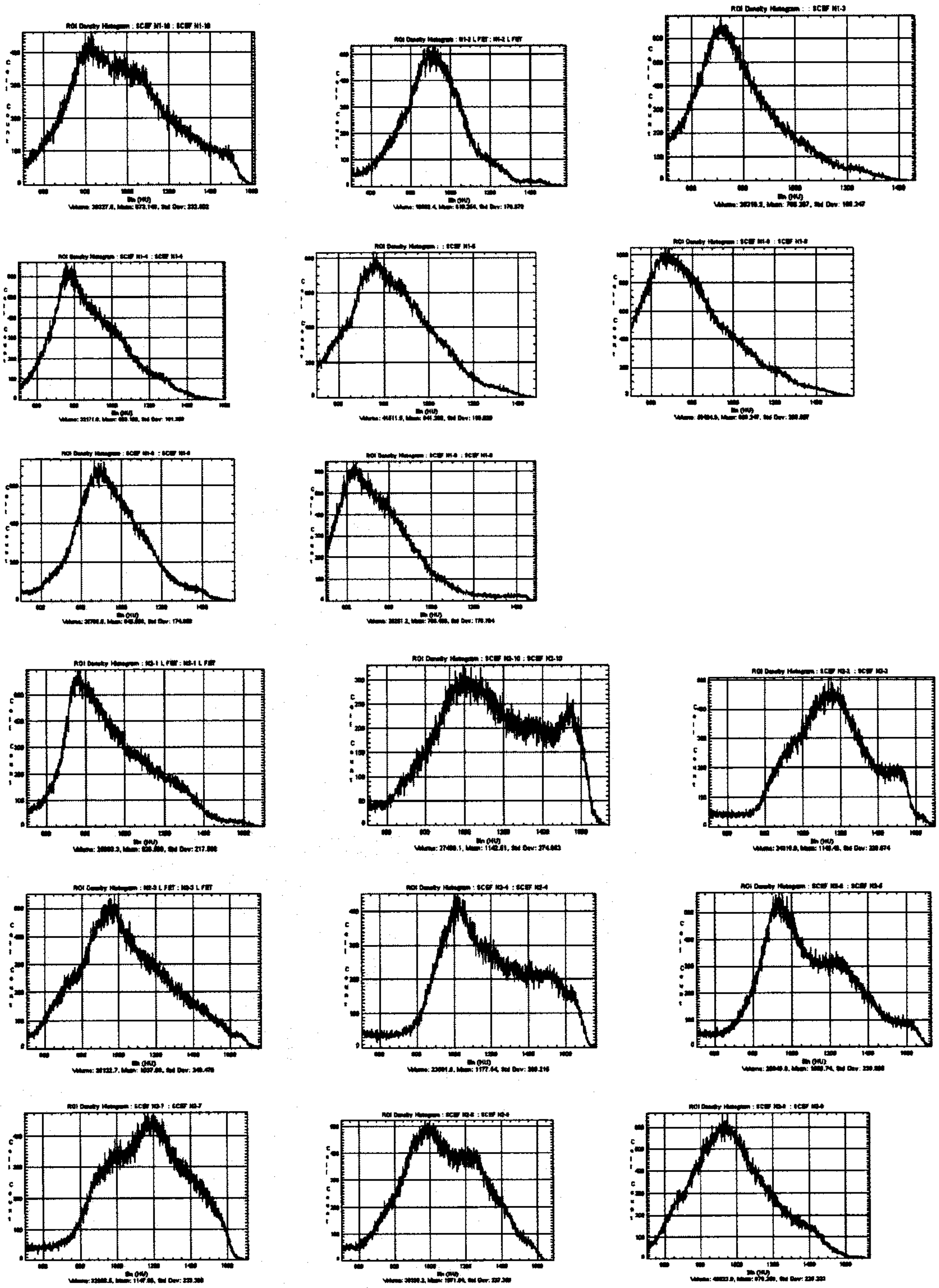

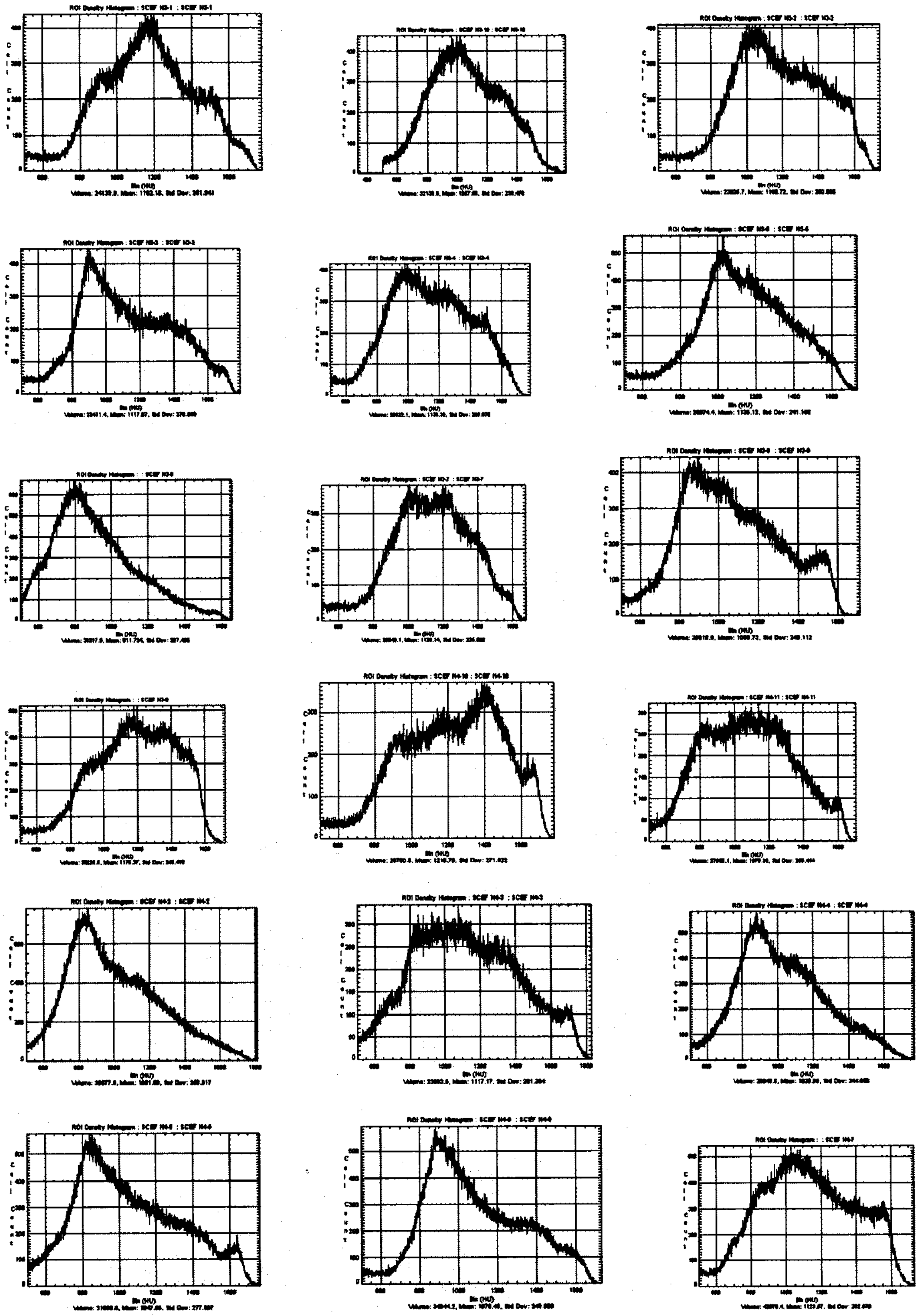

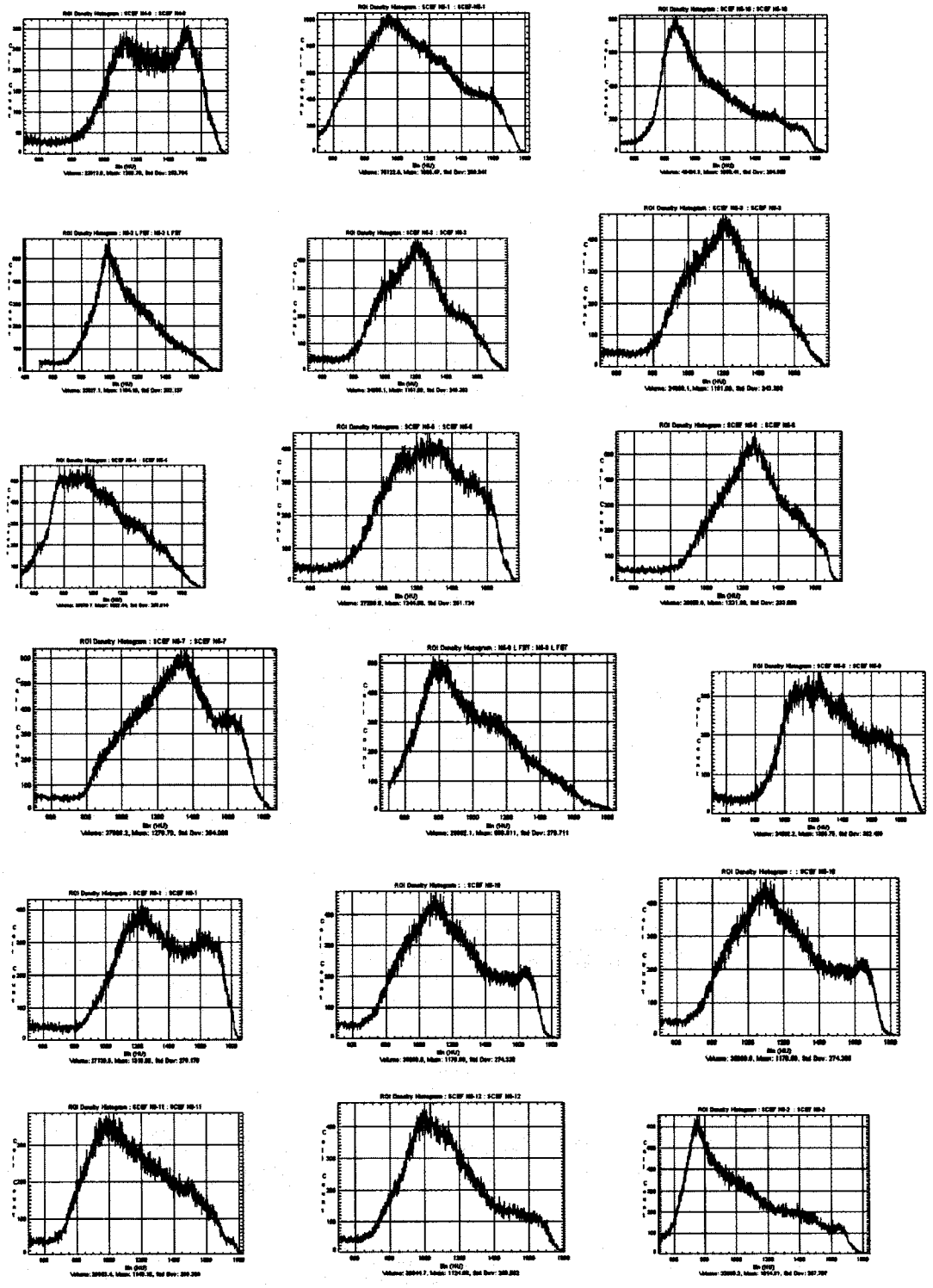

Appendix 3: CTO maps of subchondral bone density of the distal third metacarpal bone. Each map includes the subjective evaluation of the density pattern shape. Racehorses tended to have a "box" shape, exercised horses had a "flattened triangle", and non-racing horses had more triangular shaped density patterns, but also had "box" and "flattened triangle" shaped patterns. Ages are listed in addition to identification number. The following color scale represents differing densities:

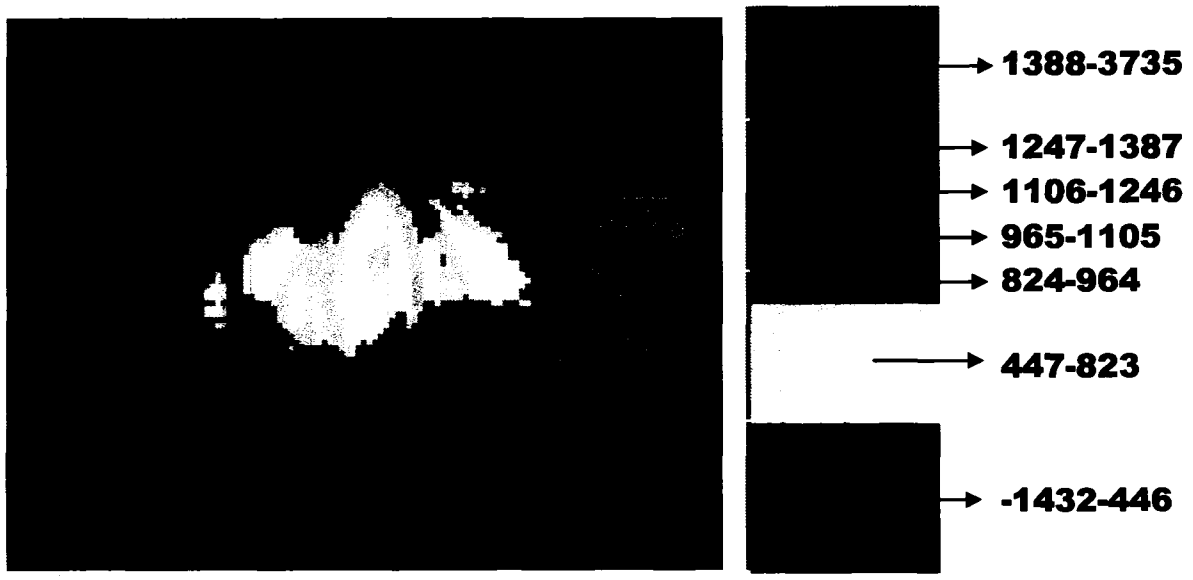

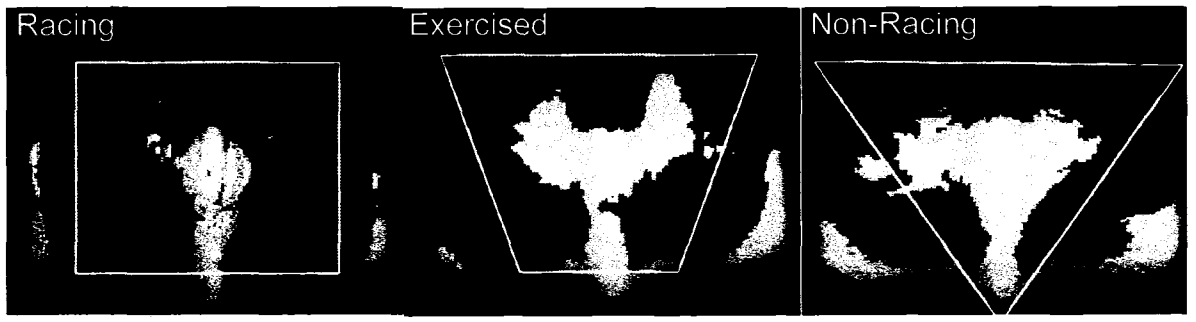

"Box" **"Flattened Triangle"** **"Triangle"**

Racing Horses

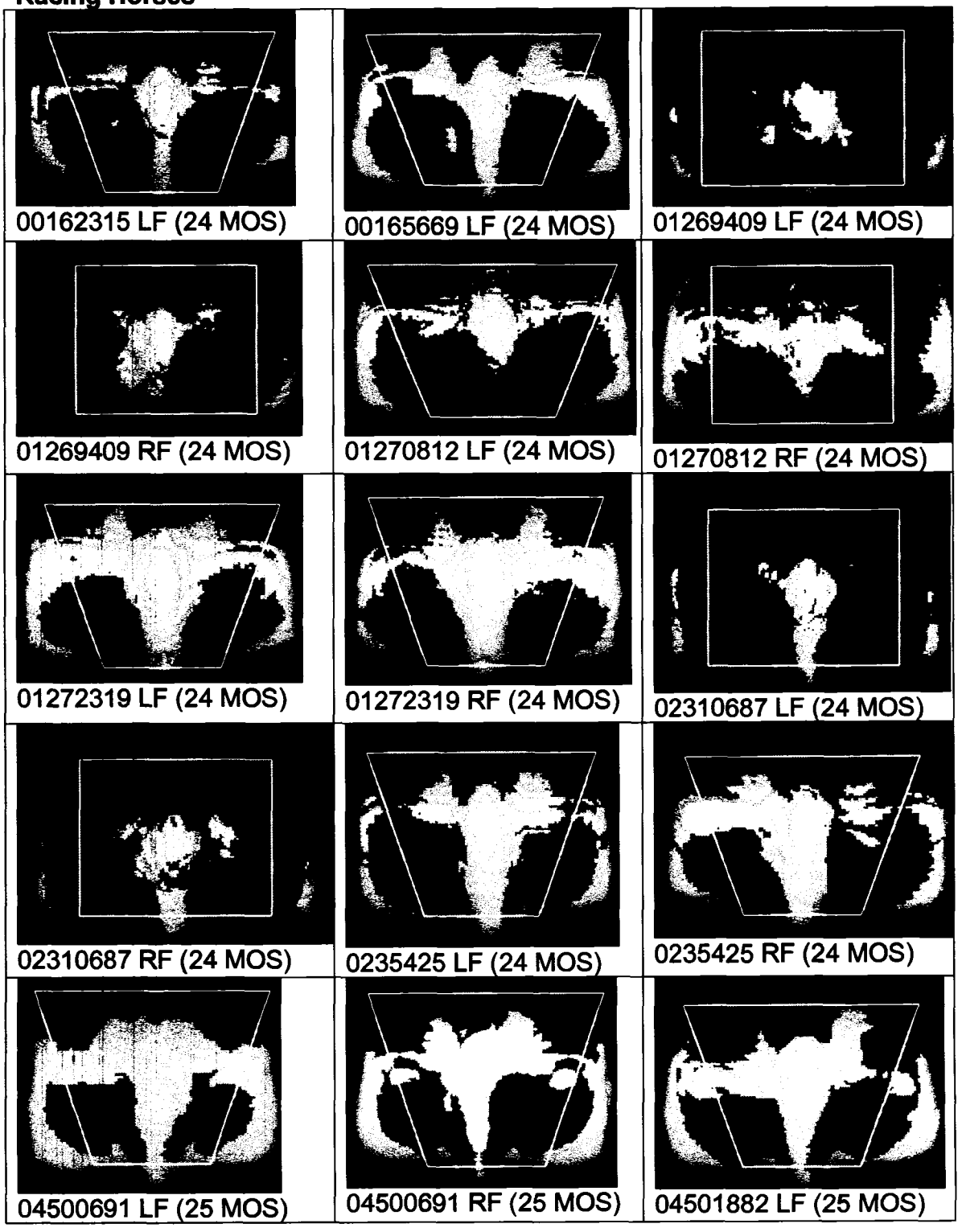

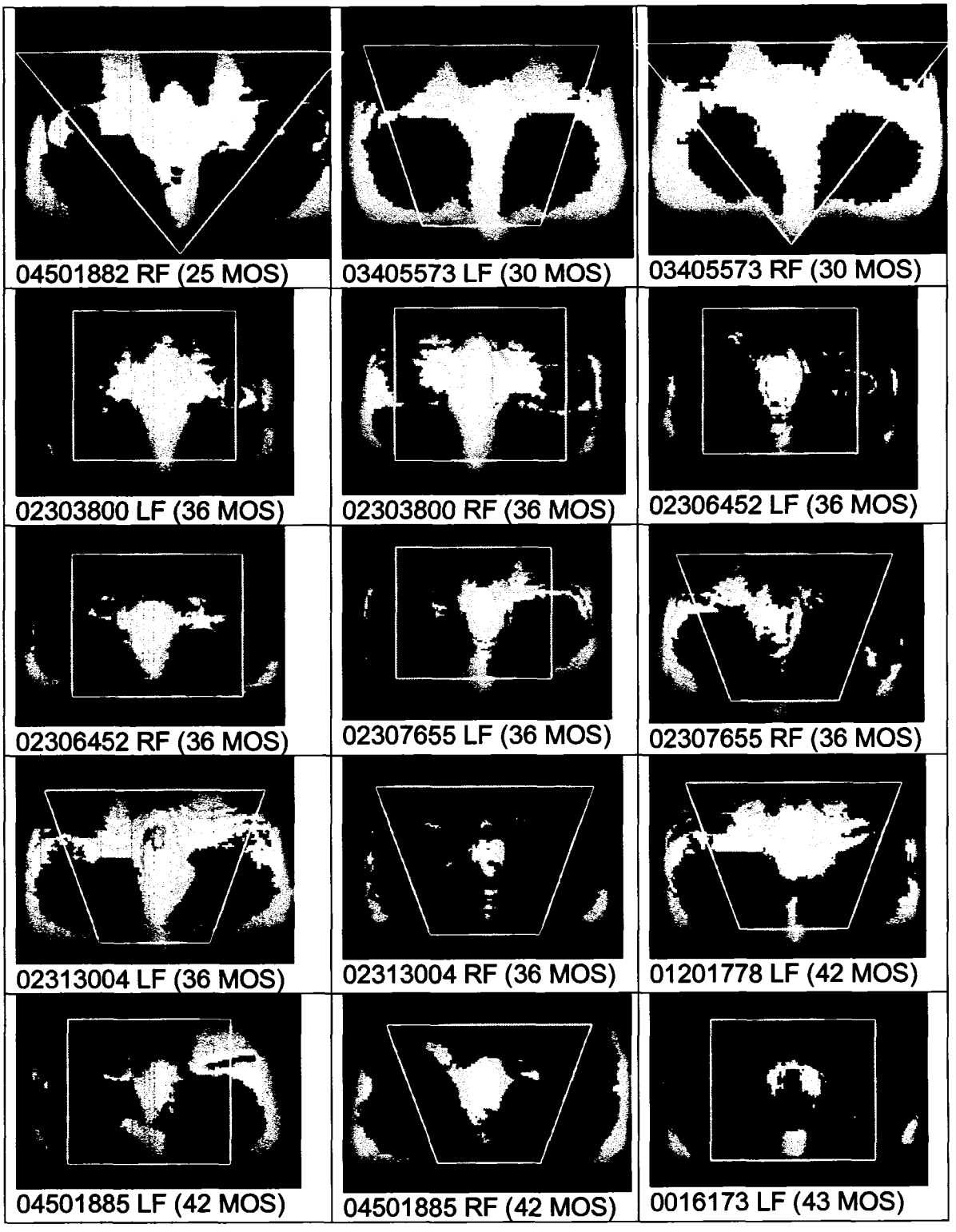

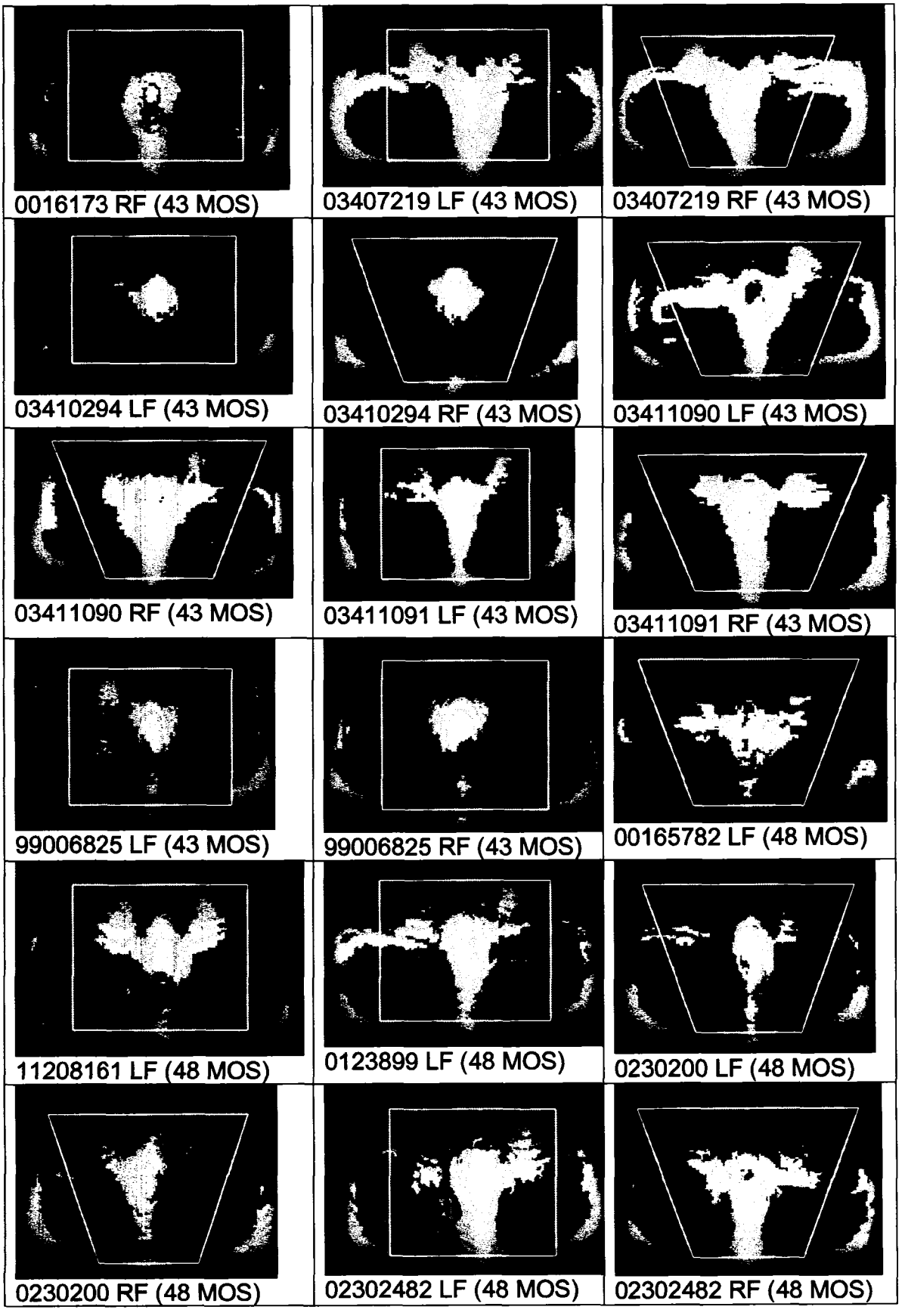

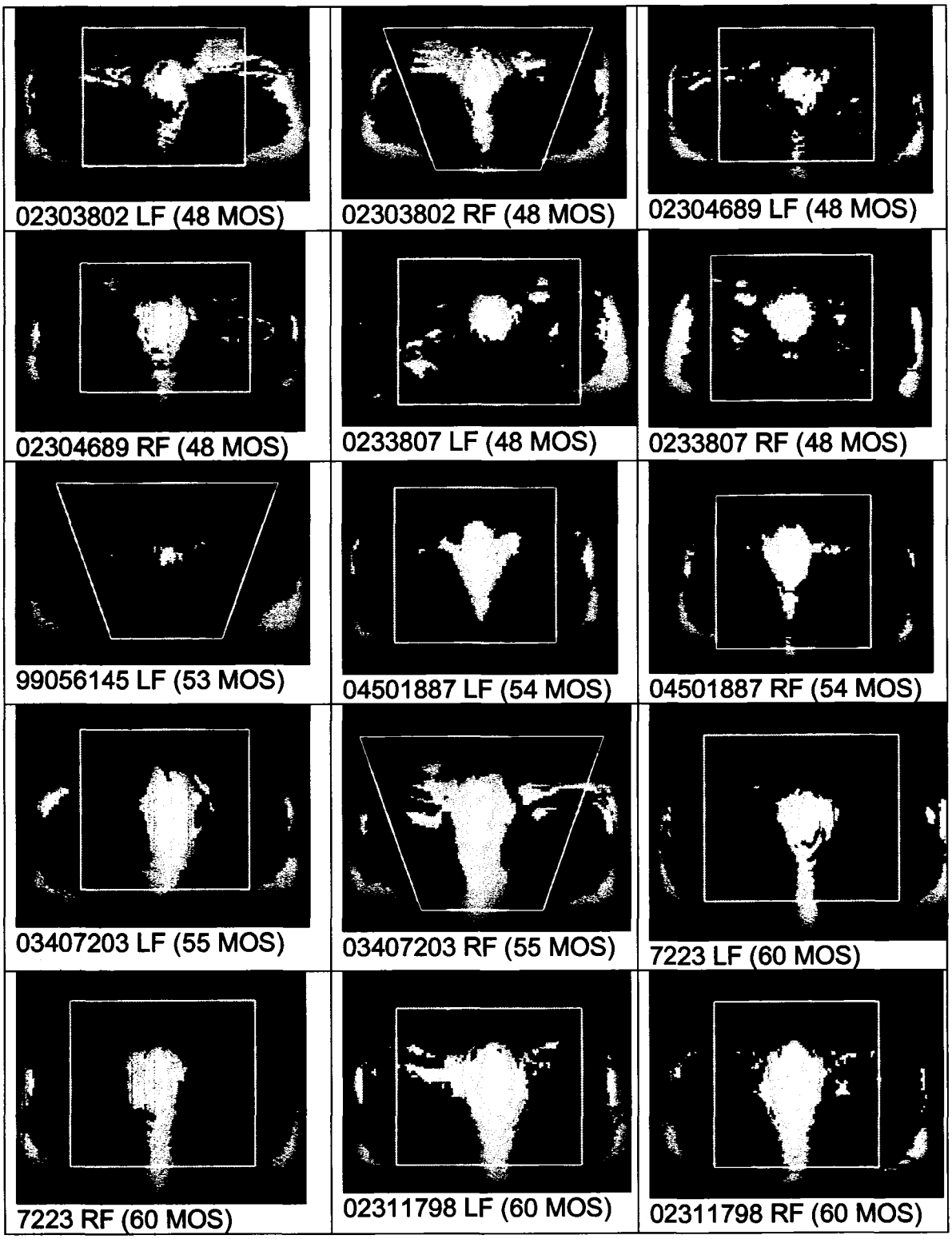

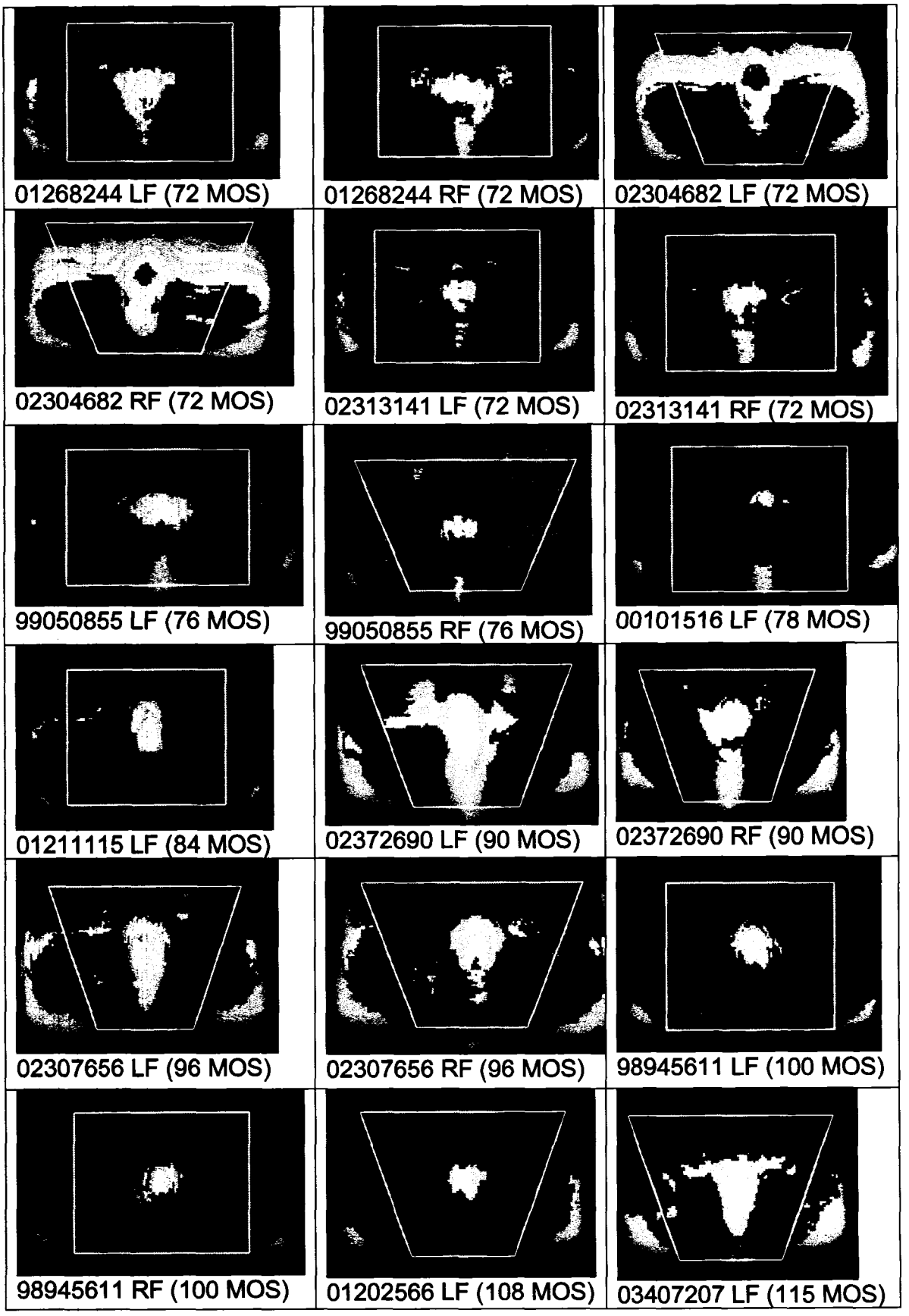

 03407207 RF (115 MOS)	 98945612 LF (136 MOS)	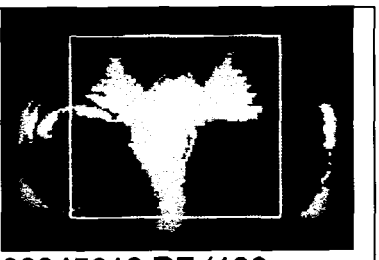 98945612 RF (136 MOS)
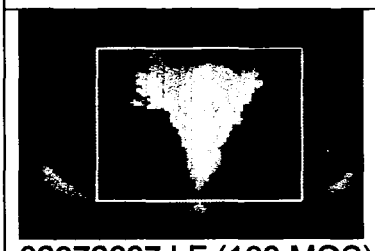 02372687 LF (138 MOS)	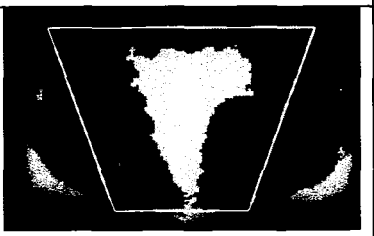 02372687 RF (138 MOS)	

Exercised Horses

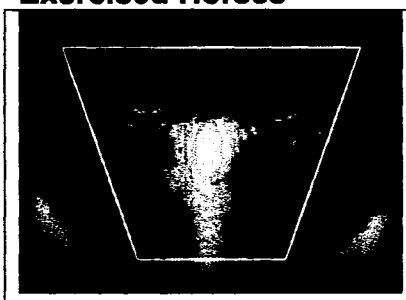
N2-2 (24 MOS)

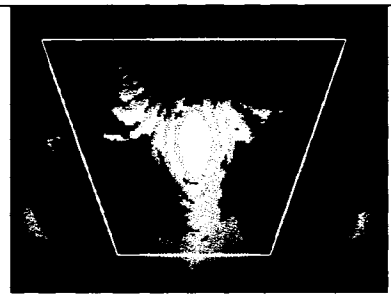
N2-3 (24 MOS)

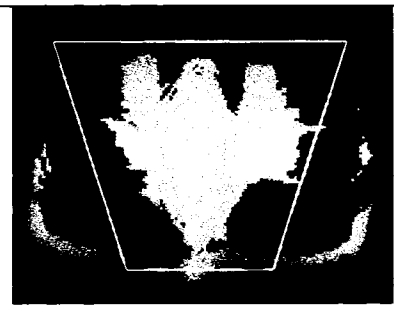
N2-1 (24 MOS)

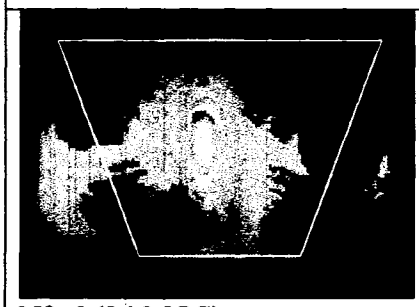
N2-6 (24 MOS)

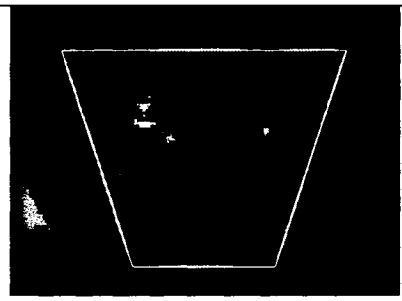
N2-7 (24 MOS)

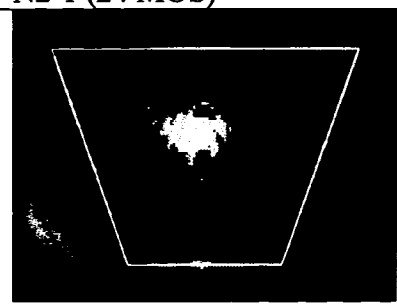
N2-5 (24 MOS)

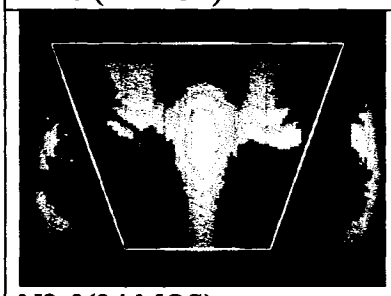
N2-9(24 MOS)

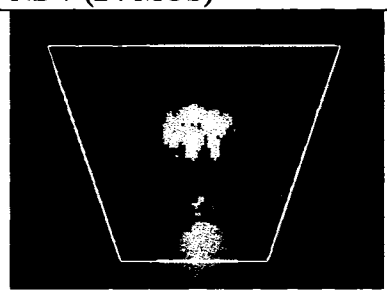
N2-10 (24 MOS)

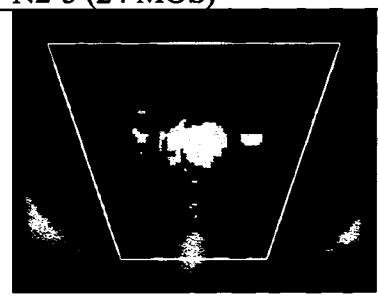
N2-8 (24 MOS)

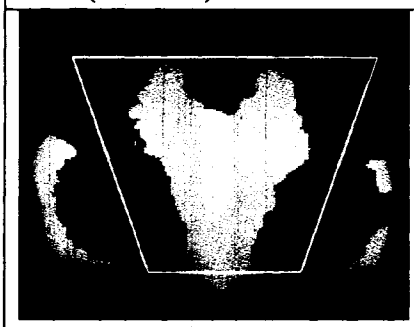
W22 R (27 MOS)

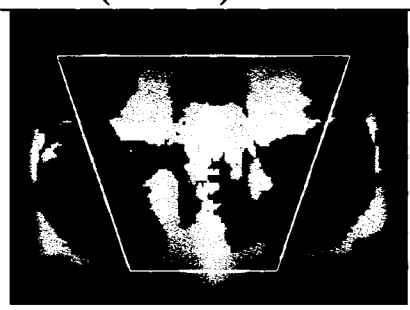
W26 L (27 MOS)

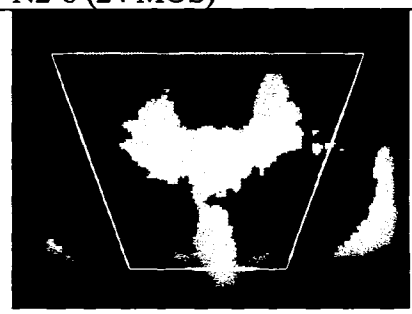
W17 L(27 MOS)

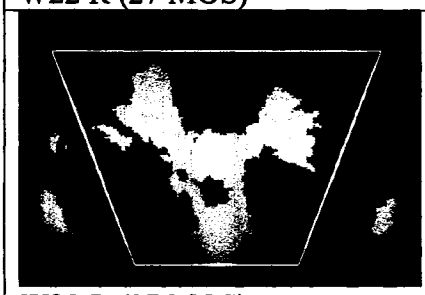
W29 R (27 MOS)

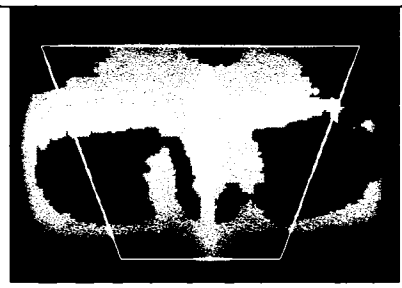
W23 L (33 MOS)

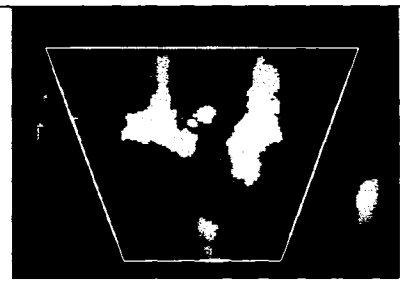
W28L (27 MOS)

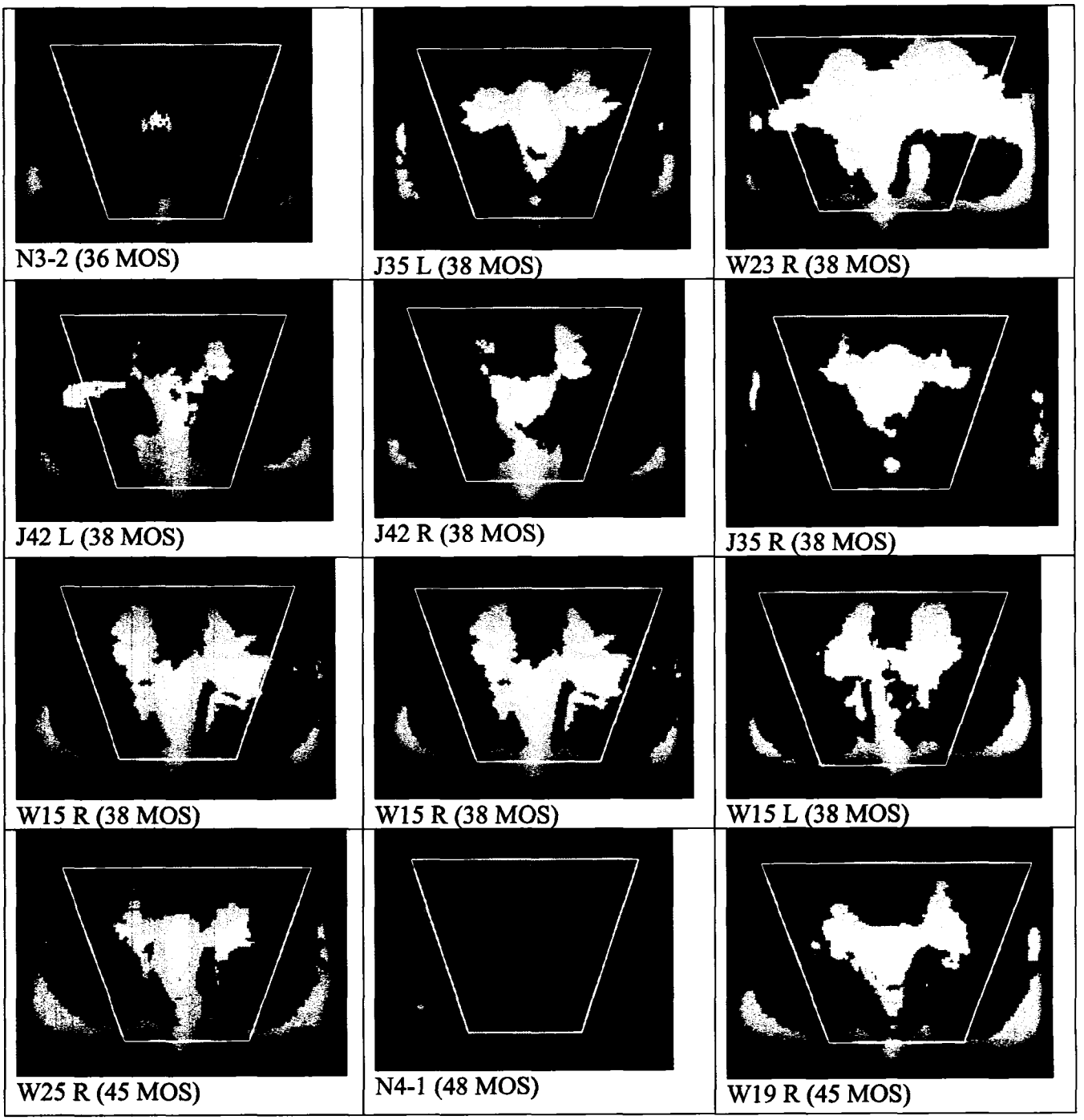

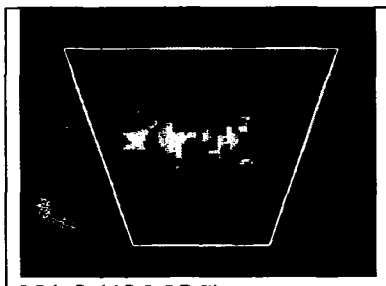

N4-5 (48 MOS)

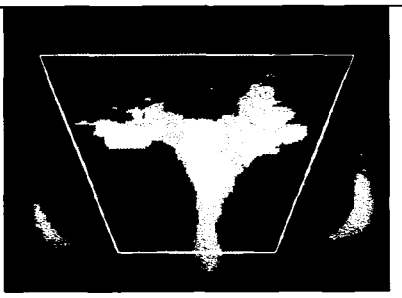

W16 L (49 MOS)

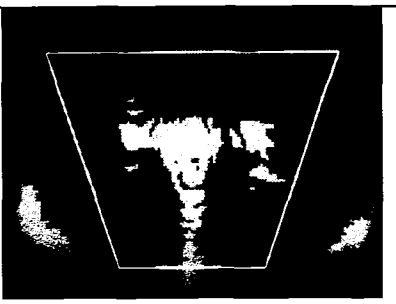

N4-4 (48 MOS)

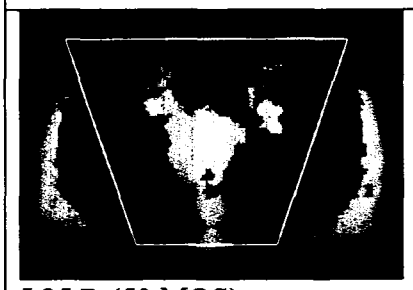

J 25 R (50 MOS)

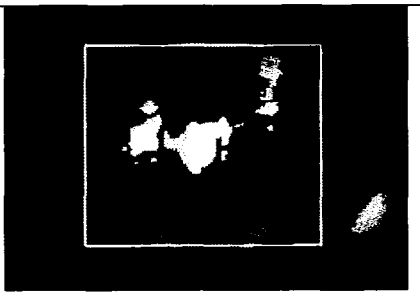

J33 L (50 MOS)

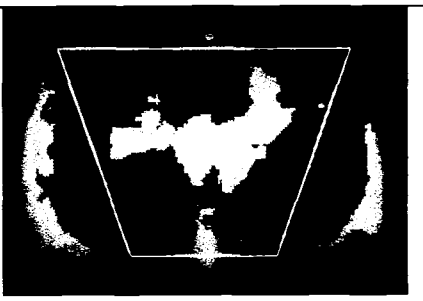

J25 L (50 MOS)

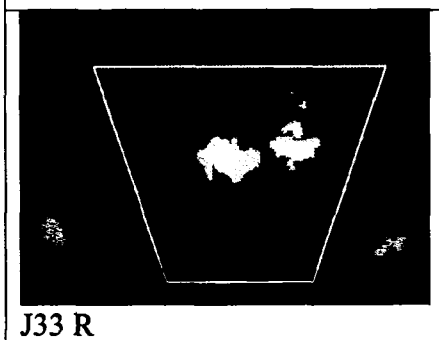

J33 R

Non-Racing Horses

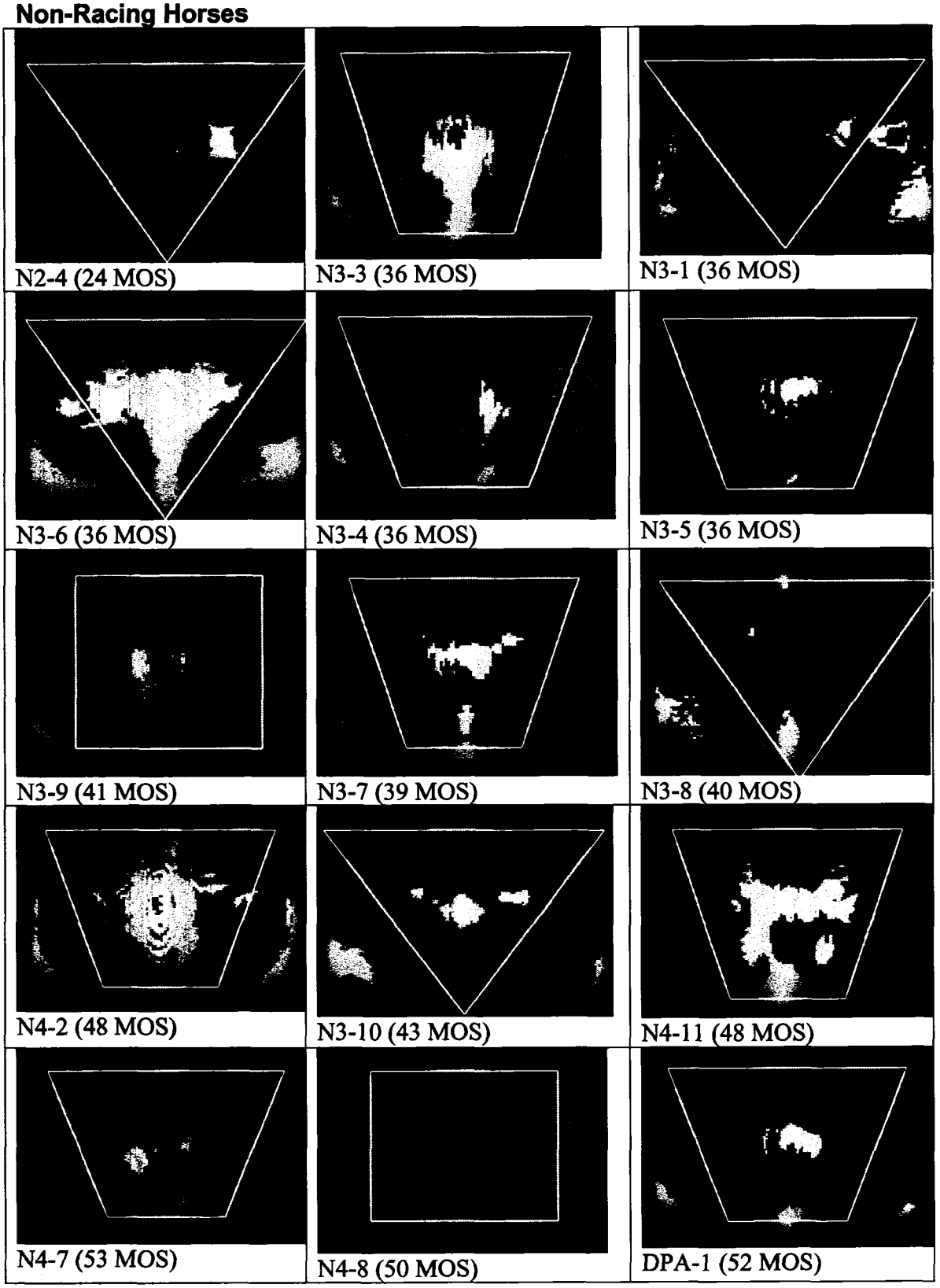

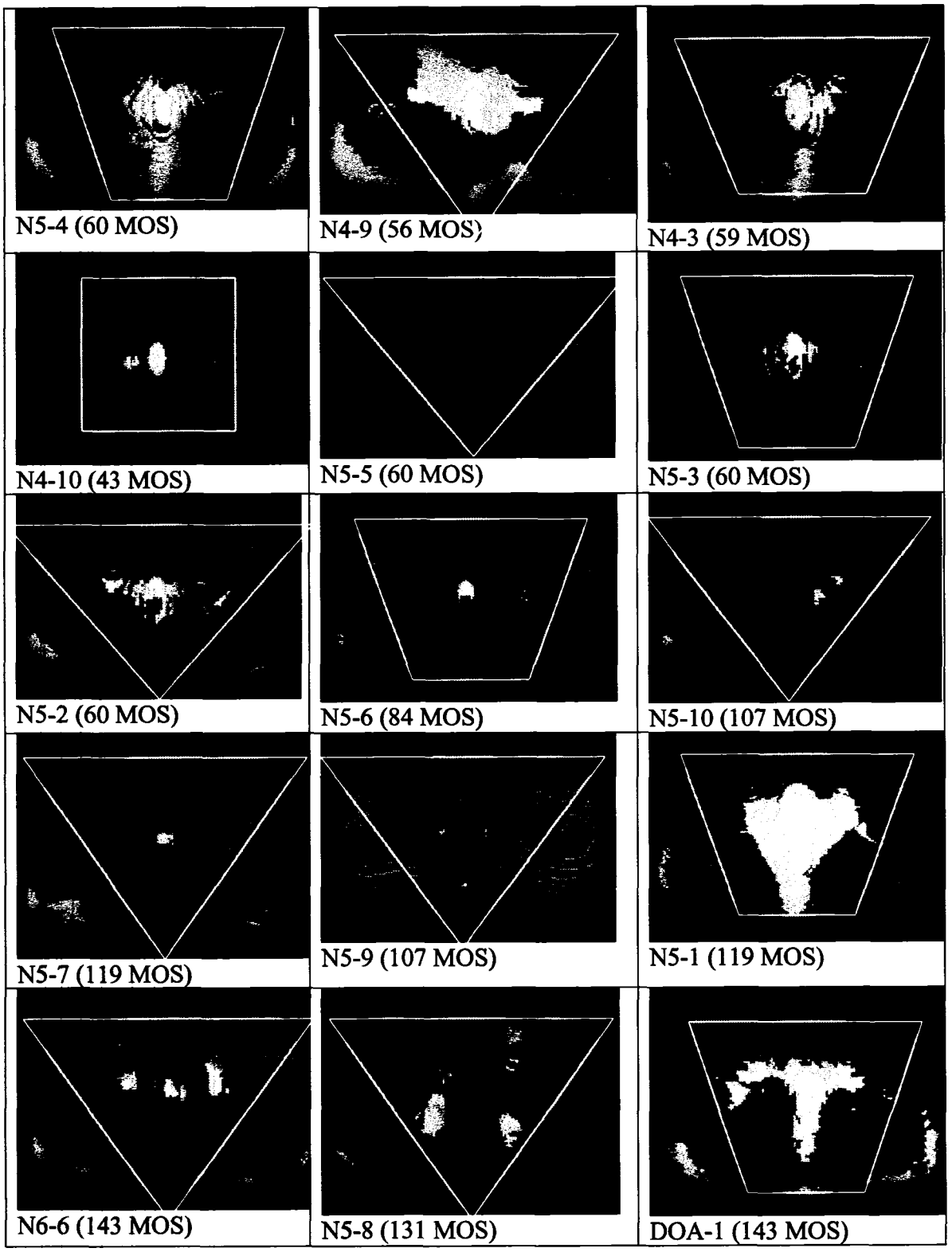

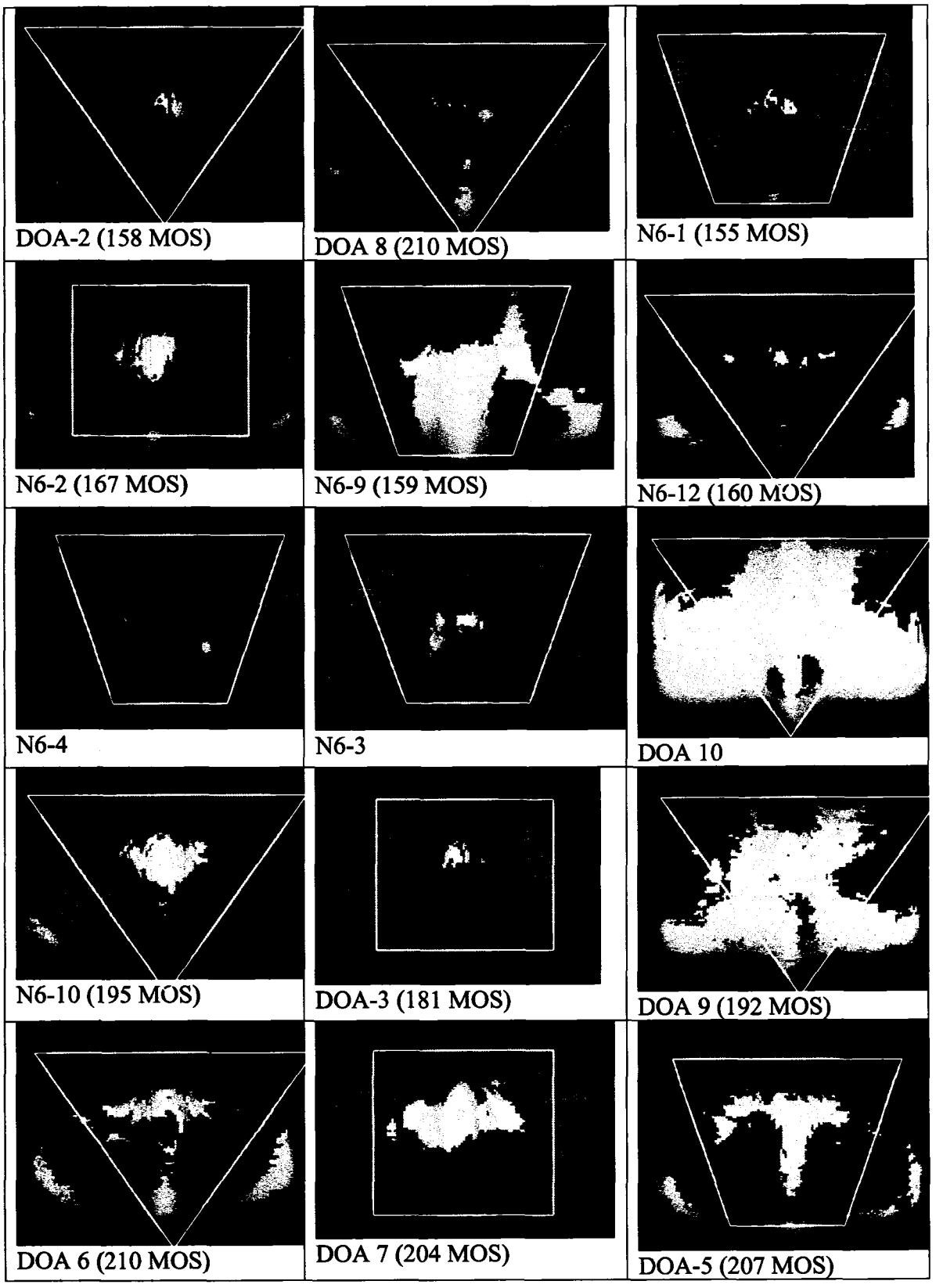

Bibliography

1. Anonymous, *National economic cost of equine lameness, colic and equine protoxoal myeloencephalitis (EPM) in the United States.* 2001, USDA:APHIS:VS, NAHMS: Web site: http://www.aphis.gov/vs/ceah/Equine/economicsfinal.PDF.
2. Estberg, L., Stover, S.M., Gardner, I.A., Johnson, B.J., Case, J.T., Ardans, A., Read, D.H., Anderson, M.L., Barr, B.C., Daft, B.M., Kinde, H., Moore, J., Stoltz, J., and Woods, L.W., *Fatal musculoskeletal injuries incurred during racing and training in thoroughbreds.* Journal of the American Veterinary Medical Association, 1996. **208**(1): p. 92-6.
3. anonymous, *Prevalence of self-reported arthritis or chronic joint symptoms among adults-United States 2001.* Morbidity & Mortality Weekly Report, 2002. **51**(42): p. 948-950.
4. anonymous, *Prevalence of disabilities and associated health conditions among adults-United States 1999.* Morbidity & Mortality Weekly Report, 2001. **50**(7): p. 120-5.
5. anonymous, *Update: Direct and indirect costs of arthritis and other rheumatic conditions--United States 1997.* Morbidity & Mortality Weekly Report, 2004. **53**(18): p. 388-389.
6. Muller-Gerbl, M., *The subchondral bone plate.* Advances in Anatomy, Embryology & Cell Biology, 1998. **141**: p. III-XI, 1-134.
7. Clark, J.M. and Huber, J.D., *The structure of the human subchondral plate.* Journal of Bone & Joint Surgery - British Volume, 1990. **72B**(5): p. 866-73.
8. Mcilwraith, C.W., Trotter G.W., *Joint Disease in the Horse.* 1996, Philadelphia: W.B. Saunders.
9. Martin, R.B., Burr, D.B., and Sharkey, N.A., *Skeletal tissue mechanics.* 1998, New York: Springer. xiv, 392.
10. Murray, R.C., Zhu, C.F., Goodship, A.E., Lakhani, K.H., Agrawal, C.M., and Athanasiou, K.A., *Exercise affects the mechanical properties and histological appearance of equine articular cartilage.* Journal of Orthopaedic Research, 1999. **17**(5): p. 725-31.
11. Murray, R.C., Whitton, R.C., Vedi, S., Goodship, A.E., and Lekeux, P., *The effect of training on the calcified zone of equine middle carpal articular cartilage.* Equine Veterinary Journal. Supplement, 1999. **30**: p. 274-8.
12. Lane, L.B., Villacin, A., and Bullough, P.G., *The vascularity and remodelling of subchondrial bone and calcified cartilage in adult human femoral and humeral heads. An age- and stress-related phenomenon.* Journal of Bone & Joint Surgery - British Volume, 1977. **59**(3): p. 272-8.
13. Diseases, N.I.o.A.a.M.a.S., *Questions and answers about arthritis and rheumatic diseases.* http://www.niams.nih.gov/hi/topics/arthritis/artrheu.htm#art_a, 2002.

14. Favus, M.J., *Primer on the Metabolic Bone Diseases and Disorders of Mineral Metabolism.* Fourth Ed. ed, ed. A.S.f.B.a.M. Research. 2003, Philadelphia: Lippencott, Williams & Wilkins.
15. Brandt, K.D., Myers, S.L., Burr, D., and Albrecht, M., *Osteoarthritic changes in canine articular cartilage, subchondral bone, and synovium fifty-four months after transection of the anterior cruciate ligament.* Arthritis & Rheumatism, 1991. **34**(12): p. 1560-70.
16. Burr, D.B., *The importance of subchondral bone in osteoarthrosis.* Current Opinion in Rheumatology, 1998. **10**(3): p. 256-62.
17. Dedrick, D.K., Goldstein, S.A., Brandt, K.D., O'Connor, B.L., Goulet, R.W., and Albrecht, M., *A longitudinal study of subchondral plate and trabecular bone in cruciate-deficient dogs with osteoarthritis followed up for 54 months.* Arthritis & Rheumatism, 1993. **36**(10): p. 1460-7.
18. Dekel, S. and Weissman, S.L., *Joint changes after overuse and peak overloading of rabbit knees in vivo.* Acta Orthopaedica Scandinavica, 1978. **49**(6): p. 519-28.
19. Frost, H.M., *Perspectives: a biomechanical model of the pathogenesis of arthroses.* Anatomical Record, 1994. **240**(1): p. 19-31.
20. Grynpas, M.D., Alpert, B., Katz, I., Lieberman, I., and Pritzker, K.P., *Subchondral bone in osteoarthritis.* Calcified Tissue International, 1991. **49**(1): p. 20-6.
21. Radin, E.L., Burr, D.B., Fhyrie D., Brown, Boyd, *Characteristics of joint loading as it applies to osteoarthrosis*, in *Biomechanics of Joint Disease*. 1990, Springer-Verlag: New York. p. 437-451.
22. Martel-Pelletier, J., *Pathophysiology of osteoarthritis.* Osteoarthritis & Cartilage, 1999. **7**(4): p. 371-3.
23. Pugh, J.W., Radin, E.L., and Rose, R.M., *Quantitative studies of human subchondral cancellous bone. Its relationship to the state of its overlying cartilage.* Journal of Bone & Joint Surgery - American Volume, 1974. **56**(2): p. 313-21.
24. Boyde, A., *The real response of bone to exercise.* Journal of Anatomy, 2003. **203**: p. 173-89.
25. Radin, E.L., Parker, H.G., Pugh, J.W., Steinberg, R.S., Paul, I.L., and Rose, R.M., *Response of joints to impact loading. 3. Relationship between trabecular microfractures and cartilage degeneration.* Journal of Biomechanics, 1973. **6**(1): p. 51-7.
26. Li, B. and Aspden, R.M., *Composition and mechanical properties of cancellous bone from the femoral head of patients with osteoporosis or osteoarthritis.* Journal of Bone & Mineral Research, 1997. **12**(4): p. 641-51.
27. Fazzalari, N.L., Forwood, M.R., Smith, K., Manthey, B.A., and Herreen, P., *Assessment of cancellous bone quality in severe osteoarthrosis: bone mineral density, mechanics, and microdamage.* Bone, 1998. **22**(4): p. 381-8.

28. Koszyca, B., Fazzalari, N.L., Vernon-Roberts, B., and ., *Microfractures in Coxarthrosis.* Acta Orthopaedica Scandinavica, 1990. **61**(4): p. 307-10.
29. Hilal, G., Martel-Pelletier, J., Pelletier, J.P., Ranger, P., and Lajeunesse, D., *Osteoblast-like cells from human subchondral osteoarthritic bone demonstrate an altered phenotype in vitro: possible role in subchondral bone sclerosis.* Arthritis & Rheumatism, 1998. **41**(5): p. 891-9.
30. Frost, H.M., *Bone's mechanostat: a 2003 update.* Anatomical Record. Part A, Discoveries in Molecular, Cellular, & Evolutionary Biology, 2003. **275A**(2): p. 1081-1101.
31. Sumner-Smith, *Bone in Clinical Orthopedics.* 2nd ed, ed. Fackelman. 2002, New York: AO Publishing.
32. Boyde, A., Haroon, Y., Jones, S.J., and Riggs, C.M., *Three dimensional structure of the distal condyles of the third metacarpal bone of the horse.* Equine Veterinary Journal, 1999. **31**(2): p. 122-9.
33. Tanck, E., Homminga, J., van Lenthe, G.H., and Huiskes, R., *Increase in bone volume fraction precedes architectural adaptation in growing bone.* Bone, 2001. **28**(6): p. 650-4.
34. Frost, H.M., *From Wolff's law to the Utah paradigm: insights about bone physiology and its clinical applications.* Anatomical Record, 2001. **262**(4): p. 398-419.
35. Kawcak, C.E., McIlwraith, C.W., Norrdin, R.W., Park, R.D., and James, S.P., *The role of subchondral bone in joint disease: a review.* Equine Veterinary Journal, 2001. **33**(2): p. 120-6.
36. McCarthy, R.N. and Jeffcott, L.B., *Monitoring the effects of treadmill exercise on bone by non-invasive means during a progressive fitness programme.* Equine Veterinary Journal. Supplement, 1988(6): p. 88-92.
37. McCarthy, R.N. and Jeffcott, L.B., *Effects of treadmill exercise on cortical bone in the third metacarpus of young horses.* Research in Veterinary Science, 1992. **52**: p. 28-37.
38. Riggs, C.M. and Boyde, A., *Effect of exercise on bone density in distal regions of the equine third metacarpal bone in 2-year-old thoroughbreds.* Equine Veterinary Journal. Supplement, 1999. **30**: p. 555-60.
39. Norrdin, R.W., Kawcak, C.E., Capwell, B.A., and McIlwraith, C.W., *Subchondral bone failure in an equine model of overload arthrosis.* Bone, 1998. **22**(2): p. 133-9.
40. Pugh, J.W., Rose, R.M., and Radin, E.L., *A possible mechanism of Wolff's law: trabecular microfractures.* Archives Internationales de Physiologie et de Biochimie, 1973. **81**(1): p. 27-40.
41. Brandt, K.D., *Animal models of osteoarthritis.* Biorheology, 2002. **39**(1-2): p. 221-35.
42. McIlwraith, C.W., Fessler, J.F., Blevins, W.E., Page, E.H., Rebar, A.H., Van Sickle, D.C., and Coppoc, G.L., *Experimentally induced arthritis of the equine carpus: clinical determinations.* American Journal of Veterinary Research, 1979. **40**(1): p. 11-20.

43. Radin, E.L. and Rose, R.M., *Role of subchondral bone in the initiation and progression of cartilage damage.* Clinical Orthopaedics & Related Research, 1986(213): p. 34-40.
44. Simmons, E.J., Bertone, A.L., and Weisbrode, S.E., *Instability-induced osteoarthritis in the metacarpophalangeal joint of horses.* American Journal of Veterinary Research, 1999. **60**(1): p. 7-13.
45. Bank, R.A., Soudry, M., Maroudas, A., Mizrahi, J., and TeKoppele, J.M., *The increased swelling and instantaneous deformation of osteoarthritic cartilage is highly correlated with collagen degradation.* Arthritis & Rheumatism, 2000. **43**(10): p. 2202-10.
46. Radin, E.L., Paul, I.L., and Tolkoff, M.J., *Subchondral bone changes in patients with early degenerative joint disease.* Arthritis & Rheumatism, 1970. **13**(4): p. 400-5.
47. Lajeunesse, D., Hilal, G., Pelletier, J.P., and Martel-Pelletier, J., *Subchondral bone morphological and biochemical alterations in osteoarthritis.* Osteoarthritis & Cartilage, 1999. **7**(3): p. 321-2.
48. Mattei, J.P. and Roux, H., *New potential therapeutic goals: subchondral bone and progression of osteoarthritis.* Osteoarthritis & Cartilage, 1999. **7**(3): p. 329-30.
49. Burr, D.B. and Schaffler, M.B., *The involvement of subchondral mineralized tissues in osteoarthrosis: quantitative microscopic evidence.* Microscopy Research & Technique, 1997. **37**(4): p. 343-57.
50. Bailey, C.J., Reid, S.W., Hodgson, D.R., Bourke, J.M., and Rose, R.J., *Flat, hurdle and steeple racing: risk factors for musculoskeletal injury.* Equine Veterinary Journal, 1998. **30**(6): p. 498-503.
51. Bailey, C.J., Rose, R.J., Reid, S.W., and Hodgson, D.R., *Wastage in the Australian thoroughbred racing industry: a survey of Sydney trainers.* Australian Veterinary Journal, 1997. **75**(1): p. 64-6.
52. Martens, P., Ihler, C.F., and Rennesund, J., *Detection of a radiographically occult fracture of the lateral palmar process of the distal phalanx in a horse using computed tomography.* Veterinary Radiology & Ultrasound, 1999. **40**(4): p. 346-9.
53. Ross, M.W. and Dyson, S.J., *Diagnosis and management of lameness in the horse.* 2003, Philadelphia, Pa. London: W. B. Saunders. xxiii, 1140 , [2] leaves of plates.
54. Steinheimer, D., McIlwraith, C., Park, R., and Steyn, P., *Comparison of Radiographic Subchondral Bone Changes with Arthoscopic Findings In the Equine Femoropatellar and Femorotibial Joints: A Retrospective Study of 72 Joints (50 Horses).* Veterinary Radiology & Ultrasound, 1995. **36**(6): p. 478-484.
55. Curry, T.S., *Christensen's Physics of Diagnostic Radiology.* 4th ed, ed. T.S. Curry, J.E. Dowdey, and J. Murry, R.C. 1990, Philadelphia: Lea & Febiger.

56. Luo, G., Kinney J.H., Kaufman J.J., Haupt D, Chiabera A, Siffert R.S., *Relationship Between Plain Radiographic Patterns and Three- dimensional Trabecular Architecture in The Human Calcaneus.* Osteoporosis International, 1999. **9**(4): p. 339-345.

57. Brandt, K.D., *Osteophytes in osteoarthritis. Clinical aspects.* Osteoarthritis & Cartilage, 1999. **7**(3): p. 334-5.

58. Buckland-Wright, J.C., Macfarlane, D.G., Lynch, J.A., Jasani, M.K., and Bradshaw, C.R., *Joint space width measures cartilage thickness in osteoarthritis of the knee: high resolution plain film and double contrast macroradiographic investigation.* Annals of Rheumatic Disease, 1995. **54**: p. 263-268.

59. Adams, O.R., *Adams' lameness in horses.* 5th ed. 2002, Philadelphia: Williams & Wilkins. xvi, 1174.

60. Innes, J.F., Costello, M., Barr, F.J., Rudorf, H., and Barr, A.R.S., *Radiographic progression of osteoarthritis of the canine stifle joint: a prospective study.* Vet Radiol & Ultrasound, 2004. **45**(2): p. 143-148.

61. Gupta, K.B., Duryea, J., and Weissman, B.N., *Radiographic evaluation of osteoarthritis.* Radiologic Clinics of North America, 2004. **42**(1): p. 11-41.

62. Twardock, A.R., *Equine bone scintigraphic uptake patterns related to age, breed, and occupation.* Veterinary Clinics of North America - Equine Practice, 2001. **17**(1): p. 75-94.

63. Innes, J.F., Barr, A.R., Patteson, M.W., and Dieppe, P.A., *Scintigraphy in the evaluation of osteoarthritis of the canine stifle joint.* Vet Comp Orthop Traumatol, 1996. **9**: p. 53-9.

64. Foreman, J.H., Kneller, S.K., Twardock, A.R., Chambers, M.D., and Inoue, O.J., *Forelimb skeletal scintigraphy responses in previously untrained Thoroughbreds undergoing initial treadmill training.* Equine Veterinary Journal. Supplement, 2002(34): p. 230-5.

65. Zubrod, C.J., Schneider, R.K., Tucker, R.L., Gavin, P.R., Ragle, C.A., and Farnsworth, K.D., *Use of magnetic resonance imaging for identifying subchondral bone damage in horses: 11 cases (1999-2003).* Journal of the American Veterinary Medical Association, 2004. **224**(3): p. 411-8.

66. Whitton, R.C., Buckley, C., Donovan, T., Wales, A.D., and Dennis, R., *The diagnosis of lameness associated with distal limb pathology in a horse: a comparison of radiography, computed tomography and magnetic resonance imaging.* Veterinary Journal, 1998. **155**(3): p. 223-229.

67. Eckstein, F., Muller-Gerbl, M., Steinlechner, M., Kierse, R., and Putz, R., *Subchondral bone density in the human elbow assessed by computed tomography osteoabsorptiometry: a reflection of the loading history of the joint surfaces.* Journal of Orthopaedic Research, 1995. **13**(2): p. 268-78.

68. Thomas, H.L., Galuppo, L.D., Wisner, E.R., Stover, S.M., and Decock, H.E. *Computed tomography for identification of early third metacarpal traumatic palmar subchondral bone lesions.* in *ACVR Scientific Program & Abstracts*. 2004. Montreal.

69. Langton, C.M. and Njeh, C.F., *The physical measurement of bone*. 2004, Bristol and Philadelphia: Institute of physics publishing.

70. Frost, H.M., *Does bone mass equate with bone health? An argument for the negative.* Journal of Clinical Densitometry, 2001. **4**(3): p. 179-84.

71. Pastoureau, P.C., Chomel, A.C., and Bonnet, J., *Evidence of early subchondral bone changes in the meniscectomized guinea pig. A densitometric study using dual-energy X-ray absorptiometry subregional analysis.* Osteoarthritis & Cartilage, 1999. **7**(5): p. 466-73.

72. Clarke, S., Wakeley, C., Duddy, J., Sharif, M., Watt, I., Ellingham, K., Elson, C.J., Nickols, G., and Kirwan, J.R., *Dual-energy X-ray absorptiometry applied to the assessment of tibial subchondral bone mineral density in osteoarthritis of the knee.* Skeletal Radiology, 2004. **33**(10): p. 588-95.

73. Bruyere, O., Dardenne, C., Lejeune, E., Zegels, B., Pahaut, A., Richy, F., Seidel, L., Ethgen, O., Henrotin, Y., and Reginster, J.Y., *Subchondral tibial bone mineral density predicts future joint space narrowing at the medial femoro-tibial compartment in patients with knee osteoarthritis.* Bone, 2003. **32**(5): p. 541-5.

74. Walker, J.E., Lewis, C.W., MacLeay, J.M., Kawcak, C.E., and Wheeler, D.L., *Assessment of subchondral bone mineral density in equine metacarpophalangeal and stifle joints.* Biomedical Sciences Instrumentation, 2004. **40**: p. 272-6.

75. Carstanjen, B., Duboeuf, F., Detilleux, J., and Lepage, O.M., *Equine third metacarpal bone assessment by quantitative ultrasound and dual energy X-ray absorptiometry: an ex vivo study.* Journal of Veterinary Medicine - Series A, 2003. **50**(1): p. 42-7.

76. Schneider, S., Breit, S.M., Grampp, S., Kunzel, W.W., Liesegang, A., Mayrhofer, E., and Zentek, J., *Comparative assessment of bone mineral measurements obtained by use of dual-energy x-ray absorptiometry, peripheral quantitative computed tomography, and chemical-physical analyses in femurs of juvenile and adult dogs.* American Journal of Veterinary Research, 2004. **65**(7): p. 891-900.

77. Nielsen, B.D., Potter, G.D., Morris, E.L., Odom, T.W., Senor, D., Reynolds, J.A., Smith, W.B., and Martin, M.T., *Changes in the third metacarpal bone and frequency of bone injuries in young quarter horses during race training: Observations and theoretical considerations.* J Eq Vet Sci, 1997. **17**(10): p. 541-549.

78. Porr, C.A., Kronfeld, D.S., Lawrence, L.A., Pleasant, R.S., and Harris, P.A., *Deconditioning reduces mineral content of the third metacarpal bone in horses.* Journal of Animal Science, 1998. **76**(7): p. 1875-9.

79. Kalender, W.A. and Fischer, M., *Quality-control and standardization of absorptiometric and computer tomographic measurements of bone-mineral mass and density.* Radiation Protection Dosimetry, 1993. **49**(1-3): p. 229-233.

80. Cann, C.E., *Quantitative CT for determination of bone mineral density: a review.* Radiology, 1988. **166**(2): p. 509-22.

81. Banse, X., Devogelaer, J.P., and Grynpas, M., *Patient-specific microarchitecture of vertebral cancellous bone: a peripheral quantitative computed tomographic and histological study.* Bone, 2002. **30**(6): p. 829-35.

82. Mulder, L., Koolstra, J.H., and Van Eijden, T.M., *Accuracy of microCT in the quantitative determination of the degree and distribution of mineralization in developing bone.* Acta Radiologica, 2004. **45**(7): p. 769-77.

83. Cann, C.E., Ettinger, B., Gordan, G.S., Kolb, F.O., Reiser, U., Arnaud, C.D., and Genant, H.K., *Osteoporosis: assessment by quantitative computed tomography.* Orthopedic Clinics of North America, 1985. **16**(3): p. 557-68.

84. Firth, E.C., Rogers, C.W., and Goodship, A.E., *Bone mineral density changes in growing and training Thoroughbreds.* Proc. of the Amer. Assoc. of Equine Prac., 2000. **46**: p. 295-99.

85. Muller-Gerbl, M., Putz, R., Hodapp, N., Schulte, E., and Wimmer, B., *Computed tomography-osteoabsorptiometry for assessing the density distribution of subchondral bone as a measure of long-term mechanical adaptation in individual joints.* Skeletal Radiology, 1989. **18**(7): p. 507-12.

86. Kawcak, C.E., McIlwraith, C.W., Norrdin, R.W., Park, R.D., and Steyn, P.S., *Clinical effects of exercise on subchondral bone of carpal and metacarpophalangeal joints in horses.* American Journal of Veterinary Research, 2000. **61**(10): p. 1252-8.

87. Pool, R.R., *Joint Disease in the Athletic Horse: A Review of Pathologic Findings and Pathogenesis.* Proc. of the Amer. Assoc. of Equine Prac., 1995. **41**: p. 20-34.

88. Pool, R.R. and Meagher, D.M., *Pathologic findings and pathogenesis of racetrack injuries.* Veterinary Clinics of North America - Equine Practice, 1990. **6**(1): p. 1-30.

89. Hornof, W., O'Brien, T., and Pool, R., *Osteochondritis dissecans of the distal metacarpus in the adult racing thoroughbred horse.* Vet Radiol, 1981. **22**(3): p. 98-106.

90. Bailey, C.J., Reid, S.W., Hodgson, D.R., and Rose, R.J., *Impact of injuries and disease on a cohort of two- and three-year-old thoroughbreds in training.* Veterinary Record, 1999. **145**(17): p. 487-93.

91. Rossdale, P.D., Hopes, R., Digby, N.J., and offord, K., *Epidemiological study of wastage among racehorses 1982 and 1983.* Veterinary Record, 1985. **116**(3): p. 66-9.

92. Jeffcott, L.B., Rossdale, P.D., Freestone, J., Frank, C.J., and Towers-Clark, P.F., *An assessment of wastage in thoroughbred racing from conception to 4 years of age.* Equine Veterinary Journal, 1982. **14**(3): p. 185-98.

93. Estberg, L., Gardner, I.A., Stover, S.M., and Johnson, B.J., *A case-crossover study of intensive racing and training schedules and risk of catastrophic musculoskeletal injury and lay-up in California thoroughbred racehorses.* Preventive Veterinary Medicine, 1998. **33**(1-4): p. 159-70.

94. Robinson, R.A. and Gordon, B., *American Association of Equine Practitioners Track Breakdown Studies-Horse Results.* Proc. of the 7th Int. Conf. of Racing Analysts and Veterinarians, 1988.

95. Johnson, B.J., Stover, S.M., Daft, B.M., Kinde, H., Read, D.H., Barr, B.C., Anderson, M., Moore, J., Woods, L., and Stoltz, J., *Causes of death in racehorses over a 2 year period.* Equine Veterinary Journal, 1994. **26**(4): p. 327-30.

96. Meagher, D. *Lateral condylar fractures of the metacarpus and metarsus in horses.* in *Proc. Amer. Assoc. Equine Pract.* 1976.

97. Riggs, C.M., *Aetiopathogenesis of parasagittal fractures of the distal condyles of the third metacarpal and third metatarsal bones--review of the literature.* Eq. Vet. J., 1999. **31**(2): p. 116-120.

98. Martin, G.S., *Factors associated with racing performance of Thoroughbreds undergoing lag screw repair of condylar fractures of the third metacarpal or metatarsal bone.* Journal of the American Veterinary Medical Association, 2000. **217**(12): p. 1870-7.

99. Ciarelli, M.J., Goldstein, S.A., Kuhn, J.L., Cody, D.D., and Brown, M.B., *Evaluation of orthogonal mechanical properties and density of human trabecular bone from the major metaphyseal regions with materials testing and computed tomography.* J of Orthop Res, 1991. **9**(5): p. 674-82.

100. Hayes, W.C., Piazza, S.J., and Zysset, P.K., *Biomechanics of fracture risk prediction of the hip and spine by quantitative computed tomography.* Radiologic Clinics of North America, 1991. **29**(1): p. 1-18.

101. Takada, M., Engelke, K., Hagiwara, S., Grampp, S., and Genant, H.K., *Accuracy and precision study in vitro for peripheral quantitative computed tomography.* Osteoporosis International, 1997. **6**: p. 207-212.

102. Kaneko, T.S., Bell, J.S., Pejcic, M.R., Tehranzadeh, J., and Keyak, J.H., *Mechanical properties, density and quantitative CT scan data of trabecular bone with and without metastases.* Journal of Biomechanics, 2004. **37**(4): p. 523-30.

103. Gluer, C.C., Reiser, U.J., Davis, C.A., Rutt, B.K., and Genant, H.K., *Vertebral mineral determination by quantitative computed tomography (QCT): accuracy of single and dual*

energy measurements. Journal of Computer Assisted Tomography, 1988. **12**(2): p. 242-58.

104. Snyder, S. and Schneider, E., *Estimation of mechanical properties of cortical bone by computed tomography.* Journal of Orthopaedic Research, 1991. **9**(3): p. 422-431.
105. Les, C.M., Keyak, J.H., Stover, S.M., Taylor, K.T., and Kaneps, A.J., *Estimation of material properties in the equine metacarpus with use of quantitative computed tomography.* Journal of Orthopaedic Research, 1994. **12**(6): p. 822-33.
106. Waite, K., Nielsen, B.D., and Rosenstein, D.S., *Computed tomography as a method of estimating bone mineral content in horses.* Equine Practice, 2000. **20**(1): p. 49-52.
107. Markel, M.D., Morin, R.L., Wikenheiser, M.A., Robb, R.A., and Chao, E.Y., *Multiplanar quantitative computed tomography for bone mineral analysis in dogs.* American Journal of Veterinary Research, 1991. **52**(9): p. 1479-83.
108. Les, C.M., Stover, S.M., Keyak, J.H., Taylor, K.T., and Kaneps, A.J., *Stiff and strong compressive properties are associated with brittle post-yield behavior in equine compact bone material.* Journal of Orthopaedic Research, 2002. **20**(3): p. 607-14.
109. Nunamaker, D.M., Butterweck, D.M., and Provost, M.T., *Fatigue fractures in thoroughbred racehorses: relationships with age, peak bone strain, and training.* Journal of Orthopaedic Research, 1990. **8**(4): p. 604-11.
110. Frost, H.M., *Bone "mass" and the "mechanostat": a proposal.* Anatomical Record, 1987. **219**(1): p. 1-9.
111. Riggs, C.M., Whitehouse, G.H., and Boyde, A., *Pathology of the distal condyles of the third metacarpal and third metatarsal bones of the horse.* Equine Veterinary Journal, 1999. **31**(2): p. 140-8.
112. Greenfield, G.B., *Radiology of Bone Diseases.* 2nd ed. 1975, Philadelphia: Lippincott.
113. Widmer, W.R., Buckwalter, K.A., Fessler, J.F., Hill, M.A., VanSickle, D.C., and Ivancevich, S., *Use of radiography, computed tomography and magnetic resonance imaging for evaluation of navicular syndrome in the horse.* Veterinary Radiology & Ultrasound, 2000. **41**(2): p. 108-16.
114. Zimmerman, C.W., Lewis, C.W., Wheeler, D.L., and Kawcak, C.E. *Site dependent subchondral bone variation within the equine fetlock.* in *Undergraduate Research Symposium Colorado State University.* 2003. Fort Collins, CO.
115. Eckstein, F., Merz, B., and Jacobs, C.R., *Effects of joint incongruity on articular pressure distribution and subchondral bone remodeling.* Advances in Anatomy, Embryology & Cell Biology, 2000. **152**: p. 1-127.
116. Porr, C.A., Ott, E.A., Johnson, E., and Madison, J.B., *Bone mineral in young Thoroughbred horses is affected by training.* Equine Practice, 1997. **19**(8): p. 28-31.

117. Barneveld, A. and van Weeren, P.R., *Early changes in the distal intertarsal joint of Dutch Warmblood foals and the influence of execise on bone density in the third tarsal bone.* Equine Veterinary Journal. Supplement, 1999. **31**: p. 67-73.
118. Meunier, P.J. and Boivin, G., *Bone mineral density reflects bone mass but also the degree of mineralization of bone: therapeutic implications.* Bone, 1997. **21**(5): p. 373-7.
119. Shamall, D., Teschler-Nicola, M., Kainberger, F., Tangl, S.T., Brandstatter, F., Patzak, B., Muhsil, J., and Plenk Jr., H., *Changes in trabecular bone structure in rickets and osteomalacia: The potential of a medico-historical collection.* International Jounral of Osteoarchaeology, 2003. **13**: p. 283-288.
120. Gerakis, A., Hadjidakis, D., Kokkinakis, E., Apostolou, T., Raptis, S., and Billis, A., *Correlation of bone mineral density with the histological findings of renal osteodystrophy in patients on hemodialysis.* Journal of Nephrology, 2000. **13**(6): p. 437-43.
121. Parfitt, A.M., *Bone age, mineral density, and fatigue damage.* Calcified Tissue International, 1993. **53**(Suppl 1): p. S82-5.
122. Boivin, G. and Meunier, P.J., *Changes in bone remodeling rate influence the degree of mineralization of bone.* Connective Tissue Research, 2002. **43**(2-3): p. 535-7.
123. Rooney, J.R., *Further studiesn in breakdown in Thoroughbred racehorses.* Equine Veterinary Data, 1983(May): p. 133.
124. Johnson, B., *A look at racetrack breakdowns.* J Eq Vet Sci, 1993. **3**: p. 129-132.
125. Davies, H.M. and Merritt, J.S., *Surface strains around the midshaft of the third metcarpal bone during turning.* Equine Veterinary Journal, 2004. **36**(8): p. 689-692.
126. Rubin, C.T. and Lanyon, L.E., *Kappa Delta Award paper. Osteoregulatory nature of mechanical stimuli: function as a determinant for adaptive remodeling in bone.* Journal of Orthopaedic Research, 1987. **5**(2): p. 300-10.
127. Lanyon, L.E., *Static vs dynamic loads as an influence on bone remodelling.* Calcified Tissue International, 1985. **37**(4): p. 411-7.
128. Butcher, M.T. and Ashley-Ross, M.A., *Fetlock joint kinematics differ with age in Thoroughbred racehorses.* Journal of Biomechanics, 2002. **35**(5): p. 563-71.
129. Ellis, D.R., *Some observations on condylar fractures of the third metacarpus and third metatarsus in young Thoroughbreds.* Eq. Vet. J., 1994. **26**(3): p. 178-183.
130. Boston, R.C. and Nunamaker, D.M., *Gait and speed as exercise components of risk factors associated with onset of fatigue injury of the third metacarpal bone in 2-year-old Thoroughbred racehorses.* American Journal of Veterinary Research, 2000. **61**(6): p. 602-8.
131. Richardson, D.W., *Medial condylar fractures of the third metatarsal bone in horses.* Journal of the American Veterinary Medical Association, 1984. **185**(7): p. 761-5.

132. Rick, M.C., O'Brien, T.R., Pool, R.R., and Meagher, D., *Condylar fractures of the third metacarpal bone and third metatarsal bone in 75 horses: radiographic features, treatments, and outcome.* Journal of the American Veterinary Medical Association, 1983. **183**(3): p. 287-96.

133. Radtke, C.L., Danova, N.A., Scollay, M.C., Santschi, E.M., Markel, M.D., Da Costa Gomez, T., and Muir, P., *Macroscopic changes in the distal ends of the third metacarpal and metatarsal bones of Thoroughbred racehorses with condylar fractures.[erratum appears in Am J Vet Res. 2003 Nov;64(11):1420].* American Journal of Veterinary Research, 2003. **64**(9): p. 1110-6.

134. Rao, G.U., Yaghmai, I., Wist, A.O., and Arora, G., *Systematic errors in bone-mineral measurements by quantitative computed tomography.* Medical Physics, 1987. **14**(1): p. 62-9.

135. Levi, C., Gray, J.E., McCullough, E.C., and Hattery, R.R., *The unreliability of CT numbers as absolute values.* AJR. American Journal of Roentgenology, 1982. **139**(3): p. 443-7.

136. Suzuki, S., Yamamuro, T., Okumura, H., and Yamamoto, I., *Quantitative computed tomography: comparative study using different scanners with two calibration phantoms.* British Journal of Radiology, 1991. **64**(767): p. 1001-6.

137. Zerhouni, E.A., Boukadoum, M., Siddiky, M.A., Newbold, J.M., Stone, D.C., Shirey, M.P., Spivey, J.F., Hesselman, C.W., Leo, F.P., and Stitik, F.P., *A standard phantom for quantitative CT analysis of pulmonary nodules.* Radiology, 1983. **149**(3): p. 767-73.

138. Cann, C.E., *Quantitative CT applications: comparison of current scanners.[erratum appears in Radiology 1987 Sep;164(3):879].* Radiology, 1987. **162**(1 Pt 1): p. 257-61.

139. Goodsitt, M.M., *Conversion relations for quantitative CT bone mineral densities measured with solid and liquid calibration standards.* Bone & Mineral, 1992. **19**(2): p. 145-58.

140. Goodsitt, M.M., Christodoulou, E.G., Larson, S.C., and Kazerooni, E.A., *Assessment of calibration methods for estimating bone mineral densities in trauma patients with quantitative CT: an anthropomorphic phantom study.* Academic Radiology, 2001. **8**(9): p. 822-34.

141. Faulkner, K.G., Gluer, C.C., Grampp, S., and Genant, H.K., *Cross-calibration of liquid and solid QCT calibration standards: corrections to the UCSF normative data.* Osteoporosis International, 1993. **3**(1): p. 36-42.

142. Markel, M.D., Morin, R.L., Wikenheiser, M.A., Lewallen, D.G., and Chao, E.Y., *Quantitative CT for the evaluation of bone healing.* Calcified Tissue International, 1991. **49**(6): p. 427-32.

143. Wachter, N., Krischak, G., Mentzel, M., Sarkar, M., Ebinger, T., Kinzl, L., Claes, L., and Augat, P., *Correlation of bone mineral density with strength and microstructural parameters of cortical bone in vitro.* Bone, 2002. **31**(1): p. 90-5.

144. Mankani, M.H., Kuznetsov, S.A., Avila, N.A., Kingman, A., and Robey, P.G., *Bone formation in transplants of human bone marrow stromal cells and hydroxyapatite-tricalcium phosphate: prediction with quantitative CT in mice.* Radiology, 2004. **230**(2): p. 369-76.

145. Augat, P., Merk, J., Genant, H.K., and Claes, L., *Quantitative assessment of experimental fracture repair by peripheral computed tomography.* Calcified Tissue International, 1997. **60**(2): p. 194-9.

146. O'Brien, T.R. *Disease of the Thoroughbred fetlock joint-a comparison of radiographic signs with gross pathologic lesions.* in *Proc. 23rd Ann. Conv., Amer. Assoc. of Equine Pract.* 1977.

147. Zekas, L.J., Bramlage, L.R., Embertson, R.M., and Hance, S.R., *Characterisation of the type and location of fractures of the third metacarpal/metatarsal condyles in 135 horses in central Kentucky (1986-1994).* Equine Veterinary Journal, 1999. **31**(4): p. 304-8.

148. Bassage, L.H., 2nd and Richardson, D.W., *Longitudinal fractures of the condyles of the third metacarpal and metatarsal bones in racehorses: 224 cases (1986-1995).* Journal of the American Veterinary Medical Association, 1998. **212**(11): p. 1757-64.

149. Otterness, I.G., Chang, M., Burkhardt, J.E., Sweeney, F.J., and Milici, A.J., *Histology and tissue chemistry of tidemark separation in hamsters.* Veterinary Pathology, 1999. **36**(2): p. 138-45.

Endnotes

[a] Philips Medical, Barthow, WA USA

[b] Computerized Image Reference Systems Inc., Fairfax, VA, USA

[c] Exakt Trennschleifsystem, Exakt-Apparatebau, Norderstedt, Germany

[d] Research Systems Inc., Boulder, CO USA

[e] Colorado State University, Fort Collins, CO USA

[f] Statistical Analysis Software, Cary, NC USA

[g] General Electric, Milwaukee, WI USA

[h] Richard-Allan Scientific Decalcifying Solution, Kalamazoo, MI USA

[i] Amberlite IR-120 (plus) ion-exchange resin, sodium form, Sigma-Aldrich Inc., St. Louis, MO USA

[j] Courtesy of Robert Zink, Diagnostic Lab Colorado State University, Fort Collins, CO USA

[k] ImagePro, Media Cybernetics, Inc, Silver Spring, MD USA

[L] Cann-Genant Liquid Phantom, San Francisco, CA USA